Inaugural dissertation

for

obtaining the doctoral degree

of the

Combined Faculty of Mathematics, Engineering and Natural Sciences

of the

Ruprecht – Karls – University

Heidelberg

Presented by

M. Sc. Sofia Libório Passos Ramos

born in: Coimbra, Portugal

Oral examination: 13th February 2025

Heparanase: a tool to improve NK cell infiltration into solid tumors

Referees:

Prof. Dr. Martin Müller

Apl. Prof. Dr. Ilse Hofmann

Dedicated to loving my mother.

And to my brave and resilient best friend, Bea.

“If you know you are on the right track, if you have this inner knowledge, then nobody can turn you off… no matter what they say.” – Barbara McClintock, winner of the 1983 Nobel Prize in Physiology or Medicine

This work was carried out from January 2021 to August 2024 under scientific supervision of Dr. Angel Cid-Arregui in the Research Group Targeted Tumor Vaccines in the Clinical Cooperation Unit Applied Tumor Immunity at the German Cancer Research Center, Heidelberg

Declaration

I hereby declare that I have written the submitted dissertation ‘Heparanase: a tool to improve NK cell infiltration into solid tumors’ myself and in this process have not used any other sources than those indicated.

I hereby declare that I have not applied to be examined at any other institution, nor have I used the dissertation in this or any other form at any other institution as an examination paper, nor submitted it to any other faculty as a dissertation.

Heidelberg, _____

Location, date Sofia Libório Passos Ramos

Summary

Clinical outcomes of adoptive cell therapy (ACT) are less favorable in solid tumors compared to those in hematological malignancies due to the higher complexity and immunosuppressive characteristics of their tumor microenvironment (TME). The extracellular matrix (ECM) barrier represents a significant limitation for ACT success, since targeting and killing of cancer cells by the immune system requires immune cell extravasation, infiltration and progression through the ECM. Heparan sulfate proteoglycans (HSPGs) are one of the major ECM components and Heparanase (HPSE) is the only known endoglycosidase which cleaves the side chains of HSPGs, therefore participating in the ECM remodeling. HPSE is highly expressed by immune cells, and it has been described to facilitate the migration and infiltration of macrophages, T cells and dendritic cells. This suggests that HPSE plays an important role in immune cell migration and infiltration through tissues. Nevertheless, tumor cells also express high HPSE levels and require its activity for all stages of tumor progression. It seems that HPSE has a dual role in cancer progression and, while being necessary for immune cells infiltration, an increase in HPSE in the tumor ECM would be detrimental. While T cells have been the primary focus of ACT, Natural killer (NK) cells are emerging as a promising alternative due to their antigen independent killing capacity, low toxicity risk and “off-the-shelf” manufacturing feasibility. However, the ECM limitation for infiltration still poses as an issue to be solved.

The main goal of my thesis was to investigate the effects of the expression of a constitutively active, membrane-bound HPSE (GS3^{TM}) on the ability of human NK cells to infiltrate tumors, using the NK-92$^{CD3/CD8}$ cells as a model. NK-92$^{CD3/CD8}$/GS3^{TM} cells displayed significantly enhanced infiltration capability into tumor spheroids, as well as into xenograft tumors in immunodeficient mice. This enhanced infiltration was translated into significant tumor growth suppression without detectable adverse effects. Moreover, I assessed the expression of HPSE upon NK cell activation and the role of this enzyme in NK infiltration capacity. My results could show that HPSE surface expression decreases upon activation of primary human NK cells and upon co-culture of NK-92$^{CD3/CD8}$ cells with target cells. Moreover, HPSE-KO (knockout) NK cells presented a significant lower capacity to infiltrate tumor spheroids, suggesting that HPSE is required for NK cell infiltration capacity.

These findings suggest that HPSE is important for NK cell infiltration and that the constitutive expression of a surface-bound active HSPE on immune effector cells enhances their capability to access and eliminate tumor cells while limiting the supply of free HPSE in the TME. This approach opens new possibilities for improving adoptive immune treatments using NK cells.

Zusammenfassung

Klinische Ergebnisse der adoptiven Zelltherapie (ACT) bei soliden Tumoren sind aufgrund deren höherer Komplexität und der immunsuppressiven Eigenschaften der Tumormikroumgebung (TME) weniger erfolgversprechend als bei hämatologischen Malignomen.

Die Barriere der extrazellulären Matrix (ECM) stellt eine erhebliche Einschränkung für den Erfolg der ACT dar, da die gezielte Bekämpfung und Abtötung von Krebszellen durch das Immunsystem die Extravasation, Infiltration und Progression von Immunzellen durch die ECM erfordert. Heparansulfatproteoglykane (HSPGs) sind einer der wichtigsten Bestandteile der ECM, und Heparanase (HPSE) ist das einzige bekannte Enzym, das die Seitenketten von HSPG spaltet und somit an der Umstrukturierung der ECM beteiligt ist. HPSE wird in hohem Maße von Immunzellen exprimiert und es wurde beschrieben, dass es die Migration und Infiltration von Makrophagen, T-Zellen und dendritischen Zellen erleichtert. Dies deutet darauf hin, dass HPSE eine wichtige Rolle bei der Migration von Immunzellen durch das Gewebe spielt. Allerdings weisen auch Tumorzellen eine hohe HPSE-Expression auf und benötigen dessen Aktivität für alle Phasen des Tumorwachstums. Es scheint, als habe HPSE eine duale Funktion bei der Tumorprogression und dass ein Anstieg von HPSE in der ECM des Tumors nachteilig wäre, obwohl es für die Infiltration von Immunzellen notwendig ist. Während das Hauptaugenmerk der ACT bisher T-Zellen darstellten, haben sich natürliche Killerzellen (NK-Zellen) als vielversprechende Alternative herausgestellt, da sie Antigen-unabhängig Zelltod induzieren können, ein geringes Toxizitätsrisiko aufweisen und serienmäßig hergestellt werden können. Die limitierte Infiltration durch die ECM stellt jedoch immer noch ein Problem dar, das es zu lösen gilt.

Das Hauptziel meiner Dissertation bestand darin, die Auswirkungen der konstitutiven Expression eines aktiven, membrangebundenen HPSE ($GS3^{TM}$) auf die Fähigkeit menschlicher NK-Zellen zur Infiltration von Tumoren zu untersuchen, unter der Verwendung von NK-$92^{CD3/CD8}$-Zellen als Modell. NK-$92^{CD3/CD8}$/$GS3^{TM}$-Zellen zeigten eine signifikant erhöhte Infiltrationsfähigkeit in Tumor-Sphäroide sowie in Xenotransplantationstumore in immundefizienten Mäusen.

Diese verstärkte Infiltration führte zu einer signifikanten Verlangsamung des Tumorwachstums ohne nachweisbare negative Auswirkungen. Darüber hinaus habe ich die Expression von HPSE bei der Aktivierung von NK-Zellen und die Rolle dieses Enzyms in Bezug auf die Fähigkeit zur Infiltration von NK-Zellen untersucht. Meine Ergebnisse zeigten, dass die HPSE-Expression an der Zelloberfläche bei der Aktivierung primärer menschlicher NK-Zellen und bei

der Ko-Kultur von NK-92$^{CD3/CD8}$-Zellen mit Zielzellen abnimmt. Darüber hinaus zeigten HPSE-KO (Knockout) NK-Zellen eine deutlich geringere Fähigkeit zur Infiltration von Tumor-Sphäroiden, was darauf hindeutet, dass HPSE für die Infiltrationsfähigkeit von NK-Zellen erforderlich ist.

Diese Ergebnisse deuten darauf hin, dass HPSE für die Infiltration von NK-Zellen wichtig ist und dass die konstitutive Expression von oberflächengebundenem aktivem HSPE auf Immuneffektorzellen deren Fähigkeit verbessert, Tumorzellen zu erreichen und zu eliminieren, während gleichzeitig die Verfügbarkeit von freiem HPSE in der TME begrenzt wird. Dieser Ansatz eröffnet neue Möglichkeiten zur Verbesserung adoptiver Immuntherapien mit NK-Zellen.

Acknowledgments

First, I would like to thank my supervisor, Dr. Angel Cid-Arregui, for giving me the opportunity to conduct my PhD studies at his lab at DKFZ and for all his scientific supervision that contributed so much for the conclusion of my PhD.

I would like to thank our collaborators in Israel, Dr. Israel Vlodavsky, Dr. Neta Ilan and all the lab members for all the help throughout the years. A special thanks for the amazing reception during my stay in Haifa. Soaad, Maram, Malik and Yasmin, I am so grateful for the opportunity to meet you and call you, my friends. Thank you for making me feel at home in Haifa and making that stay one of the best experiences of my life. I will cherish those moments.

I would like to thank my Thesis Advisory Committee (TAC) members Prof. Dr. Martin Müller, Prof. Dr. Ilse Hofmann and Dr. Anne Régnier-Vigouroux for their scientific advice and support during the TAC meetings. Additionally, I would like to thank to Prof. Dr. Ana Martin-Villalba and Prof. Dr. Nina Papavasiliou for joining my examination committee.

A big thanks goes to the current and past members of the Tarteged Tumor Vaccines lab (D122). I am especially thankful for all the help, support and guidance from Isaac Quiros-Fernandez. Also I would like to thank Elisa for all the technical help. Moreover, I would like to thank the DKFZ core facilities, including the Light Microscopy facility and the FACS core facility.

To the master's crew (and new additions) and to Marta and Rui from the camp family, thank you for the support from far away, for visiting, for welcoming me back whenever I went home and for sticking around.

I can't thank enough to the friends that I meet through the DKFZ. Carolina, Caterina, Laura, Sarah and Stefan, thank you from the bottom of my heart for all the support, the advice, the adventures, the fun, for everything. I also would like to thank Ricca for the support.

Furthermore, I would like to thank the Portuguese friends in Heidelberg, Filipa, Márcia, Rita Mariana, Sílvia and Nuno for all the support and fun times. You make Portugal feel much closer. A special thanks to Márcia and Filipa. Márcia, thank you for being my everyday support for the majority of the PhD. Thank you for all our talks, breaks and lunches, for the scientific discussions, for believing in me, for pushing me forward. Filipa, amiga, thank you for just being you, for the constant support, for all the games that we watched together (O Sporting é o nosso grande amor), for pushing me out of my comfort zone, for the patience. I am very proud of you and of our friendship.

Acknowledgments

To my therapist, thank you so much for guiding me through this journey of mental health.

I do not have words to thank by best friend, but I will try. Bea, taking you for always being there for me, for saving me from myself sometimes and for making me believe that I could finish this chapter. You are my chosen family. Até velhinhas!

Lastly, a huge thank you to my family, for always being a safe space to return to and where I am the happiest. The most important thank you goes to my mother. Thank you for believing in me, for all the support, for all the packages throughout the years, for the unconditional love. I would not be here without you.

Table of Contents

List of Figures

List of Tables

List of supplementary figures

List of abbreviations

°C	Degrees Celsius
2Ab	Secondary antibody
3D	Three-dimensional
4-1BB	Tumor necrosis factor ligand superfamily member 9
ACK	Ammonium chloride potassium
ACT	Adoptive cell therapy
ADCC	Antibody-dependent cell cytotoxicity
AF488	Alexa Fluor® 488
AF647	Alexa Fluor® 647
AMP	Ampicillin
BM	Bone marrow
CAR	Chimeric antigen receptor
CCL	C-C Motif Chemokine Ligand
CD	Cluster of differentiation
cDNA	Complementary DNA
CLP	Common lymphoid progenitors
CTLA-4	C-C motif chemokine ligand 4
CXCR	C-X-C chemokine receptor
DAPI	4′,6-diamidino-2-phenylindole
DKFZ	German Cancer Research Center
DMEM	Dulbecco’s Modified Eagle Medium
DMSO	Di-methyl sulfoxide
DNA	Deoxyribonucleic acid
ECM	Extracellular matrix
EDTA	Ethylenediaminetetraacetic acid
EGF	Epidermal growth factor

List of abbreviations

EGFR	EGF receptor
FACS	Fluorescence-activated cell sorting
FBS	Fetal bovine serum
FC	Flow Cytometry
FDA	Food and Drug Administration
FGF	Fibroblast growth factor
FGFR	FGF receptor
Fig.	Figure
GFP	Green fluorescence protein
GM-CSF	Granulocyte macrophage-colony stimulating factor
GS3	Constitutive active form of HPSE
GS3^{TM}	Cell membrane bound GS3
h	Hour(s)
HLA	Human leukocyte antigen
HNSCC	Human head and neck squamous cell carcinoma
HPSE	Heparanase
HS	Heparan sulfate
HSPGs	Heparan sulfate proteoglycans
IFNg	Interferon gamma
IL	Interleukin
ILC	Innate lymphoid cell(s)
ILCP	ILC lineage precursor
ITAMs	Immunoreceptor tyrosine-based activation motifs
ITIMs	Immunoreceptor tyrosine-based inhibition motifs
kDa	Kilodalton
KIR	Killer cell immunoglobulin-like receptor
KO	Knockout
LPS	Lipopolysaccharide
MCP-1	Monocyte chemoattractant protein-1

MFI	Median fluorescence intensity
MHC	Major histocompatibility complex
min	Minute(s)
MIP-1	Macrophage inflammatory protein-1
mL	Milliliter
mWas	mWasabi green fluorescence protein
NCR	Natural cytotoxicity receptor(s)
NK	Natural killer
NKG2	Natural killer group 2
NOD	Non-obese diabetic
ON	Overnight
P/S	Penicillin/Streptomycin
PBMCs	Peripheral blood mononuclear cells
PBS	Phosphate Buffered Saline
PD-1	Programmed cell death protein 1
PFA	Paraformaldehyde
PI	Propidium Iodide
PSMA	Prostate specific membrane antigen
RNA	Ribonucleic acid
RT	Room Temperature
RT-qPCR	Real Time quantitative polymerase chain reaction
s	Second(s)
SCID	Severe combined immunodeficiency disease
SD	Standard deviation
TCR	T cell receptor
TCR-T	TCR-transgenic T (cell)
TEM8	Tumor endothelial marker 8
TM	Transmembrane domain

List of abbreviations

TME	Tumor microenvironment
TRAIL	Tumor necrosis factor-related apoptosis-inducing ligand
VEGF	Vascular endothelial growth factor
VEGFR	VEGF receptor
WT	Wildtype
µL	Microliter

1 Introduction

The understating of cancer biology has been changing dramatically over the past decades. Solid cancers are now seen as complex ecosystems comprising of tumor cells and multiple non-cancerous cells, such as immune cells, cancer-associated fibroblasts, endothelial cells, and others, all embedded in protective extracellular matrix (ECM) [1]. The perspective that the ECM and non-cancerous cells are bystanders of tumorigenesis have been revoked, as the tumor microenvironment (TME) is seen as having key roles in the pathogenesis and progression of cancer [2].

Current cancer treatments include the conventional strategies, such as surgery, radiotherapy, chemotherapy, and the modern approaches, such as targeted therapies and immunotherapies [3]. The conventional treatments were the only option for many years, and while they can induce positive patient outcome in early-stage tumors, late-stage cancers are strongly associated with high mortally rates. Moreover, conventional strategies have several shortcomings, such as off-target effects, toxic side effects to non-cancerous tissue that leads to extensive damage, drug resistance, physique and psychological burden on patients, incomplete surgical resection and, cancer recurrence [3]. Given the need to overcome the limitations of the conventional therapies, associated with the known critical roles of the TME in the tumor context, the development of strategies to target the TME, such as immunotherapy, have been expanded in recent years.

1.1 Cancer Immunotherapies

Immunotherapies are biological therapies that aim to help the immune system to fight cancer [4]. These therapies intended to stimulate the host's anti-tumor responses and inducing a pro-tumor killing TME, by increasing the number of effector cells, by increasing the production of anti-tumorigenic soluble mediators, by decreasing the immune suppressor mechanisms, and by modulating immune checkpoints [4]. Currently, the main immunotherapy strategies are immune checkpoint inhibitors, adoptive cell transfer, cytokine therapy, and cancer vaccines [4]. Adoptive cell transfer is the strategy of particular interest for this thesis.

1.2 Adoptive cell therapy

The development of protocols to isolate and expand *in vitro* immune cells, particularly T cells, propelled the use of adoptive cell therapy (ACT). ACT comprises the *ex vivo* expansion and activation of patient immune cells, which are then reinfused into the patient to enhance its anti-tumor immune response [5].

Focusing on T cells, ACT can be carried out using three different approaches [6]. As a first approach, tumor-infiltrating lymphocytes are expanded *ex vivo* and then are infused back into the patient. However, for this strategy to elicit durable responses, it is essential that effector T cells with antitumor activity are already present within the tumor mass [6]. This is not the case for many solid tumors, which decreases significantly the efficacy of this treatment. The second approach is the use of patient cells that have been genetically engineered to express a T cell receptor (TCR) reactive to a tumor antigen epitope, presented on human leukocyte antigen (HLA) class I molecules. Thus, this strategy is limited to antigens expressed by the major histocompatibility complex (MHC) [6]. The efficacy of TCR-T therapies against tumor antigens have been assessed in several clinical trials, with low rates of success so far. This was partially attributed to the high variability of these target proteins within the tumors [7]. As a third approach and as an alternative to TCR-derived therapies, are chimeric antigen receptor (CAR) T cells [8]. These cells are genetically modified T cells designed to express a synthetic receptor with tumor antigen specificity, replicating TCR-mediated functions. This design allows the receptor to recognize target antigens with high specificity, enabling immune cells to mount a targeted anti-tumor response like that of natural T-cell receptors. CARs are comprised of an extracellular recognition domain, derived from an antibody that recognizes the tumor antigen, a hinge region, a transmembrane domain, and a cytoplasmic costimulatory domain, which drives the signal activation and amplification of CAR-T cells [8].

Adoptive cell therapies have shown remarkable clinical responses in B cell malignancies, with six CAR T-cell therapies being approved by the FDA for blood cancers [9-14]. In contrast, only very recently the first ACT therapy targeting a solid tumor antigen was approved for clinical trial [15]. In contrast to hematological cancers, solid tumors are much more complex tissues structures, which increases the difficulty of treatment.

Natural killer (NK) cells are now seen as valid alternative for immune therapies like ACT. In both clinical settings and in mouse models, studies have shown that lower percentages of NK cells, and NK cells with impaired functionality are associated with increased rates of cancer

development [16]. Conversely, a positive correlation was found between high NK cell infiltration within tumors and improved clinical outcomes [17]. NK cells are particularly effective in targeting minimal residual disease, metastasis, and hematologic malignancies. Moreover, these cells have a robust cytotoxic activity against tumor cells, do not require antigen processing and presentation to recognize their target cells and do not induce graft-versus-host disease [16].

For the success of NK or T cell therapies is necessary to overcome the main challenges for solid tumors therapies, which are the immunosuppressive TME, low infiltration of immune cells into the tumors, and the lack of targets [18].

1.2.1 Natural killer cells

1.2.1.1 NK development and subsets

NK cells are innate lymphoid cells (ILC). These cells comprised approximately 5 % of all leukocytes in human peripheral blood and 2–5% in the spleens and BM of inbred laboratory mice [19].

NK cells originate in the bone marrow (BM), from common lymphoid progenitors (CLP) that derive from $CD34^+$ hematopoietic stem cells [20]. These multipotent CLP further differentiate into a more restricted NK/ILC lineage precursor (ILCP). ILCP can be detected in circulation, which suggests that this precursor is capable of seeding in peripheral tissues and continuing the differentiation process there [20]. The last stage of differentiation is the commitment of the ILCP to the conventional NK cell lineage, which is thought to occur by the acquisition of NKp80 [20]. In mice, NK cells develop and mature in the BM [21].

Human NK cells consist of two main subsets: $CD56^{bight}$ NK cells and $CD56^{dim}$ NK cells [20, 22]. The precise mechanism of differentiation of these two subsets it not fully understood yet. The immature or regulatory $CD56^{bright}$ subset of NK cells is mostly found in secondary lymphoid organs. $CD56^{bright}$ cells have a predominantly immunomodulatory role, due to their high capacity to secrete cytokines and chemokines upon monokine activation, promoting the recruitment and modulation of immune cells [20, 22]. This NK cell subset presents low levels of perforin and granzyme secretion. The mature or cytotoxic $CD56^{dim}$ subset accounts for approximately 90 % of peripheral blood NK cells of a healthy adult. These cells present high capacity of target cell-induced cytotoxicity and cytokine production [20, 22]. Also, $CD56^{dim}$ NK

cells express the CD16 receptor, which allows them to mediate antibody-dependent cell cytotoxicity (ADCC). Upon cytokine activation, $CD56^{dim}$ NK cells are less efficient effectors, when compared to the $CD56^{bright}$ NK cells. Both subsets induce apoptosis by expressing cell death ligands such as FasL and TRAIL [20, 22].

In mice, NK cell maturation occurs by loss and gain of CD11b and CD27 expression on the cell surface [21]. Immature mouse NK cells are $CD11b^{-}CD27^{-}$ cells. Mature NK cells start expressing both proteins on the cell surface ($CD11b^{+}CD27^{+}$) and present enhanced cytotoxic capabilities and increased cytokine production. In the final maturation stage, NK cells lose the expression of CD27. The terminally mature $CD11b^{+}CD27^{-}$ NK cells have heightened cytotoxic potential but reduced cytokine secretion [21].

1.2.1.2 NK activation

NK cells are a first line of defense against multiple pathogens, viral infections, and malignant cells lacking expression of self-MHC class I [23]. These cells are capable of spontaneous or ‘natural’ cytotoxicity without the need of prior sensitization. NK cell activation is tightly regulated through a balance of signals from activating and inhibitory receptors. Activating receptors detect stress-induced ligands, expressed by virally infected of transformed cells. This allows NK cells to recognize and target potentially dangerous cells. In contrast, inhibitory receptors primarily bind self-MHC class I molecules, enabling NK cells to distinguish healthy cells from foreign or abnormal ones by sensing the absence or alteration of self-MHC-I. The input of both activating and inhibitory receptors will determine whether NK cells get activated or not, as well as the type of effector response in case of activation. This is also influenced by cytokines, chemokines, and interactions with other immune cells in the local microenvironment. In homeostasis, unnecessary NK cell activation is prevented by interaction of inhibitory receptors and self-MHC-I on normal cells (Fig. 1) [23].

To evade detection by $CD8^{+}$ T cells, tumor cells downregulate MHC-I expression, becoming then more susceptible to NK cell-mediated killing in a phenomenon known as "missing-self" recognition (Fig. 1) [24]. However, MHC-I downregulation is not sufficient to fully activate NK cells. Full activation requires the co-expression of NK receptor ligands by tumors cells (Fig. 1). Full NK activation also requires ligand-activating receptor synapse, which also helps to explain how NK cells bypass inhibitory signals if MHC-I is retained by cells, avoiding the attack on healthy cells that naturally express low or absent MHC-I such as erythrocytes or neurons [24].

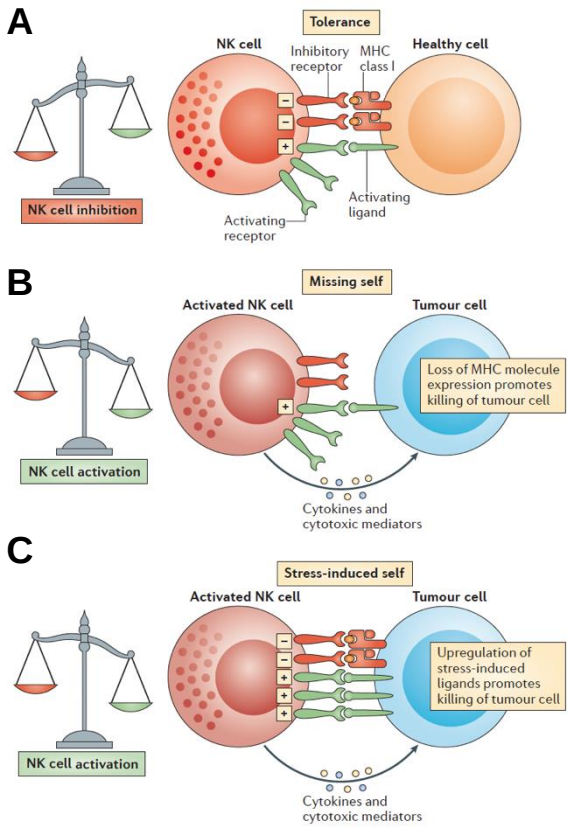

Figure 1 - NK cell tolerance or activation mechanisms.

(A) NK cells tolerance against healthy host cells duo to the presence of MHC I molecules and inhibitory receptor signaling overcoming activating receptor signaling. **(B)** The absence of MHC I molecules triggers activation receptors signaling in NK cell. This is known as the 'missing-self' activation trigger of NK cells**. (C)** Activation of NK cells by stress-induced ligands expressed by tumors cells, which overcomes inhibitory receptor signaling. Figure Adapted from Vivier et al. (2023)

1.2.1.3 NK Receptors

In contrast to B or T cells, NK cells exhibit a broad repertoire of germline encoded activating and inhibitory receptors (Fig. 2). The stimulation of either activation or inhibitory receptors by specific ligands leads to phosphorylation of immunoreceptor tyrosine-based activation motifs (ITAMs) and immunoreceptor tyrosine-based inhibition motifs (ITIMs), respectively, initiating downstream signaling cascades. In the case of activating signals, kinases such as Syk and ZAP70 are recruited, and DAP adapter molecules like DAP10 or DAP12 are engaged, leading to upregulation of genes associated with cytokine production and cytotoxicity [25]. If an

inhibitory receptor binds to an MHC class I molecule, the ITIMs become phosphorylated, subsequently blocking downstream activation pathways, and preventing NK cell activation [25].

NK cells express natural cytotoxicity receptors (NCR), namely NKp46 (NCR1; CD335) NKp44 (NCR2; CD336) and NKp30 (NCR3; CD337) [26]. NKp46 is the only NCR expressed by human and mouse NK cells. These receptors are non-MHC restricted and bind host-/pathogen-encoded ligands. Interestingly, heparan sulfate (HS) can also bind as a co-ligand to these NCR and promote tumor cell lysis [26]. The class of natural killer group 2 (NKG2) receptors are C-type lectin receptors and include both activating and inhibitory receptors [27]. NKG2D is a key activating receptor and detects stress-induced MHC class I homologue ligands, such as MIC-A and MIC-B, which are upregulated in viral or transformed cells. NKG2A is an inhibitory receptor, expressed as heterodimer with CD94, and binds to non-classical MHC-I ligand HLA-E, thus protecting self-MHC class I-expressing cells from NK cell-mediated cytotoxicity [27].

The killer cell immunoglobulin-like receptor (KIR) family comprises a group of receptors which recognize HLA-A, -B, and -C alleles [28]. KIRs are not present in mouse NK cells. Binding of inhibitory KIRs to their ligands promotes the suppression of NK effector functions. In contrast, activating KIRs bind to MHC class I or related ligands and signal NK cells to initiate cytotoxic activity and cytokine production. This family of receptors is important in the process of NK cell licensing and in building NK cell tolerance to self.

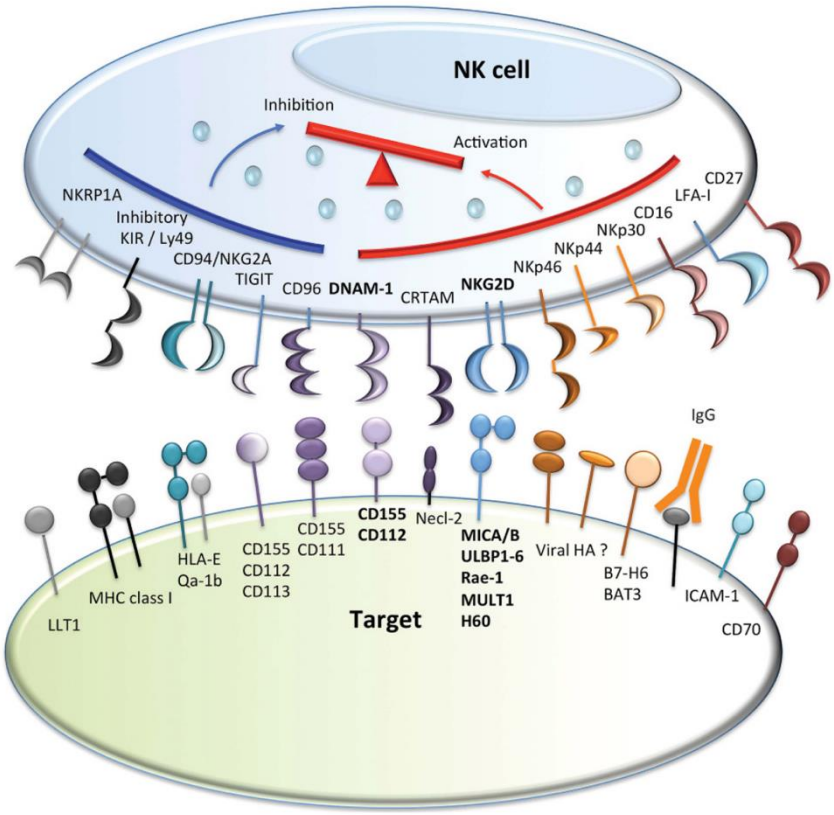

Figure 2 - NK cells activating and inhibitory receptors and their receptive ligands.

Figure adapted from Chan CJ (2014)

1.2.1.4 NK cell effector functions

NK cells mediate their effector functions via activation of death receptors on target cells or the secretion of perforins and granzymes [29]. Upon recognition of unhealthy cells, NK cells produce death ligands such as FasL, TFN and TRAIL, which will interact with death receptors on target cells and induce the formation of the death-inducing signaling complex. This complex recruit and activates caspases, initiating the enzymatic caspase cascade and promoting target cell apoptosis. NK cells are also able to kill target cells through the release of lytic granules. Upon target cell recognition, an immunological synapse is formed between NK and target cell, prompting exocytosis of cytotoxic granules, containing pre-formed perforin and granzyme [29, 30]. Perforin molecules disrupt the target cell membrane integrity by forming pore-like structures. This action also facilitates the entry of granzymes into the cytoplasm. The serine proteases granzyme A and B subsequently induce apoptosis either by activating the enzymatic

caspase cascade or through mitochondrial depolarization and DNA fragmentation mediated by proteolytic cleavage. NK cells can also recognize and lyse antibody coated cells through the ADCC process [29, 31]. B cells coat tumor target cells with IgG and NK cell CD16 receptor recognizes the Fc portion of the IgG molecules, triggering a strong cytotoxic response [29, 31]. This NK cell activation through the CD16 receptor is an exception and does not require additional co-activation [29, 31].

NK cells are also important producers of cytokines that can induce cell lysis or recruit and activate other immune cells to the TME, such as, interferon gamma (IFNg), macrophage inflammatory protein-1 alpha (MIP-1α), Interleukin (IL)-10, IL-13, granulocyte-macrophage colony-stimulating factor (GM-CSF), and monocyte chemoattractant protein-1 (MCP-1) [29].

1.3 The tumor extracellular matrix

The ECM is a major component of the TME from a structural and functional point of view [32]. The ECM composition and stiffness have major influence in cancer development and progression. It is involved in tumor metastasis, angiogenesis, and proliferation, and also regulates the immunosuppressive TME and resistance against therapeutics [32]. The complex and dynamic three-dimensional (3D) network of ECM proteins includes collagens, hyaluronic acid, proteoglycans, glycosaminoglycans, elastin, fibronectin, and laminins [33]. Heparan sulfate proteoglycans (HSPGs) are of particular interest in this thesis since HS side chains are the substrate of Heparanase (HPSE).

1.3.1 Heparan Sulfate Proteoglycans

HSPGs are composed of a protein core covalently linked to one or more HS glycosaminoglycan chains [34, 35]. These polysaccharide side chains have varying levels of sulfation, which is why they are referred to as heparan sulfate chains. They are widely present in mammalian cells and are found on the cell surface (syndecans and glypicans), within the ECM (perlecan, agrin, and type XVIII collagen), and in secretory vesicles (serglycin) [34].

The majority of HSPGs roles are mediated by their HS side chains, through binding of growth factors, of receptors, and of morphogens [34, 36]. These interactions modulate cell signalling, protect ligands from proteolysis, regulate receptor-ligand signaling complexes and modulate

receptor activities. Also, the binding of proteases and protease inhibitors to HS side chains regulates their spatial distribution and activity. Membrane-bound HSPGs cooperate with other matrix proteins (eg. Integrin) and with soluble ligands to influence cell-cell, cell-pathogen, and cell-matrix interactions, cell migration, consequently contributing to the ECM structure [34]. Moreover, HSPGs function as co-receptors for several tyrosine kinase growth factor receptors, lowering their activation threshold. HSPGs are also important in maintaining the integrity of blood vessels barriers [34].

In the context of tumors, dysregulation and overexpression of these proteins play important roles in all major stages of tumor progression [37, 38]. Tumor growth, proliferation and angiogenesis are sustained and regulated by degradation of the HS chains and shedding of the core protein and consequent release of bound factors. HPSGs are also important in the process of tumor invasion and metastasis since they modulate ECM constitution and stiffness, facilitating cancer cell migration [37, 38]. Moreover, immune responses against cancer cells are also regulated by the pro-tumorigenic changes in the ECM and consequently in the TME, with HSPGs interfering in immune cell and tumor cell interactions and regulating immune evasion of cancer cells [37, 38]. While the cleavage of the HSPGs protein core can be performed by several types of proteases, there is only one known enzyme that can directly cleave the HS side chains. This enzyme is Heparanase.

1.4 Heparanase

HPSE is an endo-acting glycoside hydrolase, which cleaves the long HS side chains of proteoglycans, releasing HS fragments of 5-7 kDa in size as well as the factors bound to these fragments. The HPSE gene in humans and in *Mus musculus* is highly conserved, with their respective amino acid sequences sharing 77% of identity [39, 40]. HPSE is initially synthesized as a single chain preproenzyme of 65 kDa, which is processed into an inactive pro-form upon removal of the signal peptide by a signal peptidase (Fig. 3) [40-42]. The pro-HPSE is then secreted from the cell and binds to the membrane bound HSPGs, such as syndecan 1. Upon binding, the (pro-HPSE)-HSPG complex undergoes rapid endocytosis into early endosomes and is subsequently trafficked to late endosomes and lysosomes for processing [41]. There, the 6 kDa linker peptide is excised by cathepsin L to yield a 50 kDa subunit and an 8 kDa subunit (Fig. 3) [43]. These two subunits from the mature HPSE as a non-covalent heterodimer [44]. Active HPSE is then either secreted from the cell or transported to the nucleus [41].

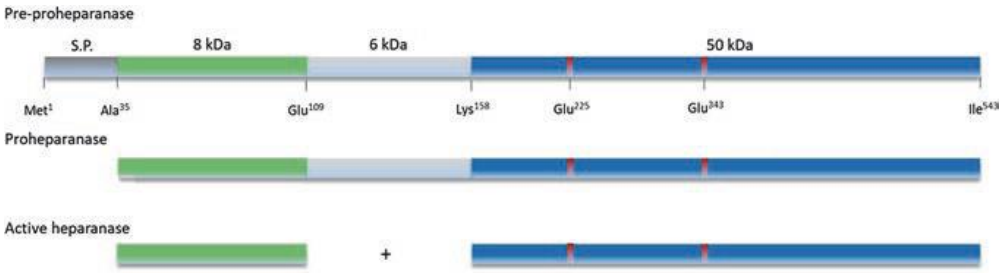

Figure 3 - Schematic representation of the processing of the 65 kDa pre-proHPSE into the active HPSE form.

Figure adapted from Gaskin, S.M. (2020)

The physiological expression of HPSE was first described in the placenta and lymphoid organs [45]. High expression was then reported in immune cells, esophagus, and lung, among others. In normal cells and tissues, the HPSE promoter is mainly silenced by methylation and negatively regulated by p53 [46]. Thus, the physiological expression and activity of this enzyme is tightly regulated to maintain tissue integrity [45]. HPSE has several physiological functions, including extracellular matrix remodeling, release of HS-bound growth factors, immune response modulation, inflammation regulation and vascularization. Consequently, HPSE is involved in wound healing, tissue repair, cell migration and extravasation, cell adhesion, cell, signaling and gene regulation. Given the abundance of HPSE expression in tumor cells, it appears that these physiological functions are required and 'hijacked' by tumor cells [45].

1.4.1 Heparanase in cancer

Expression of HPSE is dysregulated in many diseases' settings, such as atherosclerosis, diabetes and diabetic nephropathy, autoimmune and chronic inflammatory diseases, like rheumatoid arthritis and inflammatory bowel disease and cancer [47-51]. Furthermore, overexpression of HPSE has been reported in almost all cancer types. Moreover, the upregulation of this enzyme by tumor cells is correlated with enhanced tumor size, angiogenesis, enhanced metastasis and with poor patient survival [52-54].

The poorly vascularized hypoxic core of tumors provides a good environment for HS degradation by HPSE, since this enzyme maximal endoglycosidase activity is between pH 5.0 and 6.0. HPSE catalytic activity on HS side chains of HPSGs in the ECM and the basement

membrane is the key to support tumor progression [55]. By breaking down physical barriers that normally restrain tumors cells and remodeling and disrupting the ECM, HPSE activity helps cancer cells to invade neighboring tissues more easily. It also enhances tumor cells motility and capacity to enter the bloodstream and lymphatic vessels, promoting the formation of metastasis [55].

HS cleavage by HPSE not only changes the ECM physically but also liberates the HS-bound growth factors and signaling molecules, such as fibroblast growth factor (FGF), epidermal growth factor (EGF), vascular endothelial growth factor (VEGF), among others, that are stored in the ECM (Fig. 4) [56]. These HPSE regulated growth factors can also upregulate HPSE expression, maintaining a positive feedback loop for both the expression of HPSE and the regulation of these molecules. The release of active HS-bound FGF promotes the formation of HS-FGF-FGFR complexes that facilitate the dimerization of the FGF receptor and activation of downstream signaling pathways (excessive cell proliferation; inhibition of apoptosis and cellular senescence; epithelial-mesenchymal transition) [55]. EGF receptor (EGFR) is commonly overexpressed or mutated in many cancers. Syndecan cleavage by HPSE activates EGFR signaling, promoting uncontrolled cell growth, enhanced metastatic capacity and chemotherapy resistance (Fig. 4). Moreover, VEGF is an important HS-binding protein and one of the primary drivers of angiogenesis, the process by which, new blood vessels and form from pre-existing ones. By activating VEGF and FGF signaling pathways, HPSE promotes tumor angiogenesis, with numeral studies demonstrating the key role of this enzyme in promoting this hallmark of cancer progression (Fig. 4) [55].

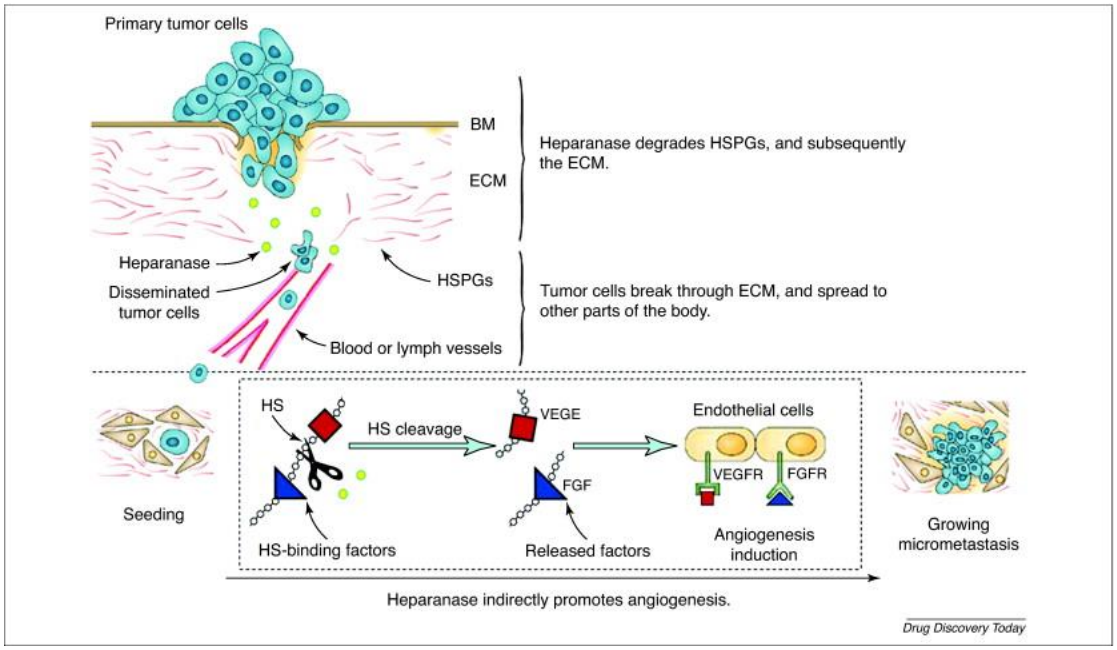

Figure 4 - Tumor cells derived HPSE promotes tumor progression.

Figure adapted from Zhang, Y. F. (2011)

Tumor cells derived HPSE also has non-enzymatic roles in cell signaling and in regulation of gene expression during cancer progression. A protein domain localized at the HPSE C-terminus has signaling capacities, independent of the enzymatic activity. Through this signaling, HPSE, is involved in regulation of cellular proliferation, evading apoptosis, chemo resistance, among others [57]. The ability of HPSE to activate the PI3K/AKT pathway, known to be dysregulated in almost all human cancer [58], promotes the bypassing of PTEN signaling and thus circumvent tumor-suppressive pathways and promote oncogenic signaling [59]. Moreover, HPSE can be passively transported to the nucleus and affect gene expression by direct interactions with chromatin and transcriptional machinery [60].

Tumor cells-derived HPSE also modulates immune cell infiltration into tumors, by realizing HS-bound cytokines, chemokines and other molecules that attract immune cells and thereby creating a chronic inflammation that supports the tumor development. This fosters immune evasion, as immune cells as reprogrammed by tumor cells to support, rather than target the tumor [55].

1.4.2 Heparanase in immune cells

In contrast to the well-studied role of HPSE in cancer cells, the contribution of HPSE produced by cells within the TME has been given far less attention [61]. HPSE expression has been described in most immune cell populations. This expression can be induced by multiple stimuli and is associated with promoting cell rolling and adhesion, cell activation and most important in the context of this work, leukocyte migration and infiltration through inflamed and tumor tissues [61].

HPSE expression plays an important role in dendritic cell migration through the ECM [62], in macrophage activation and infiltration [63] and T cells activation and infiltration [64, 65]. Despite being very important in disease context and specifically in tumor immunity, NK cells are the populations in which the role of HPSE in NK cells is less understood. Only one study reported that the cytotoxicity and activation are impaired in $HPSE^{-/-}$ NK cells, in response to poly (I:C) [66]. Further studies are necessary to understand the roles of HPSE in NK cells, specifically about HPSE contribution in NK cells migration and infiltration capacities.

2 Aims

The successful capacity of immune cells to infiltrate and degrade the dense layers of extracellular matrix that encapsulate solid tumors is essential for them to access tumor cells and exert antitumor roles. Adoptive cell therapy have had, so far, less striking therapeutic results in solid tumors than in lymphoid malignancies. Enhancing the infiltration capacity of immune cells could improve the therapeutic efficacy of adoptive cell therapy in these tumors.

The main aim of my thesis is to validate a new strategy to improve NK cell infiltration into solid tumors. To achieve this, a derivative of the NK-92 cell line, that constitutively expresses human CD3 and CD8 (NK-92$^{CD3/CD8}$), will be modified genetically to express an active form of Heparanase (GS3) on the cell surface as an integral membrane protein (GS3^{TM}).

Moreover, I aim to provide new insights into HPSE in NK cell activation and infiltration capacity. To this end, measurements of HPSE expression will be performed in primary human NK cells upon different activation stimuli, and cell infiltration will be studied in tumor spheroids, using NK cells isolated from HPSE-KO mice.

3 Materials and Methods

3.1 Materials

3.1.1 Cell lines

The cell lines used in this thesis are listed below in table 1.

Materials Table 1 - Cell lines

Name	Description	Source
FaDu	Human adherent cell line; Head and Neck squamous cell carcinoma (HNSCC); HPV-16-; HLA-A2-	Vlodavsky Lab[1]
FaDu/mWasabi	Human adherent cell line; Head and Neck squamous cell carcinoma expressing mWasabi (mWas) green fluorescence protein; HPV-16-; HLA-A2-	DKFZ
NK-92$^{CD3/CD8}$	Human suspension cell line, non-Hodgkin's lymphoma cell line expressing human CD3 and CD8	DKFZ
NK-92$^{CD3/CD8}$ /GS3-mWasabi	Human suspension cell line, non-Hodgkin's lymphoma cell line expressing human CD3 and CD8 and the GS3 on the cell surface as an integral membrane protein linked to mWas	DKFZ
NK-92$^{CD3/CD8}$ /GS3^{TM}	Human suspension cell line, non-Hodgkin's lymphoma cell line expressing human CD3 and CD8 and the GS3 on the cell surface as an integral membrane protein	DKFZ
PCI-13	Human adherent cell line; Head&Neck squamous cell carcinoma; HPV-16-; HLA-A2+	DKFZ
T2	Human lymphoblastic suspension cell line	DKFZ
TC-1	Mouse adherent cell line; Lung carcinoma	Vlodavsky Lab[1]

UPCI-SCC-154	Human adherent cell line; Head and Neck squamous cell carcinoma; HPV-16+; HLA-A2+	DKFZ
UPCI-SCC-154 /mWasabi	Human adherent cell line; Head and Neck squamous cell carcinoma expressing mWasabi green fluorescence protein; HPV-16+; HLA-A2+	DKFZ

Note: [1] - Technion Integrated Cancer Center (TICC), Rappaport Faculty of Medicine, Technion, Haifa

3.1.2 Antibodies

Antibodies used for intracellular and extracellular Flow cytometry (FC) staining of different markers are listed in table 2. Table 3 lists the antibodies used for immunofluorescence protocols.

Materials Table 2 - FC antibodies

Marker	Fluorochrome	Clone	Dilution	Supplier
Anti-myc tag	Alexa Fluor® 647	9E10	1/50	Biolegend
B7-H6	-	#875001	1/50	R&D Systems
CD107a	PE-Cy7	H4A3	1/200	Biolegend
CD137/4-1BB	PE-Cy7	4B4-1	3/100	Biolegend
CD152/CTLA-4	APC	BNI3	3/100	Biolegend
CD178/FAS-L	PE	NOK-1	3/100	Biolegend
CD25	APC-Cy7	BC96	1/50	Biolegend
CD253/TRAIL	APC	RIK-2	1/25	Biolegend
CD28	FITC	CD28.2	1/200	Biolegend
CD314/NKG2D	PE	1D11	1/25	Biolegend

CD335/NKp46	APC	9E2	1/25	Biolegend
CD336/NKp44	APC	P44-8	1/25	Biolegend
CD337/NKp30	APC	P30-15	1/25	Biolegend
CD69	PE	FN50	1/50	Biolegend
CD80	FITC	2D10	1/200	Biolegend
CD86	APC	BU639	3/100	Biolegend
CXCR2	PE	5E8/CXCR2	1/12	Biolegend
CXCR3	FITC	G025H7	3/100	Biolegend
goat anti-rabbit	Alexa Fluor® 647 (AF647)	Polyclonal	1/250	Abcam
Hpa 733	-	-	1/50	Vlodavsky Lab[1]
KIR2DL4	PE	mAb 33(33)	1/200	Biolegend
Live/Dead	ZombieViolet	-	1/300	Biolegend
Live/Dead	ZombieAqua	-	1/500	Biolegend
MICA	-	#159227	1/50	R&D Systems
MICB	-	#236511	1/50	R&D Systems
mouse IgG1	Alexa Fluor® 488	Polyclonal	1/250	SigmaAldrich
mouse IgG1	FITC	MOPC-21	variable	Biolegend
mouse IgG1	PE	MOPC-21	variable	Biolegend
mouse IgG1	PE.Cy7	MOPC-21	variable	Biolegend
mouse IgG1	APC	MOPC-21	variable	Biolegend
mouse IgG1	APC-Cy7	MOPC-21	variable	Biolegend
N-CAM1/CD56	PE	5.1H11	1/50	Biolegend

N-CAM1/CD56	FITC	HCD56	1/25	Biolegend
NKG2A	PE	S19004C	1/25	Biolegend
PD-1	Alexa Fluor® 488 (AF488)	EH12.2H7	1/200	Biolegend
TIGIT	PE	A15153G	1/100	Biolegend
ULBP-1	-	#170818	1/50	R&D Systems
ULBP-2	-	#165903	1/50	R&D Systems
ULBP-3	-	#166510	1/50	R&D Systems

Note: [1] - Technion Integrated Cancer Center (TICC), Rappaport Faculty of Medicine, Technion, Haifa

Material Table 3 - Immunofluorescence antibodies

Marker	Fluorochrome	Clone	Dilution	Supplier
N-CAM1/CD56	-	CMSSB	1/400	ThermoFisher Sicentific
goat anti-mouse	Cy3	Poly4053	1/500	Biolegend

3.1.3 Primers

Materials Table 4 - Primers used for RT-qPCR

Gene	Reactivity	Primer	Sequence
CCL1	Human	Forward	CTCATTTGCGGAGCAAGAGAT
CCL1	Human	Reverse	GCCTCTGAACCCATCCAACTG
CD56	Human	Forward	AGGATGGCAGTGAGTCAGAG
CD56	Human	Reverse	TCACACACAATCACGGCATC
GAPDH	Human	Forward	GGAGCGAGATCCCTCCAAAAT
GAPDH	Human	Reverse	GGCTGTTGTCATACTTCTCATGG

GM-CSF	Human	Forward	TCCTGAACCTGAGTAGAGACAC
GM-CSF	Human	Reverse	TGCTGCTTGTAGTGGCTGG
IFNg	Human	Forward	TCGGTAACTGACTTGAATGTCCA
IFNg	Human	Reverse	TCGGTAACTGACTTGAATGTCCA
IL-2	Human	Forward	AACTCCTGTCTTGCATTGCAC
IL-2	Human	Reverse	GCTCCAGTTGTAGCTGTGTTT

3.1.4 Plasmids

Materials Table 5 - Plasmid used and developed for this thesis

Plasmid	Manufacturer	Identifier
pCMV-SB100X	Addgene	34879
pHIV-EGFP	Addgene	21373
pHIV-GS3-CD28TM-mWasabi	I. Quiros-Fernandez/A. Cid-Arregui	N/A
pSBbi-pur	Addgene	60523
pSBbi-pur-GS3-CD28TM-mWasabi	S. Libório-Ramos/ I. Quiros-Fernandez/A. Cid-Arregui	N/A
pSBbi-pur-mWasabi	I. Quiros-Fernandez/A. Cid-Arregui	N/A
pSBbi-pur-myc-GS3-CD28TM	I. Quiros-Fernandez/A. Cid-Arregui	N/A

3.1.5 Chemicals, supplements and reagents

Materials Table 6 - List of Chemicals, Supplements and Reagents

Name	Purpose	Supplier	Reference
10X Buffer Tango	DNA cloning	ThermoFisher Scientific, Waltham	BY5
4',6-diamidino-2-phenylindole (DAPI)	Miscellaneous	ThermoFisher Scientific, Waltham	D3571
Agarose	DNA purification	Carl Roth, Karlsruhe	3810.3
Ampicilin (AMP)	Bacteria culture	Sigma-Aldrich, Steinheim	A5354
BcuI (Spe I) 10 U/µL	DNA cloning	ThermoFisher Scientific, Waltham	ER1251
Biofloat™ Flex coating solution	Cell culture	faCellitate, Mannheim Germany	F202005
Bsu15I (Cla I) 10 U/µL	DNA cloning	ThermoFisher Scientific, Waltham	ER0145
Buffer G 10X	DNA cloning	ThermoFisher Scientific, Waltham	BG5
CCL19	Cell culture	In house	-
Di-methyl sulfoxide (DMSO)	Cell culture	Sigma-Aldrich, Steinheim	67-68-5
Dulbecco's Modified Eagle's Medium (DMEM) + GlutaMAX™-I	Cell culture	Gibco, ThermoFisher Scientific, Waltham	21885-025

Dulbecco's Phosphate Buffered Saline (PBS)	Miscellaneous	Gibco, ThermoFisher Sicentific, Waltham	14190-094
Fetal Bovine Serum (FBS)	Cell culture	Gibco, ThermoFisher Sicentific, Waltham	10270-106
Ficoll® Paque Plus	Cell isolation	Merck, Darmstadt, Germany	GE17-1440-03
Geltrex™	Cell culture	ThermoFisher Sicentific, Waltham	A15696-01
Human IL-15	Cell culture	Peprotech, Hamburg, Germany	200-15
Human IL-2	Cell culture	Peprotech, Hamburg, Germany	200-02
Human TruStain FcX	FC staining	Biolegend, San Diego, USA	422301
Lipopolysaccharide (LPS)	Cell activation	Sigma-Aldrich, Steinheim	L8274
Mowiol	Tumor sections	Sigma-Aldrich, Steinheim	81381-50G
Penicillin/Streptomycin (P - 10,000 U/mL; S - 10,000 µg/mL)	Cell culture	Gibco, ThermoFisher Sicentific, Waltham	15150-122
Propidium Iodide (PI) solution	Miscellaneous	Biolegend, San Diego, USA	421301
RPMI 1640 1X + GlutaMAX™-I	Cell culture	Gibco, ThermoFisher Sicentific, Waltham	61870-010
Sfi I 10 U/µL	DNA cloning	ThermoFisher Sicentific, Waltham	ER1821
SyBR Green Master Mix	RT-qPCR	ThermoFisher Sicentific, Waltham	4385612
T4 DNA ligase	DNA cloning	ThermoFisher Sicentific, Waltham	EL0011

Tag-it Violet™ cell tracking dye	Miscellaneous	Biolegend, San Diego, USA	425101
ThinCert® 96 well HTS insert		Greiner	
Trypan blue stain (0.4 %)	Cell culture	ThermoFisher Sicentific, Waltham	15250-061
TrypLE™ Express Enzyme	Cell culture	Gibco, ThermoFisher Sicentific, Waltham	12605-010
Trypsin-EDTA (0.05 %)	Cell culture	Gibco, ThermoFisher Sicentific, Waltham	25200-056
Xbal 10 U/µL	DNA cloning	ThermoFisher Sicentific, Waltham	ER0681
X-VIVO™20	Cell culture	Lonza, Basel, Switzerland	04-448Q

3.1.6 Buffers, solutions and media

Materials Table 7 - List of Buffers, Solutions and Media

Name	Components
0.5M Ethylenediaminetetraacetic acid (EDTA)	(for 500 mL): 93.085 g of EDTA in ddH_2O, pH 8
1X Perm buffer	ddH_2O + 10 % 10X Perm buffer
4 % Paraformaldehyde (PFA)	(for 100 mL): 4g PFA + 60 mL ddH_2O, heat 60 °C + 1.87g NaH_2PO_4 + 0.428 g NaOH pH 7.2-7.4
50 mM $(NH_4)Cl$	(for 1000 mL, autoclaved): 1 L of ddH_2O + 2.6745 g of $(NH_4)Cl$
Ammonium chloride potassium (ACK) lysis buffer	(for 400 mL): 3.3 g NH_4Cl + 0.4 g $KHCO_3$ + 14.88 mg Na_2EDTA; pH 7.2-7.4
Blocking solution	PBS + 2 % Fetal calf serum + 2 % Bovine serum albumin + 0.2 % Fish gelatine
FACS buffer	PBS + 0.5 % bovine serum albumin fraction V
Freezing medium	90 % FBS + 10 % DMSO
LB medium	(for 1000 mL, autoclaved): 10 g Tryptone + 5 g yeast extract + 10 g NaCl pH 7.5
LB-Agar medium	(for 1000 mL, autoclaved): 10 g Tryptone + 5 g yeast extract + 0.10 g NaCl + 15 g Agar pH 7.5
PBS-Tween(T) 20	PBS + 0.05 % Tween 20
SOB medium	(for 1000 mL, autoclaved): 20 g Tryptone + 5 g yeast extract + 0.58 g NaCl + 0.18 g KCl + 0.95 g $MgCl_2$ + 1.20 g $MgSO_4$ pH 7
SOC medium	(for 1000 mL, autoclaved): 1L of SOB medium + 3.6 g Glucose
Sodium citrate buffer	ddH_2O + 10 Mm of Sodium citrate ($C_6H_5Na_3O_7$) + 0.05 % Tween 20

3.1.7 Kits

Materials Table 8 - List of kits

Name	Purpose	Supplier	Reference
BD Cytofix/Cytoperm™ Plus Fixation/Permeabilization Solution Kit with BD GolgiStop™	Flow Cytometry	BD (Becton Dickinson & Company) Franklin Lakes	554715
Cell Activation Cocktail	Cell activation	Biolegend, San Diego, USA	423301
NK Cell Isolation Kit, mouse	Cell isolation	Miltenyi Biotec, Bergisch Gladbach	130-115-818
NucleoSpin® RNA Plus	RNA synthesis	Macherey-Nagel, GmbH & Co. KG, Düren, Germany	740984.50
QIAGEN Plasmid Midi Kit	Plasmid DNA purification	Qiagen, Hilden	12143
QIAprep Spin Miniprep Kit	Plasmid DNA purification	Qiagen, Hilden	27104
QIAquick Gel Extraction Kit	Plasmid DNA purification	Qiagen, Hilden	28704
qScript™ cDNA Synthesis Kit	cDNA synthesis	Quantabio, Berverly MA, USA	95047-100
RevertAid First Strand cDNA Synthesis Kit	cDNA synthesis	ThermoFisher Sicentific, Waltham	K1621
SE Line 4D-Nucleofector™ X Kit S	Electroporation	Lonza, Basel, Switzerland	V4XC-1032
T Cell TransAct™ Human	Cell activation	Miltenyi Biotec, Bergisch Gladbach	130-111-160
Trans Detect PCR Mycoplasma Detection Kit	Mycoplasma screening	TransGen BioTech, China	FM311-01

ZymoPURE™ II Plasmid Midiprep Kit	Plasmid DNA purification	Zymo Research Europe GMBH, Freiburg, Germany	D4200-A

3.1.8 Consumables

Materials Table 9 - List of consumables

Name	Purpose	Supplier	Reference
96-well plates V bottom	FC staining	ThermoFisher Sicentific, Waltham	249944
Cell culture dishes (35 mm, 90 mm)	Miscellaneous	Techno Plastic Products (TPP), Trasadingen	93040, 93100
Cellstar® Cell Culture Flasks (25, 75 cm^2)	Cell culture	Greiner Bio-one, Frickenhausen	69175, 658175
Conical Tubes (15 mL, 50 mL)	Miscellaneous	Greiner Bio-one, Frickenhausen	188241, 22745
Eppendorf Safe-Lock Microcentrifuge Tubes (1.5 mL, 2 mL)	Miscellaneous	Eppendorf, Hamburg	0030120086, 0030120094
Falcon® 70 µm Cell Strainer	Cell isolation	Corning, New York	352350
Falcon® Polystyrene Round Bottom Tubes (14 mL)	Mini bacteria cultures	Corning, New York	352059
Falcon® Polystyrene Round Bottom Tubes (5 mL)	FC staining	Corning, New York	352052
Flat-bottom cell culture plates 6, 24, 48 and 96-well	Cell culture	Techno Plastic Products (TPP), Trasadingen	92006, 92024, 92048, 92096
Needles (30G)	In vivo cell injection	BD (Becton Dickinson & Company) Franklin Lakes	304000

New Brunswick Innova® 44 - Stackable Incubator Shaker	Bacteria cultures	Eppendorf, Hamburg	M1282-0010
Spheroid Microplate, 96-well black with clear round bottom ultra-low attachment	Spheroid culture	Corning, New York	4515
Superfrost slides	Tumor sections	Buddeberg GmbH, Mannheim	J1800AMNZ
TC Plate 96 Well, Suspension	Spheroid culture	Sarstedt, Nümbrecht	83.3925500
Terumo® Syringe **3-part Syringes (1 mL, 5 mL)**	Miscellaneous	Terumo Deutschland GmbH, Eschborn	MDSS01SE, MDSS05SE

3.1.9 Equipment and devices

Materials Table 10 - List of Equipment and Devices

Name	Purpose	Supplier
Azure Imager c400	Documentation agarose gels	Azure Biosystems, Dublin CA, United Sates
BD FACSAria™ Fusion	Cell sorting	BD (Becton Dickinson & Company) Franklin Lakes
BD FACSCanto II	FC measurement	BD (Becton Dickinson & Company) Franklin Lakes
Centrifuge 5415 D	Miscellaneous	Eppendorf, Hamburg
Centrifuge 5810 R	Miscellaneous	Eppendorf, Hamburg
CFX Connect™ Real-Time System	RT-qPCR	Bio-Rad Laboratories, Hercules
Easy Sep™ Magnet	Cell Isolation	StemCell Technologies, Vancouver

Heracell 240i Incubator	Cell culture	ThermoFisher Sicentific, Waltham
Heraeus Biofuge Fresco refrigerated centrifuge	Miscellaneous	M & S Laborgeräte GmbH, Wiesloch, Germany
HeraSafe™ Laminar flow hood	Cell culture	ThermoFisher Sicentific, Waltham
ImageStream X MKII	Imaging FC measurement	Cytek Biosciences B.V., Amsterdam The Netherlands
Leica DM IL LED Inverted laboratory microscope	Miscellaneous	Leica Microsystems Sales GmbH, Wetzlar, Germany
Lonza 4D Nucleofector x instrument	Electroporation	Lonza, Basel, Switzerland
NanoDrop 1000 UV	DNA/RNA isolation	ThermoFisher Sicentific, Waltham
NanoDrop One	DNA/RNA isolation	ThermoFisher Sicentific, Waltham
Neubauer cell counting chamber	Cell counting	Sigma-Aldrich, Steinheim
PowerPac Power 200 Supplies	Electrophoresis	Bio-Rad Laboratories, Hercules
RM 2135 microtome	Tumor sections	ThermoFisher Sicentific, Waltham
Step One Plus Real-Time PCR System	RT-qPCR	ThermoFisher Sicentific, Waltham
Thermomixer comfort	Miscellaneous	Eppendorf, Hamburg
Vortex Genie 2	Miscellaneous	Scientific Industries, New York
Water bath Jubalo 8A	Miscellaneous	Julabo, Seelbach
Zeiss Axio Scan.Z1	Tumor sections scanning	Carl Zeiss, Jena, Germany

Zeiss Celldiscoverer 7	Confocal Microscopy	Carl Zeiss, Jena, Germany
Zeiss LSM 900 Airyscan	Confocal Microscopy	Carl Zeiss, Jena, Germany

3.1.10 Softwares

Materials Table 11 - List of Softwares

Name	Purpose	Version	Supplier
BD FACSDiva™	FC data acquisition	V6.2	BD (Becton Dickinson & Company) Franklin Lakes
BioRender	Figures	2024	BioRender, Toronto, Canada
CellProfiler™	Microscopy images analysis	V4.2.6	Broad Institute, Cambridge, Massachusetts
EndNote™	Reference	X 20	Thomson Reuters, Carlsbad
FlowJo™	FC data analysis	V10.7.2	BD (Becton Dickinson & Company) Franklin Lakes
GraphPad Prism	Graphs; Statistical analysis	V10	GraphPad Software, San Diego, USA
Iluminex IDEAS	Imaging-FC data analysis	V5.0	Amnis, EMD Millipore
ImageJ/Fiji	Microscopy images analysis	2.15.1	National Institutes of Health, New York
Microsoft Excel	Data analysis	2016	Microsoft, Redmond
Microsoft PowerPoint	Figures	2016	Microsoft, Redmond
Microsoft Word	Writing	2016	Microsoft, Redmond
SnapGene Viewer	DNA cloning	V5.1.5	GSL Biotech LLC, Boston
Zeiss ZEN	Microscopy data analysis	V3.7	Carl Zeiss, Jena, Germany

3.2 Methods

3.2.1 Cell lines

Cells were thawed in the water bath at 37 °C and added to a 15 mL Falcon containing 6 mL of DMEM medium supplemented with 10 % of FBS. Cells were then centrifuged at 300×g for 5 min, resuspended in their respective medium and plated in the appropriate culture flask, according to the cell number. The next day, medium was changed. All cell lines were kept in a humidified incubator at 37 °C, with 5 % CO_2. Screenings for mycoplasma contamination were performed regularly, using the Trans Detect PCR Mycoplasma Detection Kit (TransGen Biotech). Cells were monitored and spilt or frozen upon reaching 70-80 % of confluency.

3.2.1.1 Adherent cell lines

HNSCC cell lines, UPCI-SCC-154, UPCI-SCC-154/mWasabi, PCI-13, FaDu and FaDu/mWasabi were cultured in DMEM, supplemented with 10 % FBS and 1 % P/S. Lung carcinoma cell line, TC-1, was cultured in RPMI-1640, supplemented with 10 % FBS and 1 % P/S. When splitting or freezing was required, the medium was removed, cells were washed with PBS and incubated with 2 mL Trypsin-EDTA (0.05 %) for 2-5 min at 37 °C. Whenever cells were split for an experiment, TrypLE™ Express Enzyme was used instead. Detached cells were collected in 5 mL medium and centrifuged at 300×g for 5 min. After removing the supernatant, cells were resuspended in 5 mL of medium and transferred back to the respective flasks in a 1:5 dilution, or counted and seeded for experiments.

3.2.1.2 Suspension cell lines

NK-92$^{/CD3/CD8}$, NK-92$^{/CD3/CD8}$/GS3-CD28TM-mWasabi (NK-92$^{CD3/CD8}$/GS3-mWas) and NK-92$^{/CD3/CD8}$/myc-GS3-CD28TM (NK-92$^{CD3/CD8}$/GS3^{TM}) cells were cultured in X-VIVO™20 supplemented with 2.5 % FBS. For splitting, or experiments, suspension cells were harvested and centrifuged at 300×g for 5 min. Cells were then resuspended in medium and handled as described in 3.2.1.1 for adherent cells.

3.2.2 Mice

NOD/SCID, Heparanase knockout (HPSE-KO) [67] and wildtype (WT) C57BL/6 mice were maintained in the animal facility of the Rappaport Faculty of Medicine (Technion, Haifa), in standard controlled environment (55 % humidity, 22-24 °C, 12 h light's cycle, food and water ad libitum) and housed in proper cages. All experiments were performed in accordance with the Technion's Institutional Animal Care and Use Committee.

3.2.3 Isolation of non-adherent peripheral blood mononuclear cells

Peripheral blood samples from healthy donors were provided by the Blood Banking Facilities (Institut für Klinische Transfusionsmedizin und Zelltherapie Heidelberg, IKTZ, GmbH). Peripheral blood mononuclear cells (PBMCs) were isolated by technicians in our laboratory using Ficoll-Paque density gradient centrifugation, following the protocol recommended by the provider. First, the blood concentrates were diluted 1:2 with PBS with 2 mM EDTA and then, in a 50 mL conical tube, 35 mL of the diluted sample was carefully layered over 15 mL of Ficoll® Paque Plus (GE Healthcare), followed by centrifugation at 400×g for 30 min at 20 °C (brake set to 0). After, the upper layer was removed, and the mononuclear cell layer was carefully transferred to a new 50 mL tube. In order to remove the platelets and obtain a more pure PBMCs population, cells were washed twice with 50 mL of PBS and centrifuged for 10 min at 200×g for 15 min at 20 °C. PBMCs were then counted and frozen in aliquots of 4-6 x 10^7 cells in freezing medium and stored in liquid nitrogen.

3.2.3.1 *In vitro* activation of PMBCs

PBMCs from 3 donors were thawed and plated overnight in 3 mL of X-VIVO™20. Then, the non-adherent cells were obtained by swirling several times the plate and collecting the medium. Cells were centrifuged at 300×g for 5 min, resuspended in X-VIVO™20, counted and plated in 48-well plates (1 x 10^6 cells per well) with cell activation cocktail (10 ng/mL of PMA and 1 x 10^3 ng/mL of Ionomycin; section 3.1.7, table 8) for 4 h. As a control, cells were plated in medium only (non-activated cells).

To evaluate indirect short-term activation of NK cells within PBMCs, cells were plated as described above and incubated with T Cell TransAct™ Human (section 3.1.7, table 8) for 24 h, 48 h, and 72 h. For long-term activation, cells were also treated with T Cell TransAct™ Human and subsequently cultured for 20 days in X-VIVO™20 supplemented with 100 U/mL of IL-2 and 0.01 ng/mL of IL-15.

Following the incubation, cells were collected and stained for CD56 and polyclonal Hpa 733 antibodies as detailed in section 3.2.7 for FC analysis of surface and intracellular expression of HPSE in NK cells.

3.2.3.2 Enrichment and activation of primary NK cells from human PBMCs

Dr. Isaac Quiros-Fernandez was responsible for the enrichment and expansion of primary NK cells from PBMCs. I proceeded with the activation and analysis of the cells. Enrichment and expansion of primary NK cells from PBMCs was performed by co-culture of these cells with T2 cells. For that, an aliquot of PBMCs was thawed and plated overnight in X-VIVO™20 supplemented with 5 % of FBS and 400 U/mL of IL-2. The following day, T2 cells were collected, centrifuged at 300×g for 5 min, resuspended in RPMI 1640 medium, counted and subjected to gamma irradiation (10 Gy). Then, non-adherent PBMCs were collected as described in 3.2.3.1, centrifuged at 300×g for 5 min, resuspended in medium and counted. A co-culture was started in a 6-well plate with 5 x 10^6 PBMCs and 5 x 10^5 irradiated T2 cells (10:1 ratio) in X-VIVO™20 supplemented with 5 % of FBS and 400 U/mL of IL-2. Cells were monitored daily and when necessary, medium was changed, or cells were transferred to a bigger flask. Every couple of days an aliquot was taken for FC staining to analyze the percentage of NK cells. After 14 days in culture, cells were collected, centrifuged at 300×g for 5 min, resuspended in X-VIVO™20 supplemented with 5 % of FBS and 400 U/mL of IL-2, counted, and plated in 48-well plates (0.5 x 10^6 cells per well) with cell activation cocktail (10 ng/mL of PMA and 1 x 10^3 ng/mL of Ionomycin; section 3.1.7, table 8) for 4 h and 20 h. As a control, cells were plated in medium only (non-activated cells). Following the incubation, cells were collected and stained for CD56 and polyclonal Hpa 733 antibodies as detail in the section 3.2.7.1 for FC analysis of surface expression of HPSE in NK cells.

3.2.4 *In vitro* activation of NK-92$^{CD3/CD8}$ cells with PMA and Ionomycin

NK-92$^{CD3/CD8}$ cells [68], a derivative of the NK-92 cell line, were harvested, added to a 15 mL tube and centrifuged at 300×g for 5 min. Supernatant was discarded, cells were resuspended in X-VIVO™20 supplemented with 5 % of FBS and counted. Cells were then plated in 48-well plates (0.5 x 10^6 cells per well) with 500 µL of medium and with cell activation cocktail (10 ng/mL of PMA and 1 x 10^3 ng/mL of Ionomycin section; 3.1.7, table 8) for 4 h and 20 h. Following the incubation, cells were collected and stained with Hpa 733 polyclonal antibody as detail in the in 3.2.7.1 for FC analysis of HPSE surface expression.

3.2.5 Generation of HNSCC cell lines with stable mWasabi expression

Generation of UPCI-SCC-154/mWasabi, FaDu/mWasabi and PCI-13/mWasabi cell lines was carried out as previously described [68]. FaDu/mWasabi, UPCI-SCC-154/mWasabi and PCI-13/mWasabi cell lines were generated in our laboratory by Dr. Quiros-Fernandez and A. Cid-Arregui (unpublished results).

A synthetic gene encoding the mWasabi fluorescent protein [69] was obtained from Twist Bioscience and cloned in the pSBbi-Pur plasmid (RRID Addgene_60523) [70] using the NcoI and XbaI restriction sites. 1x10^6 FaDu cells were washed twice with PBS and resuspended in 20 µL of SE Nucleofector solution (Lonza) containing 1 µL of DNA mix (0.6 µg pSBbi-mWasabi and 0.4 µg pCMV-SB100X) (RRID:Addgene_34879) [71]. Immediately after, electroporation was carried out with the Lonza 4D Nucleofector × instrument using the SE Cell Line 4D-Nucleofector™ X Kit S with the CA163 program. The electroporated cells were incubated at room temperature (RT) for 10 min and then cells were retrieved in DMEM with 10 % FBS and transferred to a 48-well plate with 1 mL of pre-warmed medium per well. After two weeks in culture, the expanded cells underwent two sequential sortings based on mWasabi expression, to establish the cell line with homogeneous and stable green fluorescent protein expression. Dead cells were excluded using DAPI staining, and mWasabi positive cells were sorted with a BD FACSAria™ Fusion. After each sorting, cells were placed back in culture in DMEM with 10 % FBS and 1 % of P/S and expanded from there.

3.2.6 Co-culture of NK-92$^{CD3/CD8}$ with HNSCC cell lines

UPCI-SCC-154/mWasabi and FaDu/mWasabi cells were seeded in 100 µL of medium (1 x 10^5 cells/well) in flat bottom 96-well plates (triplicates) and left to adhere for 18 h. Then, the medium of each well was removed and co-cultures were initiated by adding 1 x 10^5 NK-92$^{CD3/CD8}$ cells per well in 100 µL of X-VIVO™20 supplemented with 2.5 % FBS. As control, NK-92$^{CD3/CD8}$ cells were seeded alone. After 72 h of co-culture, cells were collected and stained with Hpa 733 polyclonal antibody as detail in the 3.2.7.1 for FC analysis of HPSE surface expression. For FC analysis 10,000 events were acquired from live cells. NK-92$^{CD3/CD8}$ cells were gated as mWasabi negative (-) single live cells.

3.2.7 Flow cytometry analysis

FC stainings were performed in 96-well V-bottom plates, on ice, in the dark. All centrifugation steps were done at 250×g for 3 min at 4 °C and supernatants were discarded by fast plate inverting. All antibodies and dyes, as well as respective dilutions, are described in section 3.1.2, table 2. Unless stated otherwise, cells were washed twice with 200 µL of FACS buffer between every step of the protocol.

3.2.7.1 Cell surface staining

Cells were collected, washed and incubated with Human TruStain FcX in 100 µL of FACS buffer for 10 min at RT. After blocking the Fc receptors to prevent non-specific immunoglobulin binding, cells were immunostained against cell surface proteins, with the respective antibodies in 50 µL of FACS buffer for 20 min, on ice, in the dark. Afterwards, cells were washed and either incubated with appropriate secondary antibodies diluted in 100 µL of FACS buffer or immediately resuspended in 200 µL of FACS buffer containing DAPI. If the incubation with a secondary antibody was necessary, then cells were washed and finally resuspended in 200 µL of FACS buffer containing DAPI and collected into FACS tubes.

3.2.7.2 Intracellular protein staining

For intracellular staining, cells were first collected, washed twice with PBS at RT and then stained with the Live/Dead marker, Zombie Violet or Zombie Aqua, diluted in 100 µL of PBS for 15 min at RT. Cells were then washed twice with FACS buffer and incubated with Human TruStain FcX diluted in 100 µL of FACS buffer for 10 min at RT. Afterwards, cells were washed and incubated in 100 µL of the fixation/permeabilization solution, using the Cytofix/Cytoperm™ Plus Kit, for 20 min, on ice, in the dark. Then, the cells were stained with the respective antibodies (section 3.1.2, table 2) diluted in 50 µL of 1X Perm Buffer for 20 min on ice and in the dark. When required, cells were washed and incubated with the appropriate secondary antibody diluted in 100 µL of FACS buffer (section 3.1.2, table 2). As a final step, cells were resuspended in 200 µL of FACS buffer and collected into FACS tubes.

3.2.7.3 Data acquisition and analysis

FC acquisition was performed on a BD FACS Canto II flow cytometer with the BD FACSDiva software. Before starting with data acquisition, single antibody stainings were used as compensation controls to generate automatic compensation and correct spectral overlap. The data was analyzed using FlowJo v10.7.1 software.

3.2.8 Isolation of primary mouse NK cells from splenocytes

WT and HPSE-KO mice were sacrificed by cervical dislocation and spleens were harvested. Spleens were then placed on top of 70 µm cell strainer fixed on a 50 mL tube. Murine spleen cells were isolated by passing the spleen through a 70 µm nylon mesh with the help of 5 mL of FACS buffer and the mechanical pressure of the back of a 5 mL syringe. Cell suspensions were centrifuged at 300×g for 10 min at 4 °C and resuspended in 5 mL of ACK lysis buffer for 10 min at RT. Lysis was stopped by adding 40 mL of cold PBS and cells then were centrifuged at 300×g for 10 min at 4 °C. Primary mouse NK cells were isolated from splenocytes by depletion of non-target cells, using the mouse NK Cell Isolation Kit. In short, cells were counted and centrifuged at 300×g for 10 min at 4 °C. The cell pellet was resuspended in 40 µL of FACS buffer per 10^7 cells plus 10 µL of NK Cell Biotin-Antibody cocktail per 10^7 cells, transferred to a

FACS tube, and incubated for 5 min at 4 °C, in the dark. Cells were then washed with 3 mL of FACS buffer and centrifuged at 300×g for 10 min at 4 °C. Supernatant was removed, the cell pellet was resuspended in 80 µL of FACS buffer per 10^7 cells plus 20 µL of Anti-Biotin MicroBeads per 10^7 cells and cells were incubated for 10 min at 4 °C, in the dark. After the incubation period, 400 µL of FACS buffer were added to the sample and the magnetic separation was carried out using the Easy Sep™ Magnet. Samples tubes were placed inside the magnet for 5 min. Afterwards, the desired unbound fraction of cells (NK cells) was poured to a new FACS tube. For each sample the magnetic labelling and separation was performed twice. For downstream analysis, NK cells from two WT or HPSE-KO mice were pooled.

3.2.9 Heparanase enzymatic activity

Measurements of HPSE activity were performed at the Technion Institute by Malik Farhoud in the laboratory of Prof. Dr. Israel Vlodavsky. For the analysis of HPSE activity in NK cells, 35-mm ECM-coated dishes were prepared as previously described [72, 73].

HPSE activity was measured by quantifying the release of sulfate labeled HS degradation fragments. To assess HPSE activity in NK cell extracts, 1 x 10^6 cells were lysed through three freeze/thaw cycles. The resulting cell extracts were then incubated with ^{35}S-labeled ECM for 18 h at 37 °C and pH 6.0. Following incubation, 1 mL of the medium containing the degradation fragments was subjected to gel filtration using a Sepharose CL-6B column. Fractions of 0.2 mL were eluted with PBS, and their radioactivity was measured using a β-scintillation counter. HPSE-generated degradation fragments of HS side chains were eluted at $0.5 < Kav < 0.8$ (fractions 15-30).

3.2.10 Optimization of tumor spheroid culture

Tumor spheroids were generated from UCPI-SCC-154, PCI-13, FaDu and TC-1 cell lines. First, 96-well tissue cultured (TC) suspension plates were coated with 100 µL of Biofloat™ Flex coating solution for 3 min. After, the liquid was completely removed and plates were left open to air-dry at RT, inside the laminar flow hood. Several seeding densities were then tested: 2.5 x 10^3 cells/well; 5 x 10^3 cells/well; 1 x 10^4 cells/well; 2 x 10^4 cells/well; 3 x 10^4 cells/well. Cells were seeded in 100 µL of respective medium. The plate was then centrifuged at 250×g for 5 min at RT and then placed in the incubator. Spheroid formation and size were monitored daily

until they reached approximately 0.3 mm. Spheroid diameters were quantified using ImageJ/Fiji software.

3.2.11 Co-culture of TC-1 spheroids with primary mouse NK cells

Tumor spheroids were generated by seeding 2 x 10^4 TC-1 cells per well in 96-well TC suspension plates as described in 3.2.10. After 3 days, WT and HPSE-KO primary mouse NK cells were isolated as described in 3.2.8 and stained with Tag-it Violet™ cell tracking dye. For that, cells were washed twice with 1 mL of PBS, centrifuged at 300×g for 5 min at RT and then resuspended in 100 µL of PBS containing the tracking dye (dilution 1:500). Cells were then incubated for 15 min at 37 °C in the water bath and then washed twice with 1 mL of X-VIVO™20 with 10 % FBS, followed by centrifugation at 300×g for 5 min at RT. NK cells were resuspended at a density of 1 x 10^5 cells/mL in X-VIVO™20 with 2.5 % FBS. To initiate co-culture, the medium from the spheroid-containing wells was removed and replaced with 100 µL of the NK cell suspension (10^4 cells/well). After 24 h, co-cultures were terminated, supernatants removed, and spheroids were washed twice with 200 µL of PBS for 5 min at RT in agitation. Spheroids were then fixed with 100 µL of 4 % PFA for 30 min at RT and in agitation. After fixation, spheroids were washed as described above and stained with 100 µL of PI (1/100) for 20 min at RT and in agitation. Z-stack images were acquired using a Zeiss LSM 900 Airyscan confocal microscope. Images were captured with a 10X objective lens, with blue channels for NK cells visualization and red channels for visualizing the spheroids. Each scanning layer was 1.96 µm thick, with a total scan depth of 72 µm. Five spheroids per condition were analyzed. To quantify NK cell infiltration, an image analysis protocol was developed using CellProfiler™ v4.2.6. First, single-channel images were converted from color to grayscale for software compatibility. A module was then implemented for the automatic recognition of blue channel intensity (NK cells) and another for the recognition of the spheroid area in the red channel. The output included the intensity of the blue channel and the area of the spheroid. NK cell infiltration was calculated as the ratio of NK cell intensity to spheroid area, multiplied by 100. Results are presented as the percentage of NK cell infiltration within a spheroid.

3.2.12 Generation of NK-92$^{CD3/CD8}$ cells stably expressing membrane-bound fusion protein of active HPSE (GS3^{TM}) linked to a green fluorescence protein (mWasabi)

The design of the synthetic gene encoding the constitutively active Heparanase (GS3) [74] linked to CD28 transmembrane domain (TM) linked to mWasabi was done in our laboratory by I. Quiros-Fernandez and A. Cid-Arregui. This gene included the insertion of a XbaI and SfiI restriction site at the 3' end of the GS3 cDNA and the insertion of a SfiI and ClaI at the 5' end of the mWasabi cDNA. Additionally, a NcoI restriction site was introduced at the 3' end of the mWasabi cDNA to enable the removal of the green fluorescent protein from the construct. The GS3-CD28TM-mWasbasi was inserted into the pSBbi-pur plasmid between the Sfi I and XbaI sites. Samples were then run on a 0.8 % agarose and the fragments were purified using the QIAquick Gel Extraction Kit, following the manufacturer instructions. DNA concentration was measured in the Thermo Scientific NanoDrop One.

3.2.12.1 Transformation of DH5α with pSBbi-pur-GS3-CD28TM-mWasbasi plasmid

DH5α bacteria were transformed by standard heat-shock protocol. In brief, 1 µL of pSBbi-pur-GS3-CD28TM-mWasbasi plasmid DNA was added to 20 µL thawed DH5α bacterial stocks and subsequently incubated for 30 min on ice. As a negative control, no plasmid DNA was added and as a positive control 1 µL of puc19 DNA was added. Next, a 30 s heat shock at 42 °C was performed, followed by a 5 min incubation on ice. After, 200 µL of SOC medium was added to the bacteria and the mix was incubated for 1 h at 37 °C in agitation. After this incubation, 150 µL of the transformed bacteria were plated onto LB AMP agar plates and incubated at 37 °C overnight.

3.2.12.2 Plasmid Minipreps

2 mL LB AMP medium based liquid mini bacterial cultures were prepared using scraped bacteria from 3 different colonies present in the agar plate plated with pSBbi-pur-GS3-CD28TM-mWasbasi transformed bacteria. These mini cultures were left to growth for 6 h at 37

°C, in agitation (180 rpm). Afterwards, 1.4 mL from each mini culture were used for DNA purification, using the QIAprep Spin Miniprep Kit. DNA concentration was measured in the Thermo Scientific NanoDrop One. Minipreps were evaluated by restriction enzyme analysis to assess successful cloning. Positive clone sequences were then confirmed by Sanger DNA sequencing.

3.2.12.3 Plasmid Midipreps

Based on sequencing results and DNA concentration, one miniprep was chosen to inoculate a maxi culture. For that, 50 µL of the liquid mini bacterial cultures were added to a 100 mL LB AMP medium based liquid culture and incubated overnight in agitation (180 rpm). Plasmid DNA purification was performed using the ZymoPURETM II Plasmid Kit, according to the manufacturer instructions. DNA concentration was measured in the Thermo Scientific NanoDrop One and plasmid DNA was stored at -20 °C.

3.2.12.4 Electroporation of NK-92$^{CD3/CD8}$ cells with pSBbi-pur-GS3-CD28TM-mWasbasi plasmid

Electroporation was carried out similarly to what is described in section 3.2.5. Briefly, 1x10^6 NK-92$^{CD3/CD8}$ cells were washed twice with PBS and resuspended in 20 µL P3 Nucleofector buffer (Lonza) containing 1 µL of DNA mix (0.6 µg pSBbi-pur-GS3-CD28TM-mWasbasi and 0.4 µg pCMV-SB100X). Immediately after, electroporation was carried out with the Lonza 4D Nucleofector × instrument using the EH115 program. The electroporated cells were incubated at RT for 10 min and then were retrieved in X-VIVO™20 with 10 % FBS and transferred to a 48-well plate well with 1 mL of pre-warmed medium. After two weeks in culture, the expanded cells were stained with anti myc-tag Alexa Fluor® 647, as described in section 3.2.7.1 but in 200 µL of antibody mix. After, cells were sorted twice based on myc expression, to establish a homogeneous and stable population of NK-92$^{CD3/CD8}$/GS3-mWas cells. Dead cells were excluded using DAPI staining, and cells were sorted with a BD FACSAria™ Fusion. After each sorting cells were placed back in culture in X-VIVO™20 with 10 % FBS and expanded from there until there were enough cells to reduce the FBS content to 2.5 %.

3.2.13 Generation of NK-92$^{CD3/CD8}$ cells stably expressing membrane-bound fusion protein of active HPSE (GS3^{TM})

The design of the synthetic gene encoding a myc tag linked to the GS3 which in turn was linked to CD28TM domain was done by I. Quiros-Fernandez and A. Cid-Arregui. The myc-GS3-CD28TM was cloned using the SpeI and XbaI restriction sites, which resulted in the plasmid p-SBbi-pur-myc-GS3-CD28TM. This cloning followed the steps described for bacterial transformation (section 3.2.12.1), plasmid miniprep preparation (section 3.2.12.2), plasmid midiprep preparation (section 3.2.12.3) and finally electroporation (section 3.2.12.4). I was responsible for several of the cloning steps and for the electroporation of NK-92$^{CD3/CD8}$ cell with the p-SBbi-pur-myc-GS3-CD28TM plasmid. The sorting of these cells to obtain a stable population of NK-92$^{CD3/CD8}$/GS3^{TM} cells was done in collaboration with I. Quiros-Fernandez.

3.2.14 Imaging flow cytometry

Imaging-FC was performed on NK-92$^{CD3/CD8}$, NK-92$^{CD3/CD8}$/GS3-mWas and NK-92$^{CD3/CD8}$/GS3^{TM} cells. Cells were harvested, centrifuged at 300×g for 5 min at RT and resuspended in 5 mL of X-VIVO™20 supplemented with 2.5 % FBS. Cells were then counted, and 1 x 10^6 cells were used for each sample. After, cells were stained with polyclonal primary antibody Hpa 733 and secondary antibody goat anti-rabbit Alexa Fluor® 647 following the cell surface staining protocol described in 3.2.7.1. In this case, incubations with antibodies were performed in 200 µL of FACS buffer and at the last step cells were resuspended in 50 µL of FACS buffer. Samples were acquired using the Cytek Amnis ImageStream X MKII at 60× magnification and images were acquired for 10^4 events/sample. Cells were excited using 405 nm (Live/Dead) and 640 nm (HPSE) lasers. Single-color controls were used to generate a compensation matrix, which was applied to all experimental files before analysis. Analysis of the data was done with IDEAS 5.0 software. Briefly, cells were initially gated using a plot of area ratio versus brightfield area (R1), and focused cells were selected within R1. From these focused cells, live cells were then gated. Total integrated channel fluorescence was used to identify live cells positive for HPSE. Once live, focused, and HPSE positive cells were identified through reductionist gating, a channel mask was adapted and applied to better delineate the pixels corresponding to HPSE staining. Results are presented as the mean value of the intensity of the HPSE mask feature.

3.2.15 *In vitro* activation of NK-92$^{CD3/CD8}$ and NK-92$^{CD3/CD8}$/GS3^{TM} cells with LPS

This protocol was done during my stay in Dr. Israel Vlodavsky lab in Israel. NK-92$^{CD3/CD8}$ and NK-92$^{CD3/CD8}$/GS3^{TM} cells were harvested and added to a 15 mL tube and centrifuged at 300×g for 5 min. Supernatants were discarded, cells were resuspended in X-VIVO™20 and counted. Cells were then plated in 24-well plates (1 x 10^6 cells/well) with 1 mL of medium and 1 µg/mL of LPS and incubated overnight (ON). After the ON period, cells were collected and processed for analysis by real time quantitative PCR (RT-qPCR).

3.2.15.1 RNA extraction from NK-92$^{CD3/CD8}$ and NK-92$^{CD3/CD8}$/GS3^{TM} cells

Cells were washed once with PBS and centrifuge at 300×g for 5 min. Supernatants were discarded and cell pellet total RNA was extracted using NucleoSpin® RNA Plus (Macherey-Nagel™), according to the manufacturer instructions. RNA concentration was measured in the NanoDrop 1000 UV. Purified RNA was stored at -20 °C for downstream use.

3.2.15.2 cDNA synthesis

cDNA was generated from the total RNA obtained in 3.2.15.1 using the qScript^{TM} cDNA Synthesis Kit (Quantabio) and following the manufacturer instructions. In short, all necessary components were thawed, mixed thoroughly, briefly centrifuged and then maintained on ice. A mix was prepared for each sample in PCR tubes containing: 1000 ng of RNA, nuclease-free water (variable amount), 4 µL of qScript Reaction Mix (5X) and 1 µL of qScript reverse transcriptase (final volume of 20 µL). Samples were gently vortexed and centrifuged. Tubes were placed in the thermal cycler programmed as follows:

Step	Temperature	Time (hh:mm:ss)
1	22 °C	00:05:00
2	42 °C	00:30:00
3	85 °C	00:05:00
4 °C hold		

After completion of cDNA synthesis, tubes were centrifuged and samples were stored at -80 °C for downstream use.

3.2.15.3 Real Time-Quantitative PCR

For the RT-qPCR, all necessary components and samples were thawed, mixed thoroughly, briefly centrifuged and then maintained on ice. PCR amplification was performed in a total reaction of 10 µL, containing 5 µL of SyBR Green Master Mix, 0.5 µL of the primer mix (10 mM of Forward Primer plus 10mM of Reverse Primer) and 2 µL of PCR-grade water. This mix was gently vortexed, centrifuged and 7.5 µL were distributed to each well of the RT-qPCR plate. The PCR primers used are listed in section 3.1.3, table 4. Afterwards, 2.5 µL of the cDNA from each sample were added to respective wells. The plate was then sealed with an optically transparent film and centrifuged at 300×g for 1 min. RT-qPCR was performed according to the following steps:

Step	Temperature	Time (hh:mm:ss)
1	95 °C	00:00:20
2	95 °C	00:00:03
3	60 °C	00:00:30
Go to step 2 – 40 cycles		
4	95 °C	00:00:15
5	60 °C	00:01:00
4 °C hold		

The results were analyzed following the manufacturer's instructions.

3.2.16 Measurement of NK cell degranulation upon co-culture with target cells

UPCI-SCC-154/mWasabi and FaDu/mWasabi cells were seeded as described in section 3.2.6 (1 x 10^5 cells/well). Co-cultures were then initiated by removing the medium and adding 1 x 10^5 NK-92$^{CD3/CD8}$ cells or 1 x 10^5 NK-92$^{CD3/CD8}$/GS3^{TM} cells per well in 100 µL of X-VIVO™20 supplemented with 2.5 % FBS per well. As control, both cell lines were seeded alone. After 24 h of co-culture, cells were collected and stained with CD107a PECy7 antibody as detail in the 3.2.7.1 for FC analysis as a measure of NK cell degranulation. For FC analysis 10,000 events were acquired from live cells. NK cells were gated as mWasabi- single live cells.

3.2.17 Transwell migration assay

Migration assay was carried out using ThinCert® 96 well HTS insert (Greiner). Transwell inserts (0.4 µm pore size, 14 mm² growth area, and polycarbonate membrane) were coated with 100 µL of Geltrex^{TM} and let to solidify for 18 h in the incubator at 37 °C, with 5 % CO_2. The next day, NK-92$^{CD3/CD8}$ and NK-92$^{CD3/CD8}$/GS3^{TM} cells were harvested, added to respective 15 mL tubes and centrifuged at 300×g for 5 min. After, cells were resuspended in serum-free X-VIVO^{TM}20

and counted. To initiate the migration assay, 3 x 10^4 NK-92$^{CD3/CD8}$ cells or 3 x 10^4 NK-92$^{CD3/CD8}$/GS3^{TM} cells were seeded in triplicates on top of the solidified geltrex. To the bottom well were added 200 µL of X-VIVO^{TM}20, supplemented with 300 ng/mL of CCL19. As control, only medium was added to the bottom wells, again in triplicates. Migration was allowed to occur for 24 h at 37 °C, with 5 % CO_2. After this period, cells that had migrated to the bottom well were collected, washed twice with FACS buffer and centrifuged at 300×g for 5 min at 4 °C. Finally, supernatants were discarded and cells were resuspended in FACS buffer containing DAPI. For FC analysis 10,000 events were acquired from live cells. NK cells were identified as single live cells, and their migration was expressed as the fold change between +CCL19 migrated cells and control migrated cells.

3.2.18 Co-cultures of HNSCC spheroids and NK-92$^{CD3/CD8}$ and NK-92$^{CD3/CD8}$/GS3-mWasabi cells

Tumor spheroids were generated by seeding either 2 x 10^4 UPCI-SCC-154 cells per well or 3 x 10^4 PCI-13 cells per well in 96-well TC suspension plates as described in 3.2.10. After 2 days, NK-92$^{CD3/CD8}$ and NK-92$^{CD3/CD8}$/GS3-mWas cells were harvested and stained with Tag-it Violet™ cell tracking dye as described for primary mouse NK cells in 3.2.3.11. To initiate co-cultures, the medium from the spheroid-containing wells was removed and replaced with 100 µL of the NK cell suspension (10^4 cells/well). After 24 h and 48 h, co-cultures were terminated, the supernatant was gently removed, and spheroids were gently washed twice with 200 µL of PBS for 5 min at RT and in agitation. Spheroids were then incubated with 50 µL of Trypsin-EDTA (0.05 %) for 3 min in the incubator, followed by pipetting up and down and another incubation for 2 min. After, 200 µL of medium were added to each well and cell suspensions were transferred to eppendorf tubes, washed twice with FACS buffer and centrifuged at 300×g for 3 min. Cells were then resuspended in 200 µL of FACS buffer containing PI. For FC analysis 1 x 10^5 events were acquired from live cells. Dead cells were excluded using PI staining and NK cells were gated as Tag-it Violet+ single live cells.

3.2.19 Co-cultures of HNSCC spheroids and NK-92$^{CD3/CD8}$ and NK-92$^{CD3/CD8}$/GS3^{TM} cells

3.2.19.1 Confocal microscopy

This protocol was done during my stay in Dr. Israel Vlodavsky lab in Israel. Tumor spheroids were generated by seeding 1.5 x 10^4 FaDu cells per well in 96-well TC suspension plates as described in section 3.2.10. In this protocol spheroids were allowed to form only for 24 h. After this time, NK-92$^{CD3/CD8}$ and NK-92$^{CD3/CD8}$/GS3^{TM} cells were stained with Tag-it Violet™ cell tracking dye as described in section 3.2.11. To initiate co-cultures, the medium from the spheroid-containing wells was removed and replaced with 100 µL of the NK cell suspension (10^4 cells/well). After 24 h, co-cultures were terminated, the supernatant was gently removed, and spheroids were gently washed twice with 200 µL PBS for 5 min at RT and in agitation. Spheroids were then fixed with 4 % PFA and stained with PI as described in section 3.2.11 and imaged by confocal microscopy using a Zeiss LSM 900 Airyscan. Images were captured with a 10X objective lens, with blue channel for visualizing NK cells and red channel for visualizing the spheroids. Each scanning layer was 1.96 µm thick, with a total scan depth of 72 µm. Three spheroids per condition were analyzed. Quantification of NK cell infiltration was done with CellProfiler™ v4.2.6, using the same protocol described in section 3.2.11. Results are presented as the percentage of NK cell infiltration within a spheroid.

3.2.19.2 Live cell confocal microscopy

Tumor spheroids were generated by seeding either 2 x 10^4 UPCI-SCC-154/mWasabi cells/ well or 3 x 10^4 FaDu/mWasabi cells/well in 96 well black bottom ultra-low attachment plates as described in section 3.2.10. After 2 days, NK-92$^{CD3/CD8}$ and NK-92$^{CD3/CD8}$/GS3^{TM} cells were harvested and stained with Tag-it Violet™ cell tracking dye as described in section 3.2.11. The medium from the spheroid-containing wells was then removed and replaced with 100 µL of the NK cell suspension (10^4 cells/well for co-culture with UPCI-SCC-154-mWasabi spheroids and 5 x 10^3 cells/well for co-culture with FaDu/mWasabi spheroids). The plate was incubated in the Zeiss Celldiscoverer 7 automated confocal chamber at 37 °C, with 5 % CO_2 for 45 min, before initiating a 12-24 h time course live cell imaging experiment. Using the ZEN 3.7 software (Carl Zeiss) positions were defined for the z-stack image in each well (10 images/spheroid). Z-stack

images were then taken hourly in the green (tumor cells) and blue (NK cells) channels, using a 10X/0.5X lens combination (final magnification of 5X). Quantification of NK cell infiltration was done with CellProfiler™ v4.2.6, as described in section 3.2.11, with the exception that for spheroid identification the green channel was used instead of the red channel.

3.2.20 *In vivo* experiments

3.2.20.1 Tumor xenografts

Animal experiments were carried out by Dr. Neta Ilan and Dr. Soaad Soboh at the animal facilities of the Technion Institute (Haifa, Israel). FaDu cells were harvested, washed with PBS and centrifuged at 300×g for 5 min. Cells were then resuspended in PBS, counted and brought to a concentration of 50 x 10^6 cells/ml. The cell suspension of 5 x 10^6 cells (100 µL per mouse) was subcutaneously injected into the right flank of 6-week-old female NOD/SCID mice (day 0). Mice were monitored over time and tumor growth was measured externally with calipers. Once the tumors became palpable (day 15), mice were divided into three study groups with 7 animals per group. Mice were then either injected intravenously with 5 x 10^6 NK-$92^{CD3/CD8}$ cells or 5 x 10^6 NK-$92^{CD3/CD8}$/GS3^{TM} cells, stained with the Tag-it Violet™ cell tracking dye, as described in section 3.2.11. As a control, mice were only injected with the vehicle, PBS. NK cell injections were administered three times, at four-day intervals. The day after the last NK cells injection, the experiment was terminated, and mice were sacrificed by cervical dislocation. Tumors were removed, weighed, a portion of each tumor was fixed in formalin and another portion was immediately processed for RNA extraction, using NucleoSpin® RNA Plus (Macherey-Nagel™) and described in section 3.2.3.15.1.

3.2.20.2 cDNA synthesis and RT-qPCR

cDNA synthesis and RT-qPCR protocol were performed by Dr. Quiros-Fernandez. cDNA was obtained using RevertAid First Strand cDNA Synthesis Kit (ThermoFisher) and RT-qPCR was performed using SYBR Green PCR master mix, following the manufacturer recommendations. CD56 primers used are described in are listed in section 3.1.3, table 4.

Step	Temperature	Time (hh:mm:ss)
1	50 °C	00:02:00
2	95 °C	00:05:00
3	95 °C	00:00:15
4	60 °C	00:01:00
Go to step 2 – 40 cycles		
4 °C hold		

The results were analyzed following the manufacturer's instructions.

3.2.20.3 Tissue processing and Immunofluorescence

Tumors fixed in formalin were received from the Technion Institute and were cut into sections of 5 µm using a RM 2135 microtome (Leica) and placed onto superfrost slides (Epredia Netherlands B.V). On each slide, two tumor sections were placed. I performed the cutting of the sections and the immunostaining of sections was performed by Ruken Süleymanoglu and A. Cid-Arregui. For immunostaining, the sections were first deparaffinized in two rounds of 5 min incubation in xylene and then rehydrated by gradually exposing them to decreasing concentrations of ethanol (2x 100 %, 95 %, 70 %, 50 %), each for 5 min. Finally, sections were incubated in distilled water (dH_2O) for 5 min. Antigen retrieval was performed using 10mM sodium citrate (pH 6) in a cooking pot, pre heated with water at 95-100 °C, for 30 min. After, sections were left to cool down at RT for 20 min, followed by washing three times with PBS-Tween 20 (PBS-T0.05 %), for 5 min each. Sections were placed in a humidified chamber and incubated for 10 min with 50 mM $(NH_4)Cl$ to reduce background fluorescence, followed by incubation with the blocking solution, described in section 3.1.6, table 7, for 1 h. Slides were then washed three times with PBS-T, for 5 min each and the primary antibody CD56 (section 3.1.6, table 3), diluted in blocking solution, was incubated overnight at RT. The next day, the antibody solution was discarded, slides then washed three times with PBS-T, for 5 min each and the secondary antibody goat anti-mouse Cy3 (section 3.1.6, table 3), diluted in blocking solution, was incubated for 1 h at RT in the dark. Slides were then washed three times with

PBS-T, for 5 min each, incubated with DAPI for 15 s and rinsed with DH_2O. Finally, slides were mounted using Mowiol and stored at 4 °C in the dark. Sections were visualized and scanned with the Zeiss Axio Scan.Z1, using a 20X objective. Images were analyzed with the ZEN 3.7 software.

3.2.21 Statistical analysis

Statistical analysis was performed using GraphPad Prism software v9. All data is shown as mean ± Standard Deviation (SD). Group means ± SD were plotted. Applied statistical tests are listed in the figure legends. p values were considered as follows: *$p < 0.05$, **$p < 0.01$, ***$p < 0.001$, ****$p < 0.0001$.

4 Results

4.1 Heparanase in NK cells

4.1.1 Expression of Heparanase is diminished on the surface of primary NK cells upon activation

With the goal of providing new insights into HPSE in NK cell activation, I started by assessing whether HPSE expression in primary human NK cells is affected by different activation stimuli.

NK cells activated with PMA and Ionomycin presented a slight decrease in intracellular HPSE expression (Fig. 5A) and a significant decrease in surface HPSE expression (Fig. 5B).

Indirect short-term activation (24 h, 48 h and 72 h) of NK cells via T cell stimulation with T Cell TransAct™ didn't lead to significant alterations in the HPSE surface expression (Fig. 5C). Resting for 17 days after 72h of activation led to a significant decrease of surface HPSE expression in NK cells, when comparing with the NK cells activated for 48 h and 72 h (Fig. 5C). Also, these activated cells presented a tendency to lower surface HPSE expression when compared to non-activated cells, under the same conditions (Fig. 5C). Non-activated cells presented similar surface expression of HPSE throughout the analyzed time points (Fig. 5C).

In both activation methods described above, NK cells were in the presence of other immune cells. These cells play important roles in shaping NK cell phenotypes and could, therefore, influence their HPSE expression. I then asked if the HPSE expression would be differently affected in an enriched and expanded NK cell population. NK cells presented a decrease in HPSE surface expression upon 4 h and 20 h of stimulation with PMA and Ionomycin (Fig. 5D). This result was similar to what was observed in Figure 1B, when NK cells were stimulated within the PBMCs population.

These findings indicate that different kinds and durations of activation stimuli promote an overall reduction in surface HPSE expression in primary NK cells.

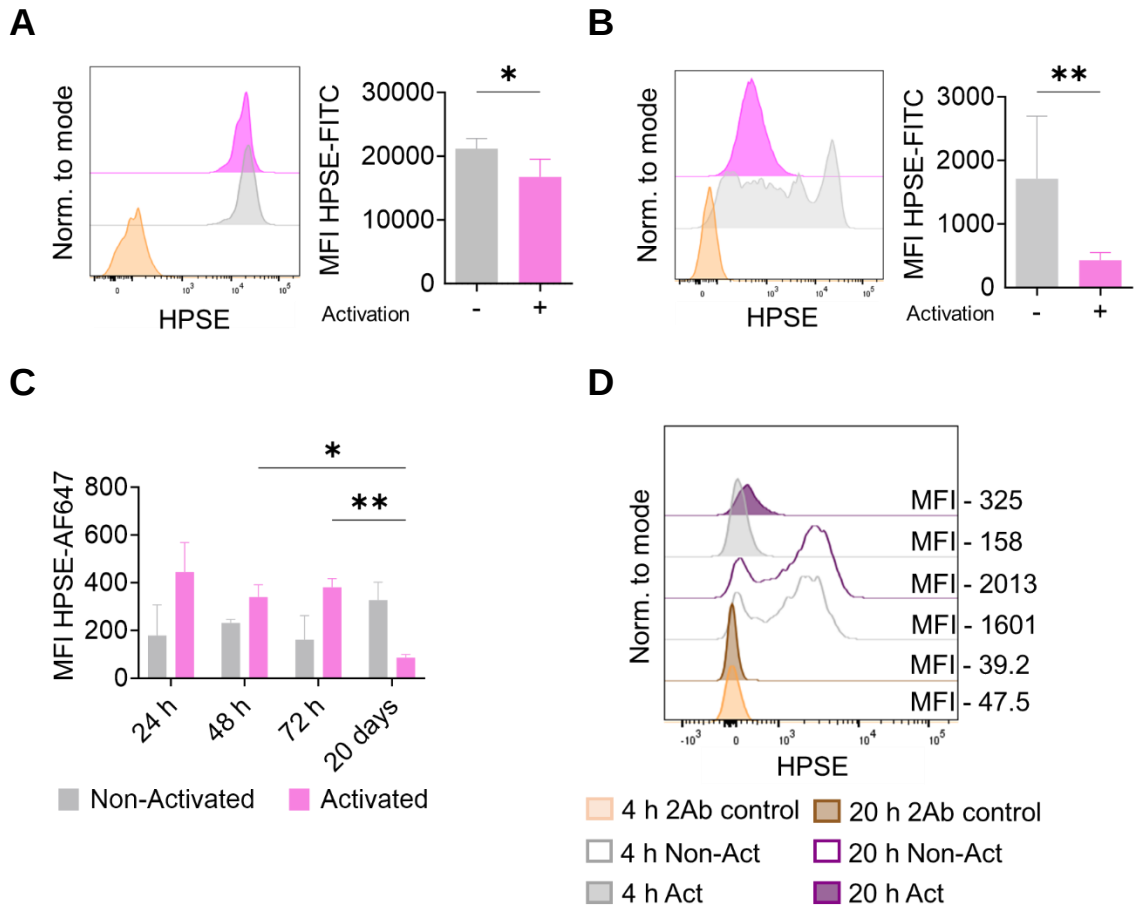

Figure 5 - Heparanase expression in primary human NK cells

(A) Intracellular expression of HPSE in NK cells within PBMCs upon 4 h of activation with PMA + Ionomycin. PBMCs were fixed and then stained with polyclonal Hpa 733 and CD56 antibodies and analyzed by FC. Histograms are normalized to mode and represent the median fluorescence intensity (MFI) of HPSE expression in secondary antibody (2Ab) only control (orange), non-activated NK cells (grey) and activated NK cells (pink). **(B)** Surface expression of HPSE in NK cells within PBMCs upon 4 h of activation with PMA + Ionomycin. PBMCs were stained with polyclonal Hpa 733 and CD56 antibodies and analyzed by FC. Colors as in (A). **(C)** Indirect activation of NK cells with T Cell TransAct^{TM}. Cells were incubated for 24 h, 48 h, 72 h and 20 days. **(D)** Surface expression of HPSE in enriched human NK cells after 4h and 20 h of activation with PMA + Ionomycin. Histograms show MFI of surface HPSE expression in 4 h 2Ab only control (orange), 20 h 2Ab only control (brown), 4 h non-activated cells (grey line), 4 h activated cells (purple line), 20 h non-activated cells (grey), and 20 h activated cells (purple).

Results are shown as the mean ± SD. Statistics: * p-value <0.05; ** p-value <0.01. Mann-Whitney U test was applied to compare two independent groups. Mixed model ANOVA was applied to compare two independent groups with repeated measures and statistical testing of multiple groups was performed with the Tukey's multiple comparison test.

I. Quiros-Fernandez was responsible for the enrichment and expansion of primary NK cells from PBMCs. I proceeded with the activation and analysis of the cells.

4.1.2 Expression of Heparanase is diminished on the surface of primary NK cells upon activation with target cells

NK-92$^{CD3/CD8}$ cell line is a NK-92 derived cell line generated previously in our laboratory [68]. These cells constitutively express the human CD3 and CD8 genes, while maintaining the NK-92 characteristics of cytotoxicity. The NK-92$^{CD3/CD8}$ cell line is also suited for co-expression and study of TCRs or CARs. Since the NK-92$^{CD3/CD8}$ cell line was chosen as the NK cell model for this work, the HPSE expression upon activation was also assessed in these cells. In contrast to what was observed for the enriched primary NK cells, the stimulation for 4 h with PMA and Ionomycin promoted a slight increase of HPSE intracellular expression and the stimulation for 20 h promoted a significant increase of the HPSE intracellular expression (Fig. 6A). Regarding HPSE surface expression, a slight increase was observed upon 20 h of stimulation (Fig. 6B).

NK-92$^{CD3/CD8}$ cells presented an almost 2-fold decrease in HPSE surface expression upon 72 h co-culture with FaDu/mWasabi cells and 1-fold decrease in HPSE surface expression upon co-culture with UPCI-SCC-154/mWasabi (Fig. 6C).

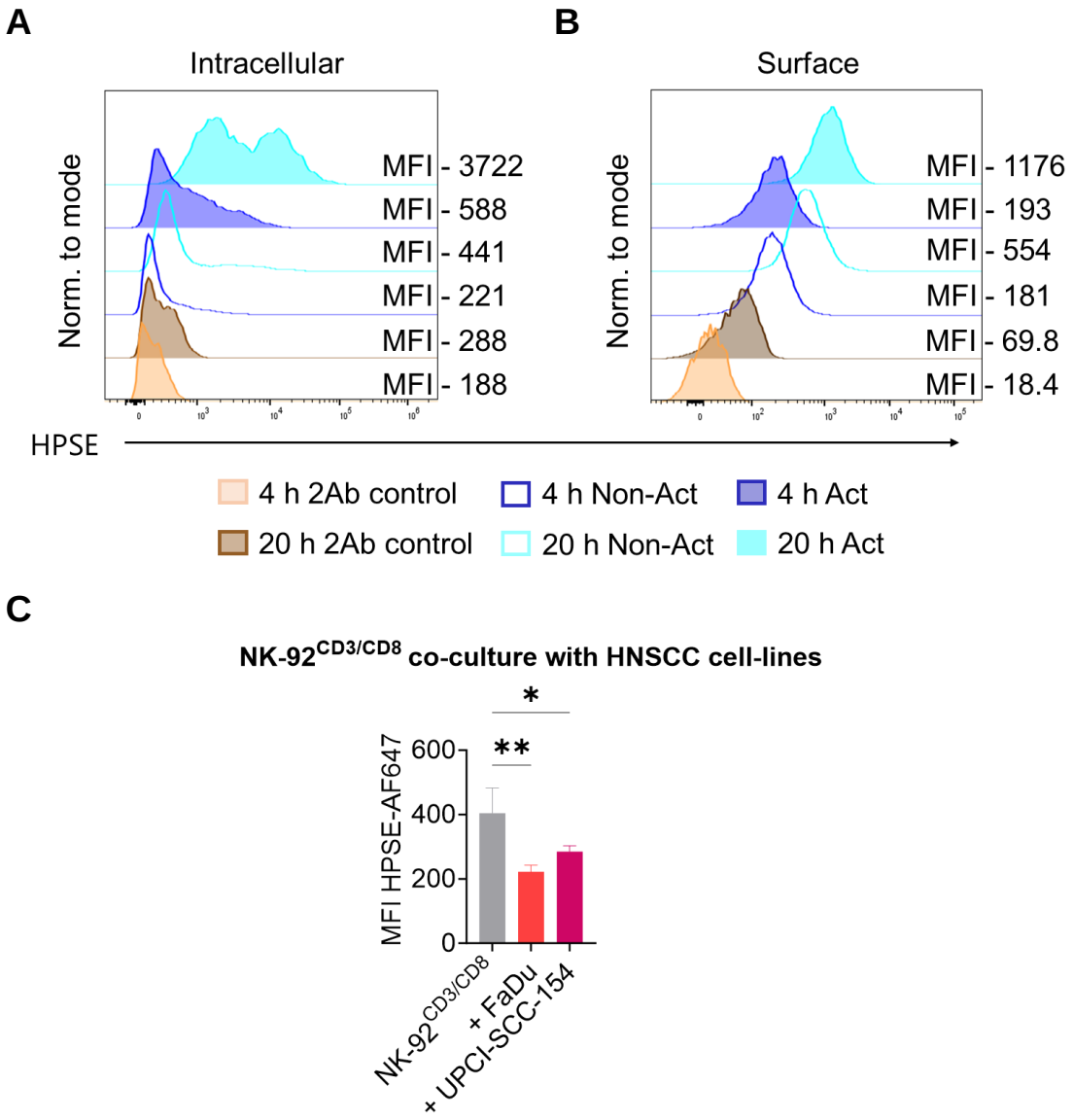

Figure 6 - Heparanase expression in NK-92$^{CD3/CD8}$ cells

(A) Intracellular expression of HPSE in NK-92$^{CD3/CD8}$ after 4 h and 20 h of activation with PMA + Ionomycin. NK-92$^{CD3/CD8}$ cells fixed and then stained with Hpa 733 polyclonal antibody and analyzed by FC. Histograms are normalized to mode and represent the MFI of HPSE expression in 4 h 2Ab only control (orange), 20 h 2Ab only control (brown), 4 h non-activated cells (dark blue line), and 4 h activated cells (light blue line), 20 h non-activated cells (dark blue curve) and 20 h activated cells (light blue curve). **(B)** Surface expression of HPSE in NK-92$^{CD3/CD8}$ after 4h and 20h of activation with PMA + Ionomycin. NK-92$^{CD3/CD8}$ cells were stained with Hpa 733 polyclonal antibody and analyzed by FC. Colors as in (A). **(C)** Surface expression of HPSE in NK-92$^{CD3/CD8}$ upon co-culture with HNSCC cell lines. Results are shown as the mean ± SD (n=3). FC plots are from a single representative experiment. Statistics: * p-value <0.05; ** p-value <0.01. One-way ANOVA was used to compare every group with the control (NK-92$^{CD3/CD8}$ only) and statistical testing of multiple groups was performed with the Dunnett's multiple comparison test.

4.1.3 NK cells need Heparanase to efficiently infiltrate growing tumor spheroids

To investigate the role of HPSE on the infiltration capacity of NK cells, HPSE-KO cells were used [67]. I started by isolating NK cells from HPSE-KO and WT mice spleens as described in Figure 7A and in the methods section 3.2.8. Then, the HPSE activity of these cells was measured by quantification of released sulfate labeled HS fragments from ECM, upon degradation by NK cell extracts. As expected, HPSE-KO NK cells presented no HPSE activity (Fig. 7B). HPSE-KO and WT NK cells were then co-cultured for 24 h with spheroids of the lung carcinoma TC-1 cell line, to check their infiltration capacity. HPSE-KO NK cells presented significantly lower infiltration capacity (Fig. 7C-D), while the WT NK cells were found in higher numbers and distributed throughout the tumor spheroid sections (Fig. 7C left). Cell number quantification and microscopy analysis demonstrated that HPSE-KO NK cells were present in significantly lower numbers, primarily localized in the periphery of the spheroid (Fig. 7C right-D).

These findings suggest that HPSE is essential for NK cells the infiltration into 3D tumor structures.

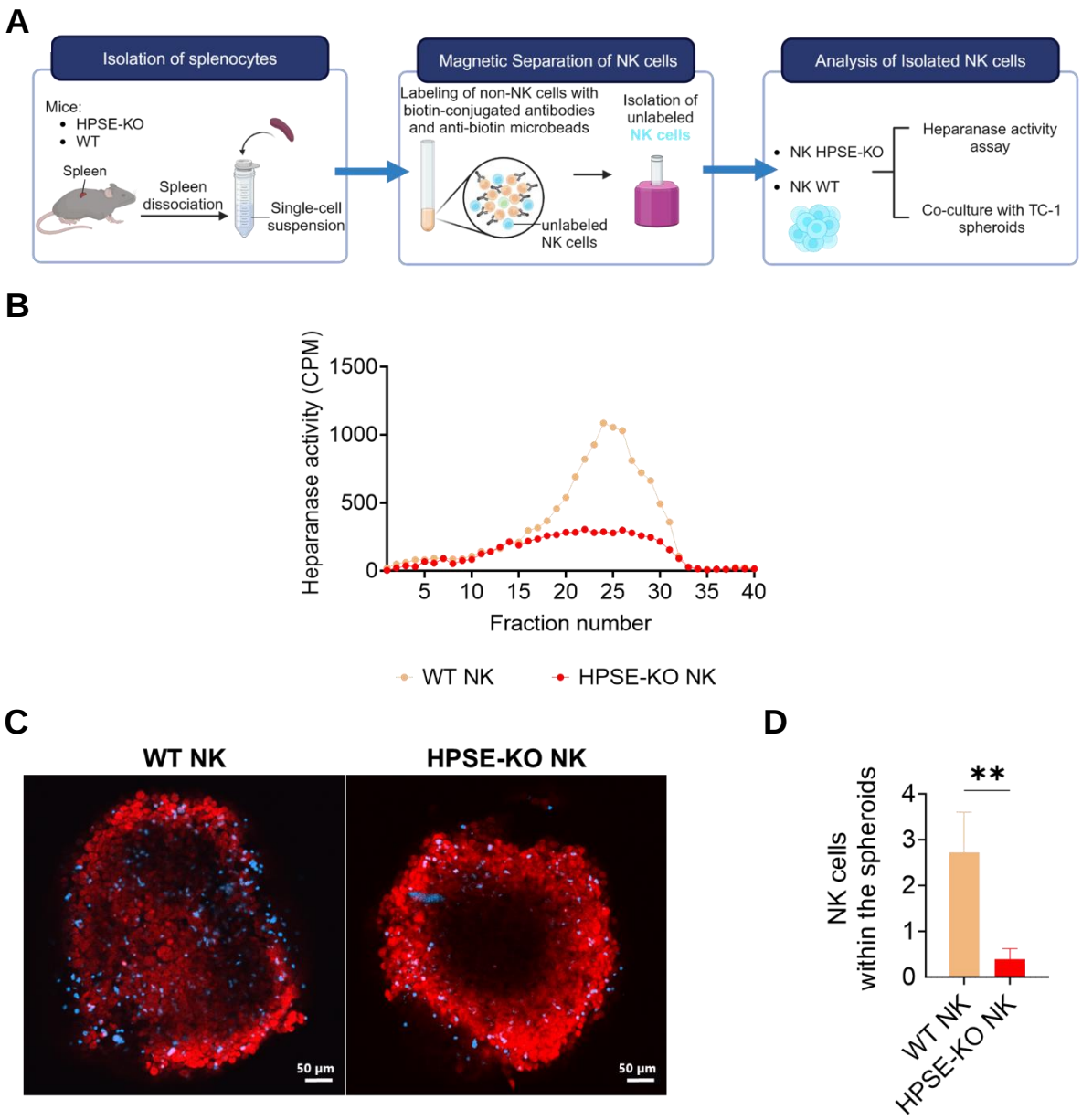

Figure 7 - Knockout of Heparanase reduces the infiltration capacity of mouse NK cells

(A) Flow-chart of the isolation and analysis of NK cells from WT and HPSE-KO mice. (**B**) HPSE activity in NK cells isolated from either WT or HPSE-KO mice. (**C**) Illustrative confocal microscopy image of infiltrating NK cells. Tumor spheroids generated from TC-1 cells were co-cultured for 24 h with HPSE-KO or WT isolated primary NK cells, previously labeled with a violet proliferation dye (Cell Trace Violet). Scalebar – 50 µm. (**D**) Infiltrating NK cells were quantified using an automatic image analysis software that identifies violet NK cells within the red spheroid area. The percentages of infiltrating NK cells were calculated by the ratio of violet fluorescence intensity per Spheroid area.

Results are shown as the mean ± SD (n = 5). Statistics: ** p-value <0.01. Mann-Whitney U test was applied to compare two independent groups.

4.1.4 NK-92$^{CD3/CD8}$ cells with stable surface expression of a membrane bound constitutive active Heparanase, the GS3^{TM}

After demonstrating that HPSE is required for NK cells to efficiently infiltrate tumor spheroids, I hypothesized that HPSE overexpression could be beneficial to improve NK cell infiltration. However, it must be taken into consideration that this enzyme is secreted as part of its activation and activity processes and that tumor cells use soluble HPSE present in the TME to sustain the excessive HSPG degradation, reorganization of the ECM and consequent facilitation of cancer growth and metastasis. So, to promote NK cell infiltration without increasing HPSE availability for tumor cells in the TME, this thesis proposal is to arm NK cells with the constitutive active form of HPSE (GS3) as an integral membrane protein.

4.1.4.1 The GS3-mWasabi fusion protein doesn't increase Heparanase expression and activity in NK-92$^{CD3/CD8}$ cells

The first strategy was to construct a fusion gene coding for a chimeric protein composed of an N-terminal extracellular GS3 linked to a CD28TM and an intracellular monomeric green fluorescence protein, mWasabi (Fig. 8A). The GS3-CD28TM-mWas gene was integrated with the Sleeping Beauty transposon system and delivered via electroporation, which allowed the integration of the gene in the genome of the transfected NK cells. Following electroporation, cells were sorted based on mWasabi expression (Fig. 8B). Cells were then expanded and maintained in culture. This fusion gene was designed and constructed in our lab by I. Quiros-Fernandez and A. Cid-Arregui.

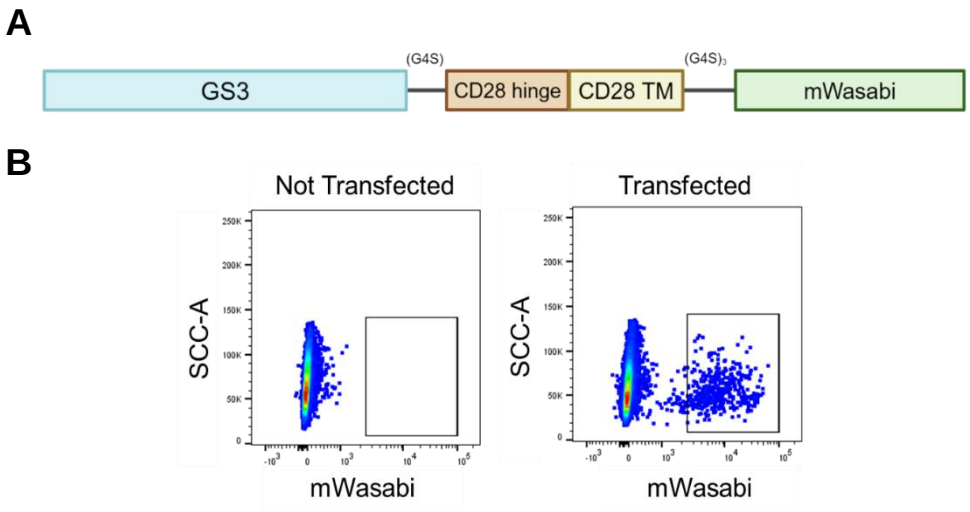

Figure 8 - GS3-CD28TM-mWasabi fusion gene construct and NK-92$^{CD3/CD8}$/GS3-mWasabi sorting strategy

(A) Schematic representation of the GS3-mWasabi fusion gene: [GS3-CD28hinge-CD28TM-mWasabi] used to generate the NK-92$^{CD3/CD8}$/GS3-mWas cell line. **(B)** Gating strategy for sorting of NK-92/GS3-mWas cells two weeks after electroporation.
Results obtained in collaboration with I. Quiros-Fernandez. E. Arias Romero and A. Cid-Arregui.

Comparison of the parental cell line and the newly generated wasabi version did not reveal any significant differences in surface marker expression. (Fig. 9A). Then, the expression of GS3-CD28TM-mWas fusion protein in NK-92$^{CD3/CD8}$/GS3-mWas cells was examined via three different strategies. First, cells were analyzed by conventional FC, using the Hpa 733 polyclonal antibody. No differences were observed in the MFI of surface HPSE between NK-92$^{CD3/CD8}$/GS3-mWas cells and the NK-92$^{CD3/CD8}$ cells (Fig. 9B). Hpa 733 staining was also applied to analyze these cells by imaging-FC, allowing to verify the expression and distribution of HPSE/GS3-mWas throughout the cells surface. The images showed that mWasabi was being expressed in the intracellular compartment of NK-92$^{CD3/CD8}$/GS3-mWas cells, as expected, but no differences were observed regarding HPSE expression or distribution (Fig. 9C-D). Moreover, HPSE activity was measured and similar levels of HPSE enzymatic activity were verified between the two cell lines (Fig. 9E).

These results indicate that this strategy to increase the GS3 expression on NK-92$^{CD3/CD8}$ cells surface was not successful.

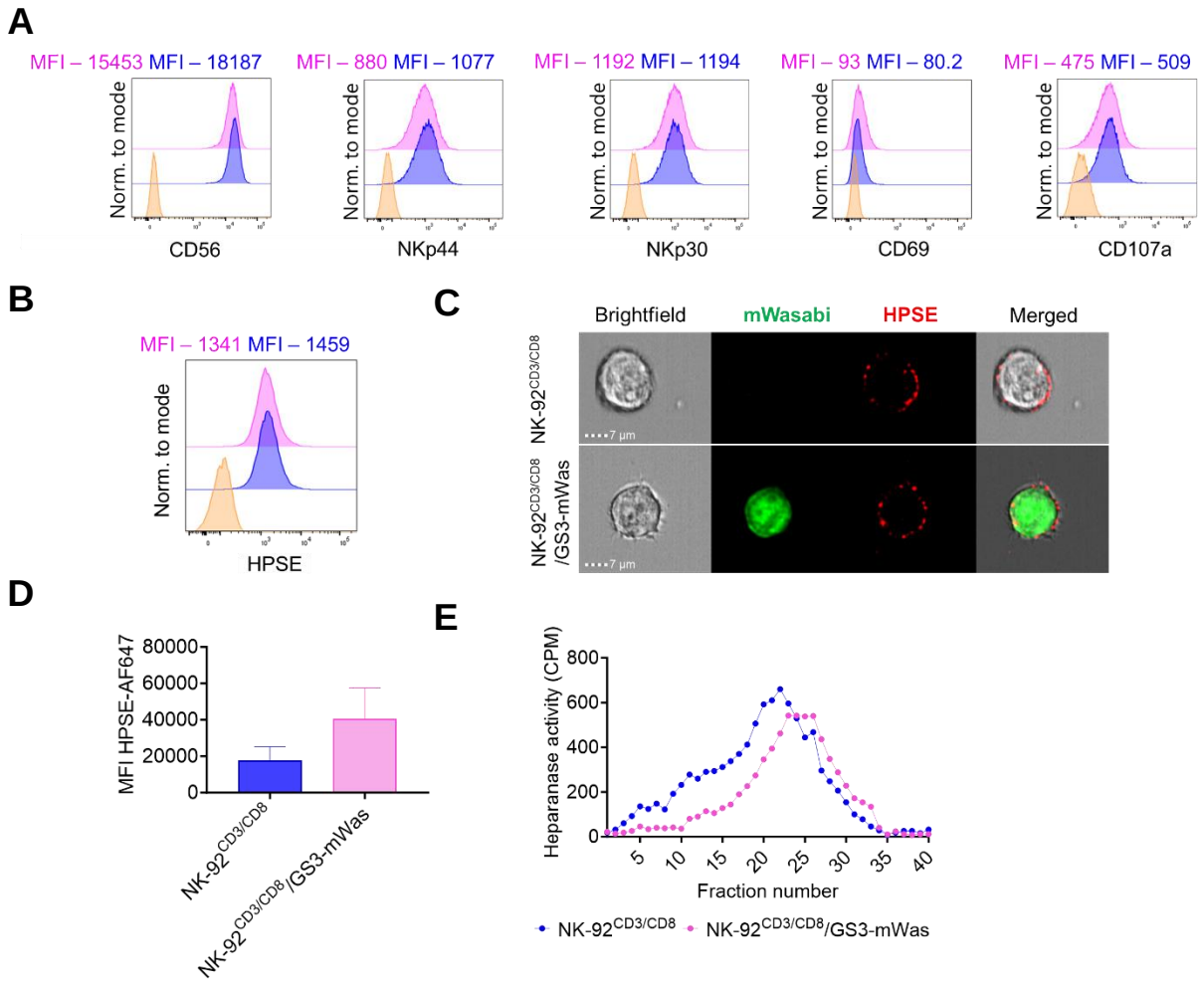

Figure 9 - Characterization of the NK-92$^{CD3/CD8}$/GS3-mWasabi cell line

(A) FC receptor profile of NK-92$^{CD3/CD8}$ and NK-92$^{CD3/CD8}$/GS3-mWas cells. Histogram colors represent 2Ab only control (orange curve), NK-92$^{CD3/CD8}$ cells (blue curve) and NK-92$^{CD3/CD8}$/GS3-mWas cells (pink curve). **(B)** FC analysis of HPSE and GS3 surface expression on NK-92$^{CD3/CD8}$ cells and NK-92$^{CD3/CD8}$/GS3-mWas cells after staining with the Hpa 733 polyclonal antibody. The histograms show the results of one representative experiment and represent same conditions as in (A). **(C)** Surface distribution of HPSE and GS3-mWas on NK-92$^{CD3/CD8}$ and NK-92$^{CD3/CD8}$/GS3-mWas cells stained with the Hpa 733 polyclonal antibody and analyzed by imaging-FC. Illustrative pictures are shown for the brightfield, mWasabi (528/65) and AF647 (702/85) channels. **(D)**. Quantification of HPSE/GS3-mWas. Results are shown as the mean ± SD. (n = 1 of three independent experiments). **(E)** HPSE activity measured in NK cell lysates that were incubated for 18 hours on sulfate-labeled ECM dishes. Representative results of two independent experiment are shown (Results obtained by Malik Farhoud at the Technion Institute in Israel). No statistical analysis was performed.

Mann-Whitney U test was applied to compare two independent groups.

NK-92$^{CD3/CD8}$/GS3-mWas cell line infiltration capacity in a 3D context was also assessed. UPCI-SCC-154 spheroids and PCI-13 spheroids were co-cultured with NK-92$^{CD3/CD8}$ cells (stained with CFSE) and with NK-92$^{CD3/CD8}$/GS3-mWas cells for 24h. NK cells infiltration was then assessed by FC. As expected, no significant differences were observed in the percentages of infiltrating NK cells (Fig. 10).

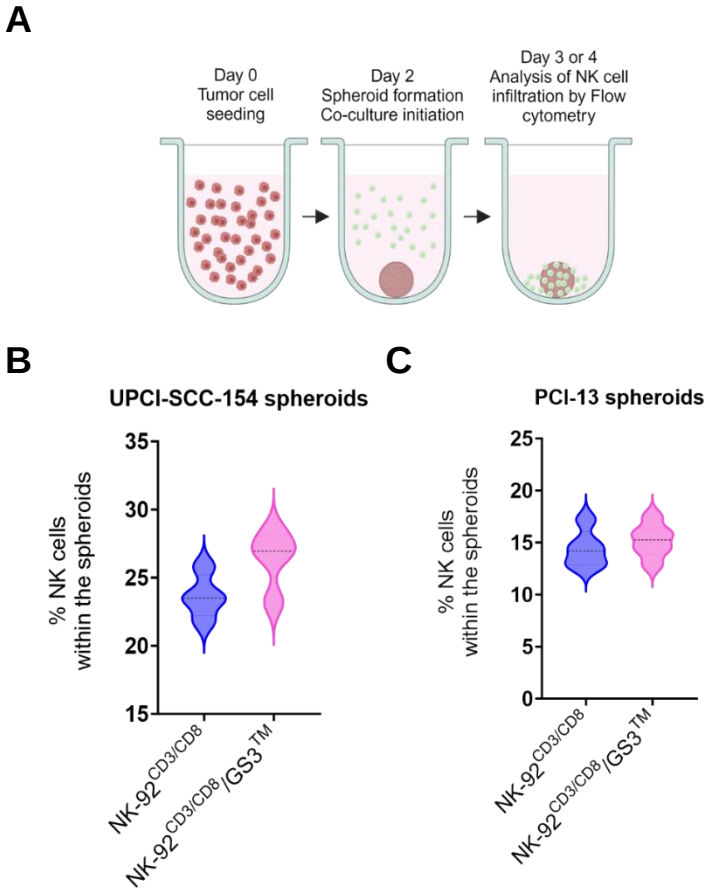

Figure 10 - NK-92$^{CD3/CD8}$/GS3-mWas cells and NK-92$^{CD3/CD8}$ cells present similar infiltration capacity

(A) Experimental protocol of UPCI-SCC-154 or PCI-13 spheroids co-culture with NK-92$^{CD3/CD8}$ cells or NK-92$^{CD3/CD8}$/GS3-mWas cells. **(B)** Quantification of NK cells infiltration using the CellProfiler software.
Results are shown as the mean ± SD. Mann-Whitney U test was applied to compare two independent groups.

4.1.4.2 Constitute expression of the GS3^{TM} fusion protein in NK-92$^{CD3/CD8}$ cells lead to increased Heparanase enzymatic activity, and cytokine release upon activation

A new strategy was adopted, in which the intracellular mWasabi was removed from the construct and a Myc-tag was added to the N-terminus of the GS3, linked at its C-terminus to the CD28 hinge and transmembrane domains (Fig. 11A). The Myc-tag was added to facilitate the detection of the fusion protein in the stable transfected cells for the sorting step (Fig. 11B).

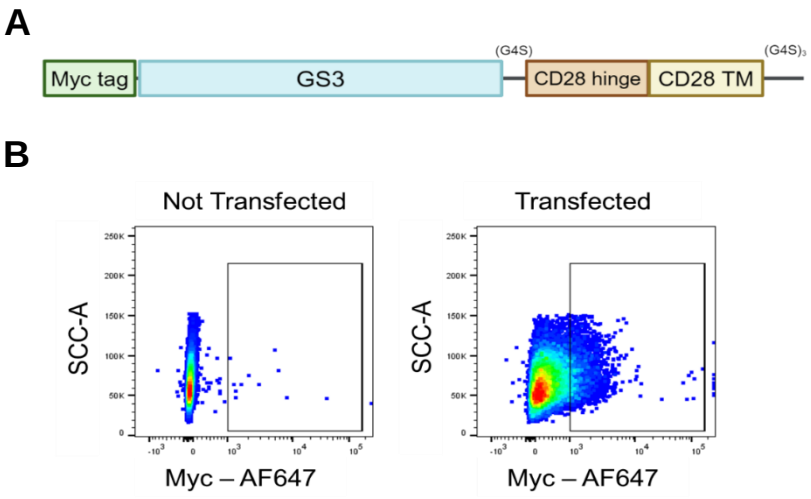

Figure 11 - Myc-GS3-CD28TM fusion gene construct and NK-92$^{CD3/CD8}$/GS3^{TM} sorting strategy

(A) Schematic representation of the Myc-GS3 fusion gene: [Myc-GS3-CD28hinge-CD28TM] used to generate the NK-92$^{CD3/CD8}$/GS3^{TM} cell line. **(B)** Gating strategy for sorting of NK-92$^{CD3/CD8}$/GS3^{TM} cells two weeks after electroporation.
Results obtained in collaboration with I. Quiros-Fernandez. E. Arias Romero and A. Cid-Arregui.

After sorting and expansion of NK-92$^{CD3/CD8}$/GS3^{TM} cells, the analysis of GS3-CD28TM expression was performed using the same three strategies applied for the first construct. By conventional FC staining, using the Hpa 733 polyclonal antibody to detect HPSE and GS3^{TM}, it was observed that the NK-92$^{CD3/CD8}$/GS3^{TM} cells presented a 4-fold higher MFI than the non-transfected NK-92$^{CD3/CD8}$ cells (Fig. 12A). This significant increase was confirmed by imaging-FC (Fig. 12B-C). Additionally, I could also assess HPSE/GS3^{TM} expression throughout the cell surface (Fig. 12B). Furthermore, NK-92$^{CD3/CD8}$/GS3^{TM} cells presented a 3-fold higher HPSE

enzymatic activity compared to the activity detected in non-transfected NK-92$^{CD3/CD8}$ cells (Fig. 12D), indicating that the desired increase in GS3^{TM} surface expression on NK-92$^{CD3/CD8}$ cells was successful.

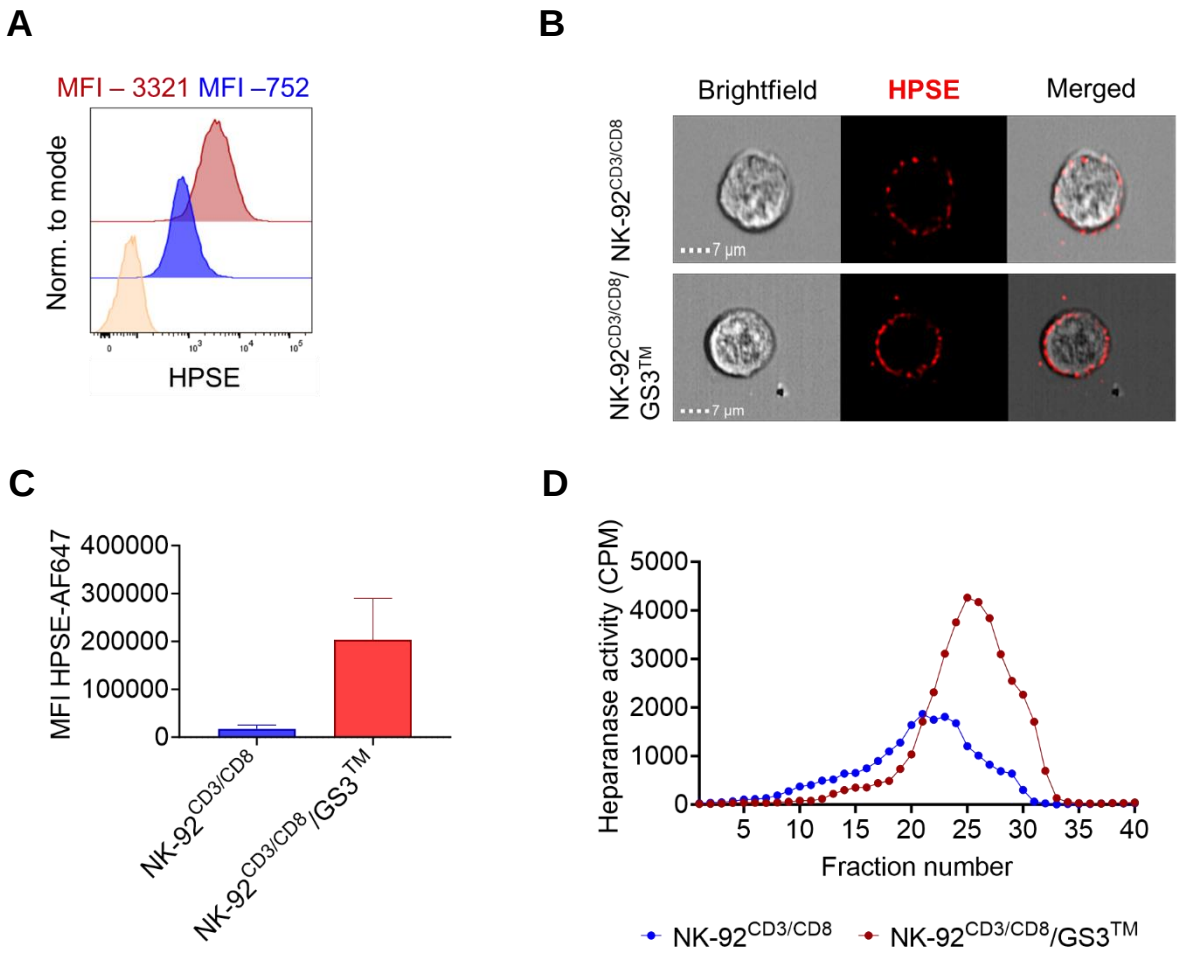

Figure 12 - NK-92$^{CD3/CD8}$/GS3^{TM} cells have higher Heparanase expression and higher Heparanase enzymatic activity

(**A**) FC analysis of HPSE and GS3^{TM} surface expression on NK-92$^{CD3/CD8}$/GS3^{TM} and NK-92$^{CD3/CD8}$ cells after staining with the Hpa 733 polyclonal antibody. Histograms represent the 2Ab only control (orange curve), NK-92$^{CD3/CD8}$ (blue curve) and the NK-92$^{CD3/CD8}$/GS3^{TM} cells (red curve). Results are from of one representative experiment. (**B**) Surface distribution of HPSE and GS3^{TM} on NK-92$^{CD3/CD8}$ and NK-92 $^{CD3/CD8}$/GS3^{TM} cells stained with the Hpa 733 polyclonal antibody and analyzed by imaging-FC. Illustrative pictures are shown for the brightfield and AF647 (702/85) channels. (**C**) Quantification of HPSE/GS3^{TM}. Results are shown as the mean ± SD. (n = 1 of three independent experiments). Mann-Whitney U test was applied to compare two independent groups. (**D**) HPSE activity measured in NK cell lysates that were incubated for 18 hours on sulfate-labeled ECM dishes. Representative results of two independent experiment are shown (Results obtained by Malik Farhoud at the Technion Institute in Israel). No statistical analysis was performed.

To test whether the constitutive expression of the GS3^{TM} fusion protein on the surface of NK-92$^{CD3/CD8}$ cells would influence the surface expression of several important membrane proteins, an extensive panel of lineage-specific NK receptors was analyzed (Fig. 13, Supplementary fig. 1). The expression of CD56, NKp30, NKG2A and KIR2DL4 was similar between the two analyzed cell lines (Fig. 13). Moreover, the expression of NKp44, NKp46 and NKG2D was slightly lower in the NK-92$^{CD3/CD8}$/GS3^{TM} cells when compared to non-transfected NK-92$^{CD3/CD8}$ cells (Fig. 13). No differences were observed in the expression levels of the remaining receptor analyzed (Supplementary fig. 1). Additionally, the basal activation status of the NK-92$^{CD3/CD8}$/GS3^{TM} in comparison to the parental cell line NK-92$^{CD3/CD8}$ cells was analyzed to understand if the insertion of the GS3^{TM} was promoting any changes in the cells. Similar low levels of CD69 expression were found between the two cell lines (Fig. 13), suggesting that the basal activation status NK-92$^{CD3/CD8}$ was maintained upon insertion of the GS3^{TM}.

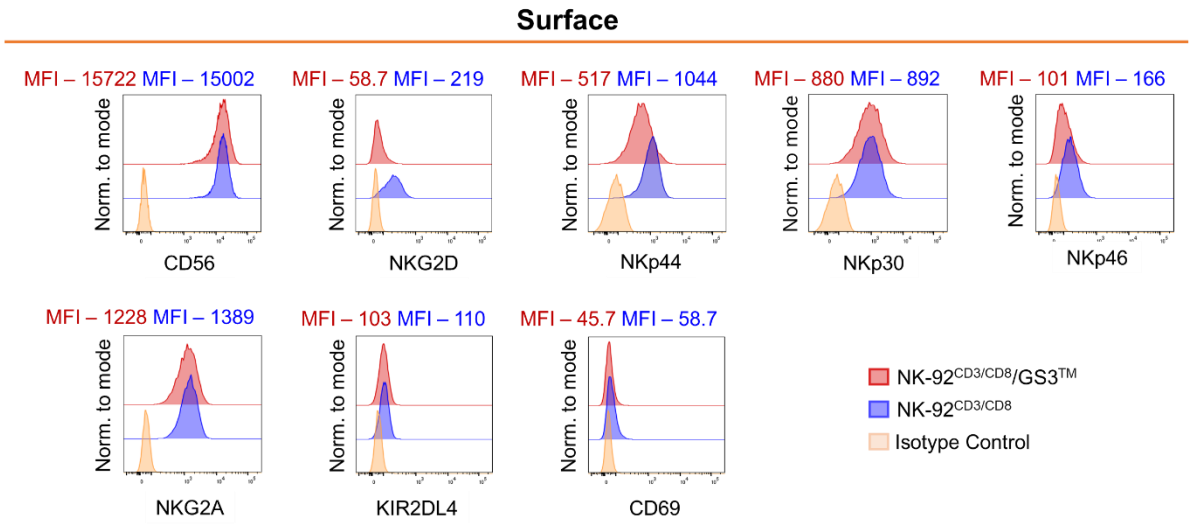

Figure 13 - Characterization of flow cytometric profile of NK-92$^{CD3/CD8}$/GS3^{TM}

Surface receptors were stained on live cells with the indicated antibodies. Histograms are normalized to the mode. Results of three independent experiment are shown as MFI of each condition. No statistical analysis was performed.

Finally, I investigated whether the constitutive expression of the GS3^{TM} fusion protein would modulate the activation capacity of NK-92$^{CD3/CD8}$ cells. For that, NK cells were stimulated with LPS or co-cultured with target tumor cells. It was observed that the NK-92$^{CD3/CD8}$/GS3^{TM} cells presented a 0.5 fold increase in IFNg, IL-2 and CCL1 expression upon activation with LPS, when comparing with non-transfected NK-92$^{CD3/CD8}$ cells also stimulated with LPS (Fig. 14A). GM-CSF expression increase significantly in both stimulated and unstimulated NK-92$^{CD3/CD8}$/GS3^{TM} cells, when comparing to the expression of the non-transfected NK-92$^{CD3/CD8}$ cells in the same conditions (Fig. 14A).

Degranulation is a known hallmark of NK cell activation [75]. When I looked at the expression of the degranulation marker CD107a, NK-92$^{CD3/CD8}$/GS3^{TM} cells plate alone presented a higher basal expression of this marker, comparing to the expression of NK-92$^{CD3/CD8}$ cells in the same condition (Fig. 14B). This increased expression of CD107a expression was also verified upon co-culture with target cells (Fig. 14B). Moreover, a significantly higher expression of CD107a by NK-92$^{CD3/CD8}$/GS3^{TM} cells was observed upon co-culture with FaDu cells (1.5 fold) when compared with of NK-92$^{CD3/CD8}$/GS3^{TM} cells co-cultured with UPCI-SCC-154 cells (1 fold) (Fig. 14B). This correlates with the observation that FaDu cells presented higher expression levels of NKG2D ligands, an important NK activation receptor (Supplementary Fig. 3).

These results suggest that the constitute expression of the GS3^{TM} fusion protein in NK-92$^{CD3/CD8}$ cells promotes a phenotype more prone to activation.

Overall, the results of the characterization of NK-92$^{CD3/CD8}$/GS3^{TM} cell line support that arming NK-92$^{CD3/CD8}$ with GS3^{TM} on the cell surface is translated into an increased HPSE expression and activity.

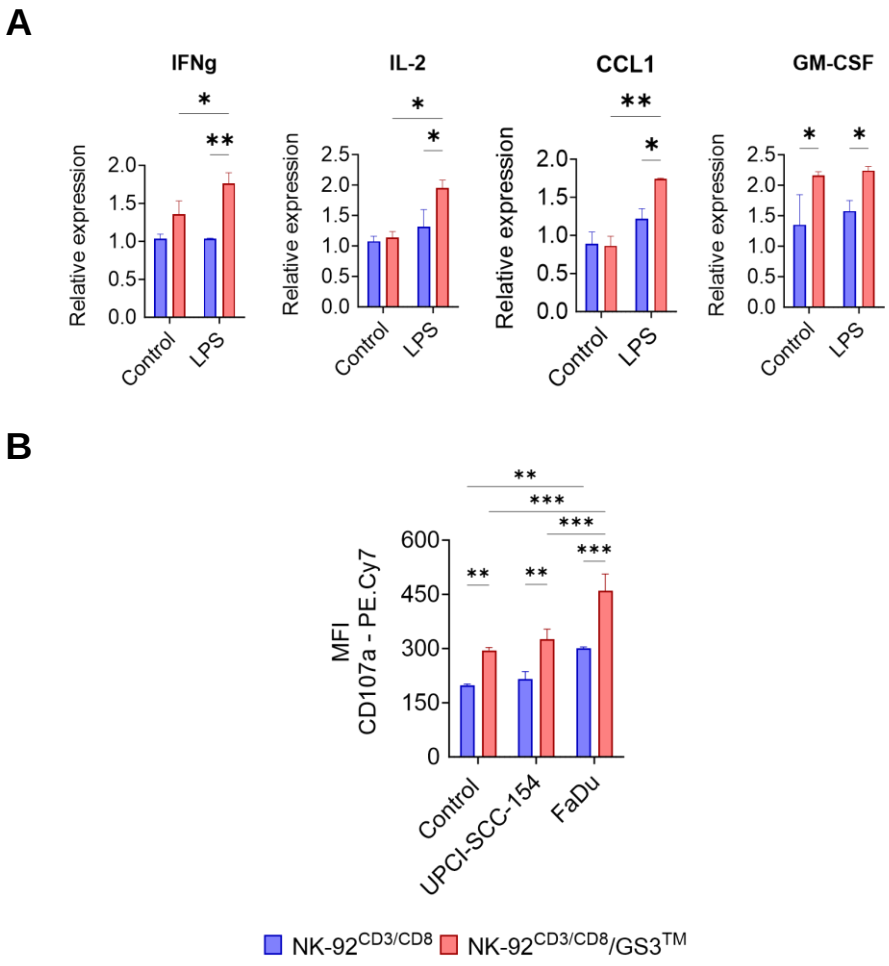

Figure 14 - NK-92$^{CD3/CD8}$/GS3^{TM} cells are prone to activation upon stimulation with LPS and co-culture with tumor cells

(A) Cytokine and chemokine expression during resting state and upon stimulation with LPS (Results obtained in collaboration with Soaad Soboh at the Technion Institute in Israel). **(B)** Surface expression of degranulation maker CD107a in NK-92$^{CD3/CD8}$ cells and NK-92$^{CD3/CD8}$/GS3^{TM} cells upon 24 h co-culture with HNSCC cell lines. Cell were stained with CD107a antibody and analyzed by FC.

Results are shown as the mean ± SD (n=3). Statistics: * p-value <0.05; ** p-value <0.01; *** p-value <0.001. Two-way ANOVA was applied to compare two independent groups with repeated measures and statistical testing of multiple groups was performed with the Tukey's multiple comparison test.

4.1.4.3 Constitute expression of the GS3^{TM} fusion protein promotes enhanced migration capacity through ECM

The next step was to test if the GS3^{TM} constitutive expression on the cell surface of NK cells and the consequent higher HPSE enzymatic activity would be translate into enhanced migration and infiltration capacity. To this end, a transmigration assay was performed (Fig. 15A). The number of NK-92$^{CD3/CD8/}$GS3^{TM} cells present in the lower chamber was significantly higher than that of the non-transfected NK-92$^{CD3/CD8}$ cells incubated under the same conditions (Fig. 15B).

These results suggest that GS3^{TM} promotes increased migration capacity of cells through the ECM.

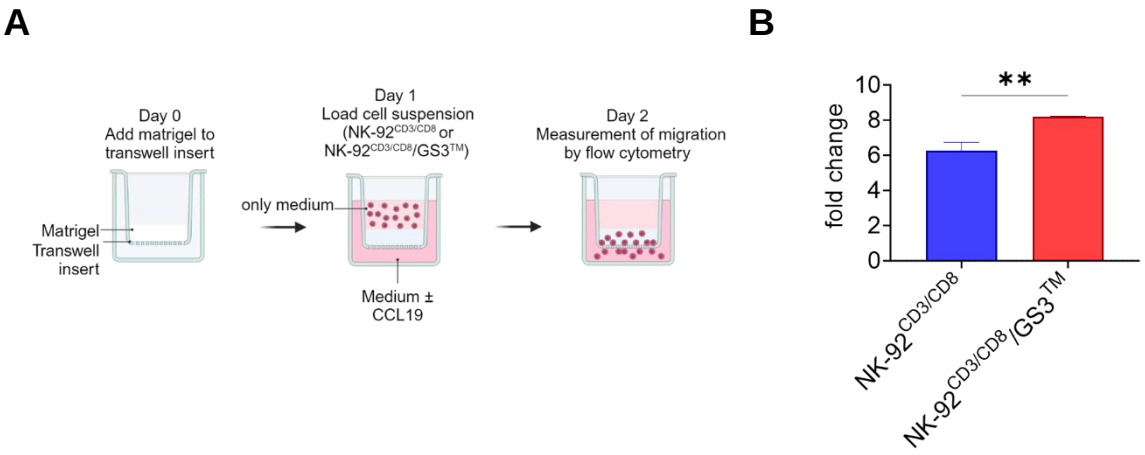

Figure 15 - NK-92$^{CD3/CD8}$/GS3^{TM} cells have enhanced migration capacity through ECM *in vitro*

(A) Transwell migration assay of NK-92$^{CD3/CD8}$ or NK-92$^{CD3/CD8}$/GS3^{TM} cells toward medium with CCL19. **(B)** The number of migrated cells was determined as the fold change between the +CCL19 migrated cells and the control migrated cells.

Results are shown as the mean ± SD (n=3). Statistics: ** p-value <0.01. Unpaired t test was applied to compare two independent groups.

4.1.4.4 Constitute expression of the GS3^{TM} fusion protein promotes enhanced infiltration into tumor spheroids

NK cells infiltration capacity was assessed in 3D structures known as tumor spheroids, which resemble more closely the state of actual tumors than cells cultured in monolayers. FaDu tumor spheroids were generated and co-cultured with NK-92$^{CD3/CD8}$ cells and NK-92$^{CD3/CD8}$/GS3^{TM} cells for 24 h (Fig. 16A). NK infiltration was analyzed by confocal microscopy (Fig. 16A). NK-92$^{CD3/CD8}$/GS3^{TM} cells were found more evenly distributed throughout the tumor spheroid sections (Fig. 16B), while the NK-92$^{CD3/CD8}$ cells were found mainly in the periphery of the sections (Fig. 16B). The quantification of NK cells infiltration was in agreement with the previous result, since a significantly increased number of NK-92$^{CD3/CD8}$/GS3^{TM} cells was found within the FaDu spheroids in comparison to the number of non-transfected NK-92$^{CD3/CD8}$ cells (Fig. 16C).

These findings demonstrate that the constitutive expression of GS3^{TM} on the surface of NK-92$^{CD3/CD8}$ cells is increasing their infiltration capacity into FaDu spheroids.

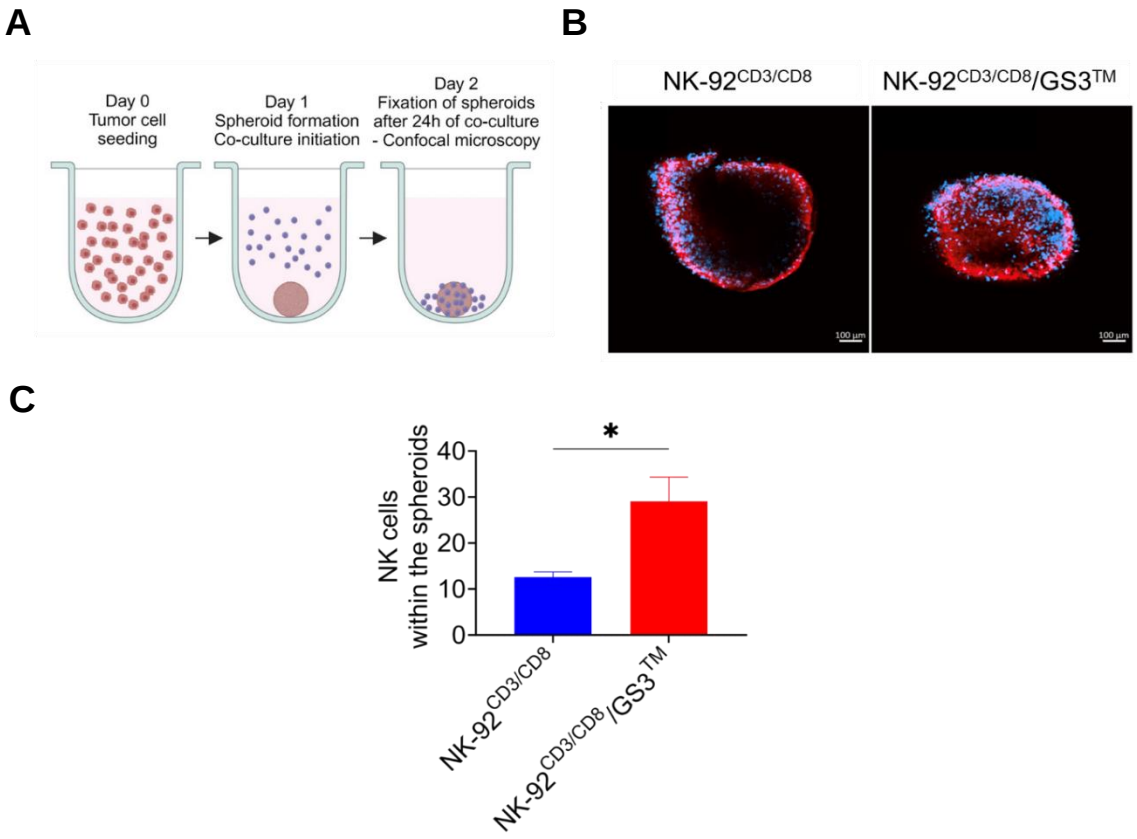

Figure 16 - NK-92$^{CD3/CD8}$/GS3^{TM} cells present higher capacity of infiltration into FaDu spheroids

(A) Experimental protocol of FaDu spheroids co-culture with NK-92$^{CD3/CD8}$ cells or NK-92$^{CD3/CD8}$/GS3^{TM} cells. **(B)** Representative images of the same stack showing NK-92$^{CD3/CD8}$ cells or NK-92$^{CD3/CD8}$/GS3^{TM} cells after 24h of co-culture with FaDu spheroids. Z-Stack pictures in the red (target cells), violet (effector cells) channel were taken using a 10X objective. Scalebar – 100 µm. **(C)** Quantification of NK cells infiltration. Identification and quantification of the NK cells (intensity of blue channel) was performed with the CellProfiler software. Results are shown as the mean ± SD (n=3). Statistics: ** p-value <0.01. Unpaired t test was applied to compare two independent groups.

To assess the kinetics of NK cell infiltration over time, spheroids were generated with the FaDu/mWasabi cells (Fig. 17A). Co-culture with NK-92$^{CD3/CD8}$ or NK-92$^{CD3/CD8}$/GS3^{TM} cells was followed by live-cell confocal fluorescence microscopy for 24 h (Fig. 17A-B). Z-stack images of different time points showed that, while NK-92$^{CD3/CD8}$/GS3^{TM} cells are distributed throughout the entire structure, infiltrating the FaDu/mWasabi spheroids deep into the core, NK-92$^{CD3/CD8}$ cells are mainly located in the periphery of the spheroid (Fig. 17B-C). Moreover, as early as 6 h time point, a higher decrease in spheroid area was observe in the spheroids co-cultured with NK-92$^{CD3/CD8}$/GS3^{TM} cells (Fig. 17B). This decrease continues until the end point of the experiment (Fig. 17B).

To quantify the number of infiltrating NK cells, images were applied to an automatic image analysis pipeline, using the Cell profiler software (Supplementary Fig. 2). After 24 h of co-culture it could be observed a significant increase in the number of NK-92$^{CD3/CD8}$/GS3^{TM} cells that had infiltrated the FaDu/mWasabi spheroids, in comparison to NK-92$^{CD3/CD8}$ cells (Fig. 17D). The difference in infiltration capacity between the two cell lines was first verified after 18 h after the start of the experiment (Fig. 17D).

These results demonstrated the enhanced capacity of NK-92$^{CD3/CD8}$ cells expressing the GS3^{TM} fusion protein to move through the compacted 3D structure of FaDu tumor cells.

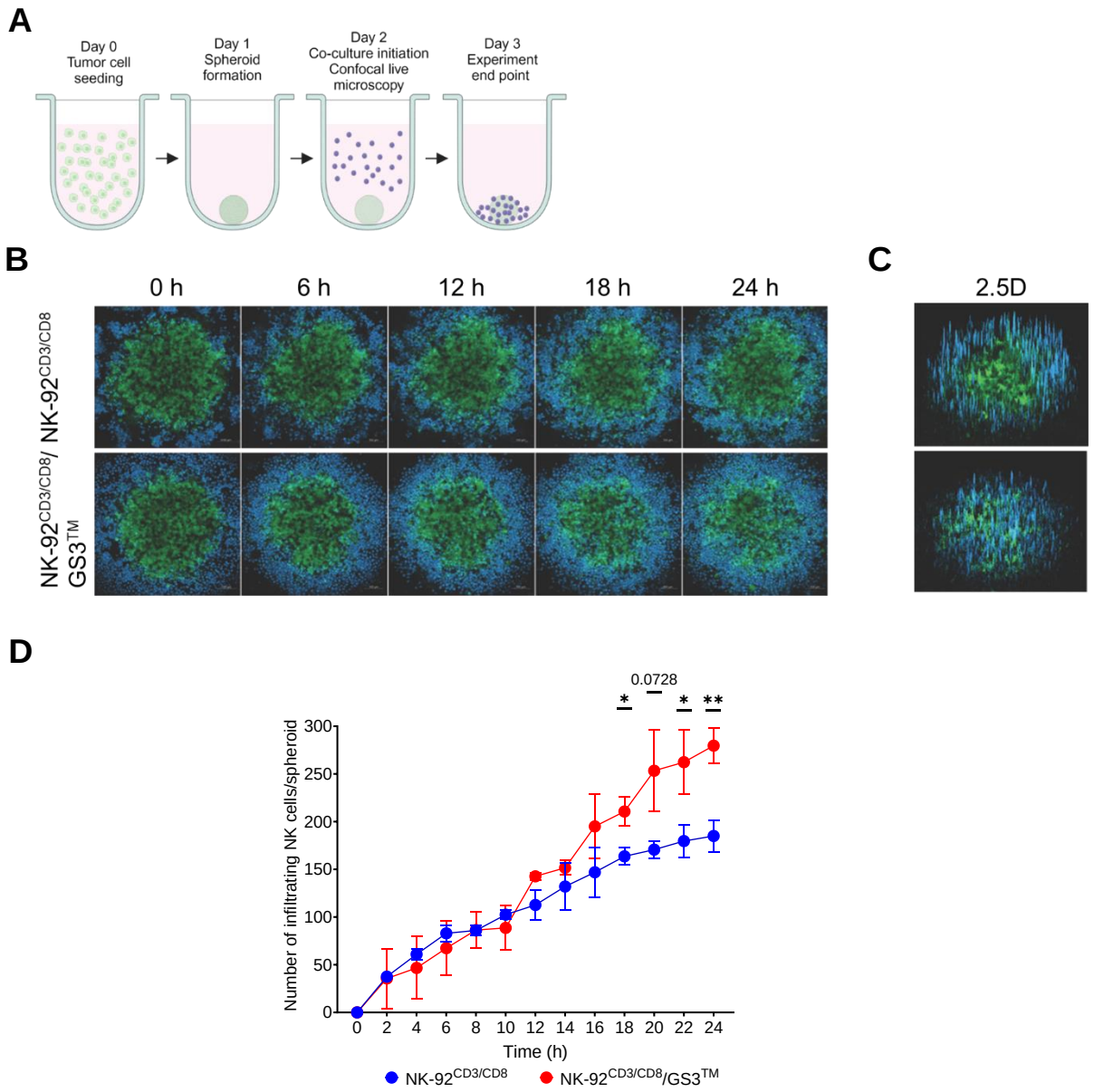

Figure 17 - Live microscopy analysis of NK-92$^{CD3/CD8}$/GS3^{TM} infiltrating into FaDu/mWasabi spheroids

A) Experimental protocol of Infiltration of NK-92$^{CD3/CD8}$/GS3^{TM} cells and NK-92$^{CD3/CD8}$ cells into FaDu/mWasabi spheroids. (**B**) Confocal images in the violet (NK cells) and green (FaDu/mWasabi cells) channels were taken every hour for 24 h using a 5X magnification. Representative images are shown for the co-cultures at the indicated time points. (**C**) Representative 2.5D images of the NK-92$^{CD3/CD8}$ and NK-92$^{CD3/CD8}$/GS3^{TM} cells distribution within the FaDu/mWasabi spheroids. (**D**) The number of infiltrating NK cells were quantified in a time-resolved manner and expressed as mean ± SD (n=3) using the CellProfiler software. Two-way ANOVA was applied to compare two independent groups with repeated measures across time and statistical testing of multiple groups was performed with the Šídák's multiple comparison test.

Results obtained by I. Quiros-Fernandez

A similar experiment was performed with UPCI-SCC-154/mWasabi spheroids but this time spheroids were generated with tumor cells and Geltrex™. Geltrex™ was used to increase the complexity of the 3D structures and to increase HPSE/GS3™ substrate, since it contains HSPGs. Co-cultures were followed as explained above, by live-cell confocal fluorescence microscopy. After 12 h of co-culture, it was observed that spheroids incubated with NK-92$^{CD3/CD8}$/GS3™ cells had significant lower diameters, when compared to the ones incubated with NK-92$^{CD3/CD8}$ cells (Fig. 18A-B). This difference in size is visible as early as 6 h after the start of the experiment (Fig. 18A-B). Moreover, a higher number of infiltrating NK-92$^{CD3/CD8}$/GS3™ cells were observed throughout the experiment (Fig. 18C).

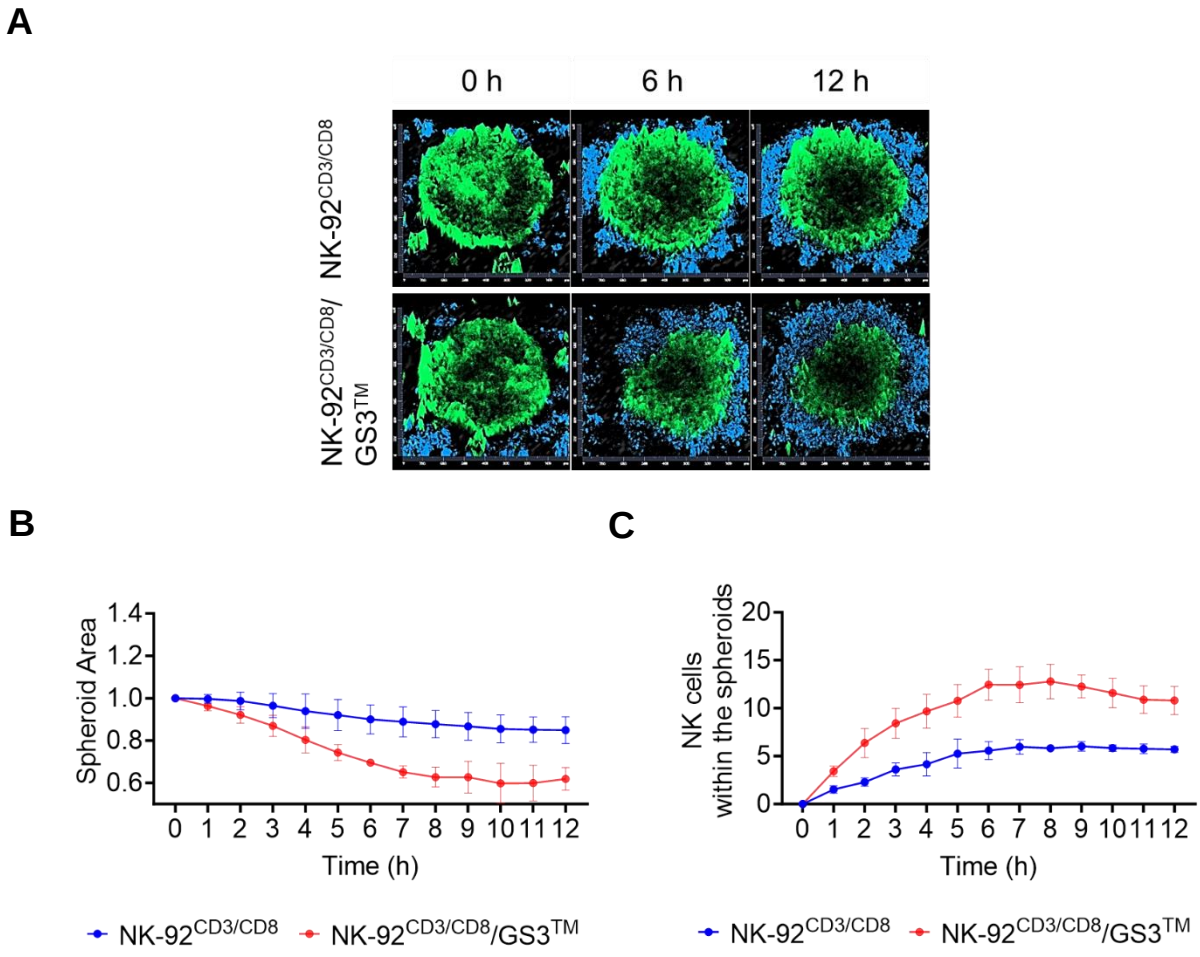

Figure 18 - Live microscopy analysis of NK-92$^{CD3/CD8}$/GS3^{TM} cells infiltrating into UPCI-SCC-154/mWasabi spheroids

(A) Representative 2.5D images, generated with the ZEN image analysis software, are shown for the co-cultures of NK-92$^{CD3/CD8}$ and NK-92$^{CD3/CD8}$/GS3^{TM} cells with UPCI-SCC-154/mWasabi spheroids at the indicated time points. Pictures in the violet (NK cells) and green (UPCI-SCC154/mWasabi cells) channels were taken hourly during 12 h using a 10X objective. (B) Quantification of spheroid area. Identification of primary object (spheroid) and quantification of spheroid area was performed with the CellProfiler software. (C) Quantification of NK cells infiltration. Identification and quantification of the NK cells (intensity of blue channel) was performed with the CellProfiler software.

Results are shown as the mean ± SD (n=5). Two-way ANOVA was applied to compare two independent groups with repeated measures across time and statistical testing of multiple groups was performed with the Šídák's multiple comparison test.

4.1.4.5 Constitute expression of the GS3^{TM} fusion protein promotes enhanced infiltration *in vivo*

So far, the NK-92$^{CD3/CD8}$/GS3^{TM} cells showed enhanced infiltration capacity cells in *in vitro* settings. Thus, the next step was to investigate their ability to infiltrate *in vivo*. Towards this goal, NK-92$^{CD3/CD8}$/GS3^{TM} were injected tumor bearing immunodeficient mice (Fig. 19A). A reduction in tumor volume in mice receiving NK-92$^{CD3/CD8}$/GS3^{TM} cells (significant at day 23) was observed, in comparison to those receiving NK-92$^{CD3/CD8}$ cells (mean 310.7 ± 131.6 mm^3 vs 681.4 ± 153 mm^3; p=0.0177) (Fig. 19B). Likewise, a significant reduction on tumor weight was observed at the endpoint of the experiment, in mice infused with NK-92$^{CD3/CD8}$/GS3^{TM}, when compared to mice infused with NK-92$^{CD3/CD8}$ cells (mean 1.1±0.2 g vs 1.71±0.3 g; p=0.0030) (Fig. 19C).

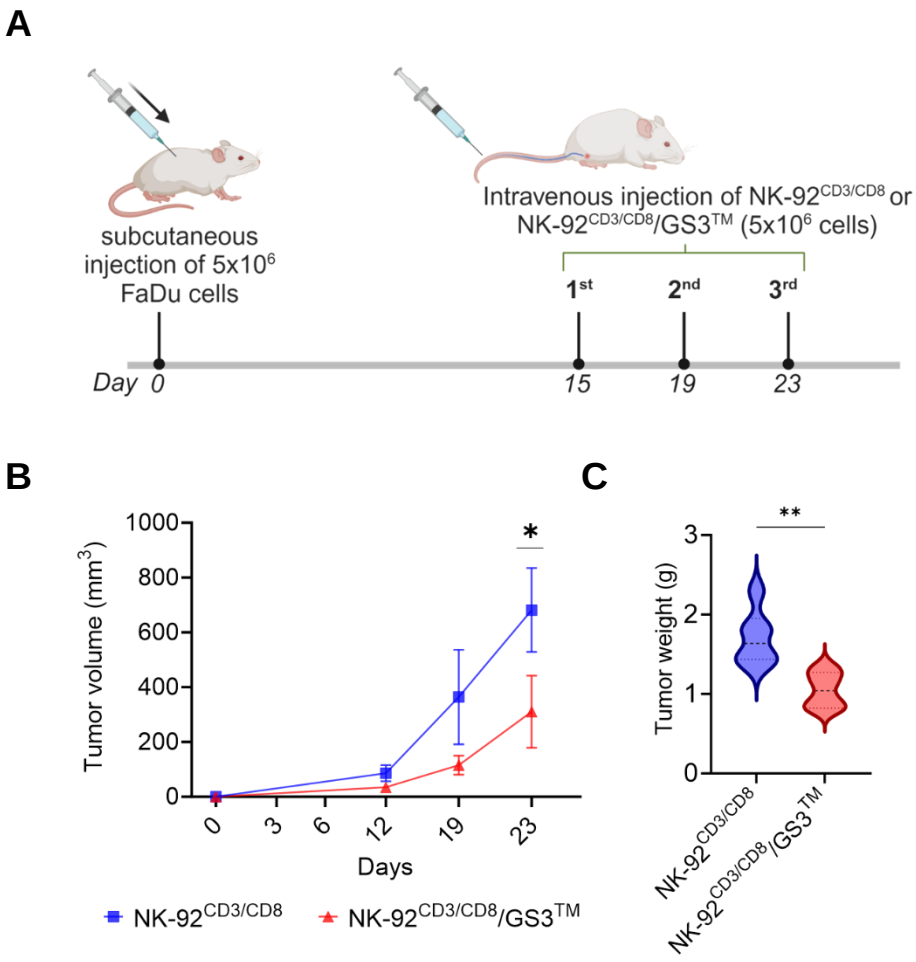

Figure 19 - Tumors from mice injected with NK-92$^{CD3/CD8}$/GS3^{TM} cells present lower volume and size

(A) Experimental protocol of the xenograft mouse model used. (B) Tumor volume was calculated from external caliper measurements, every 3-4 days. Two-way ANOVA was applied to compare two independent groups with repeated measures across time and statistical testing of multiple groups was performed with the Šídák's multiple comparison test. (C) Comparison of the weight of the tumors at the end of the experiment. Mann-Whitney U test was applied to compare two independent groups.

Neta Ilan and I performed the injections of tumor cells into the immunodeficient mice. NK cell infusions and processing of tumors were done by Neta Illan and Soaad Soboh at the Technion Institute in Israel.

The next step was to analyze the presence of NK-92$^{CD3/CD8}$/GS3^{TM} cells or non-transfected NK-92$^{CD3/CD8}$ cells in the tumors.

SCID mice (SCID stands for severe combined immunodeficiency disease), possess a genetic autosomal recessive mutation designated Prkdc^{scid}, which promotes a severe immunodeficiency that genetically affects the development of T and B lymphocytes [76, 77]. Moreover, the NOD/SCID mice are mice in which the SCID mutation has been transferred onto a non-obese diabetic background (NOD), resulting in additional defective NK cell function [78]. As a result, interference from the endogenous mouse NK cells in this experiment is not anticipated.

At end point, total RNA was extracted from a portion of the tumors and the amount of tumor infiltrating NK cells was assessed by RT-qPCR using a set of primers specific for CD56, a human NK cell lineage marker. Since mouse NK cells don't express CD56, this assay would only quantify the NK-92$^{CD3/CD8}$/GS3^{TM} cells and NK-92$^{CD3/CD8}$ cells in the samples. It is important to mention that these two cell lines express comparable levels of CD56, as shown in Figure 13. Notably, the CD56 expression was increased by 2-fold in samples from mice that had been injected with NK-92$^{CD3/CD8}$/GS3^{TM}, in comparison to the expression of NK-92$^{CD3/CD8}$ cells (Fig. 20A).

Moreover, tumor sections were stained with CD56 antibody and scanned with the Zeiss Axio Scan.Z1, which automatically scans complete sections. Tumors from mice treated with NK-92$^{CD3/CD8}$/GS3^{TM} showed significantly higher numbers of CD56+ cells compared to those injected with NK-92$^{CD3/CD8}$ cells (Fig. 20B).

Taken together, these results show that the constitutive expression of GS3^{TM} fusion protein on the surface of NK-92$^{CD3/CD8}$ cells is giving an advantage in their infiltration capacity and could be potentially used as a tool to improve adoptive cellular therapies that lack efficacy due to their decreased capacity to overcome the tumor microenvironment.

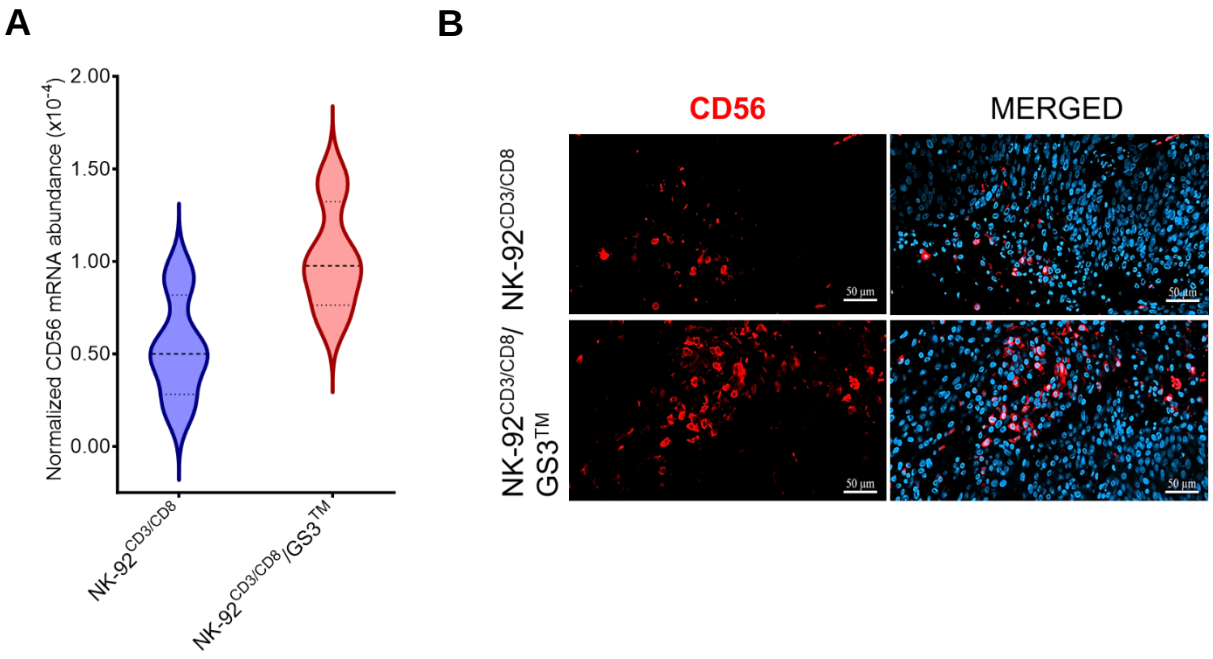

Figure 20 - NK-92$^{CD3/CD8}$/GS3^{TM} cells present higher capacity of infiltration into tumor xenograft

(A) Total RNA was extracted from the tumors and the corresponding cDNA was subjected to RT-qPCR, using a specific set of primers for CD56. Results were normalized with vehicle values (Graph from I. Quiros-Fernandez). **(B)** Representative microscopic images of 5-µm tumor sections from animals injected with NK-92$^{CD3/CD8}$ cells (top row) or NK-92$^{CD3/CD8}$/GS3^{TM} cells (bottom row). Sections were stained with anti-CD56 antibody (red) and with DAPI (blue). Scale – 50 µm (section staining and images obtained by R. Süleymanoglu and A. Cid-Arregui). Results are shown as the mean ± SD. No statistical analysis was performed.

5 Discussion

Immune cells are known as an important player within the TME and the presence of a higher number of immune cells, such as T and NK cells, is correlated with a longer overall patient survival in several types of cancer [79]. To overcome the mechanisms by which cancer cells evade immune detection, multiple immunotherapies are being developed, such as ACT, with CAR-T cell therapies having a considerable success in hematological malignancies. However, the application of ACT in solid tumors faces several limitations including target antigen heterogeneity and antigen escape, immunosuppressive tumor microenvironment and immune cell trafficking and infiltration [80].

In solid tumors, the clear identification of a target tumor antigen is a difficult process, since normally these tumors have high intratumoral antigen heterogeneity, resulting from genomic instability [81]. Additionally, the selected tumor antigen needs to have a much higher expression in the tumor than in healthy cells to avoid unwanted toxicity (on-target/off-tumor effects) [80]. Another challenge that limits the clinical efficacy of these therapies are the TME immunosuppressive properties. The entry of effector cells is physically blocked by the tumor associated stroma, such as fibroblasts and the ECM. Thus, one of the requirements for a successful cell therapy is the capacity of the cells to migrate and infiltrate solid tumor, thus surpassing ECM barriers, through the degradation of ECM components, such as HSPGs [82]. Moreover, the migration and function of cytotoxic immune cells towards the tumor is overshadowed by the tumor aberrant vasculature, dysregulation of adhesion molecules and production of immune-dampening chemokines gradients. All this supports the recruitment of immunosuppressive cells and decreases the lifetime and cytotoxicity capacity of ACT [83]. Strategies to overcome all these barriers are being developed.

This thesis is focused on the improvement of effector cells infiltration into solid tumors, by genetically modifying NK cells to constitutively express an active form of Heparanase (GS3) on the cell surface as an integral membrane protein (GS3^{TM}). Moreover, HPSE is highly expressed by immune cells and has been described to be important for to facilitate the migration and infiltration of macrophages, T cells and dendritic cells. However, little is known about the role of this enzyme in NK cells. Thus, I also investigated the expression of HPSE upon NK cell activation and its role in NK cell infiltration.

5.1 Heparanase expression in NK cells

HPSE expression by immune cells can be can be modulated by activation or inhibitory stimuli [61]. Despite existing evidence that HPSE is required for proper NK cell activation and cytotoxicity [66], this data derives from one study only, supporting the necessity to further investigate the roles of HPSE in NK cells.

My results showed that upon activation with a chemical activation cocktail (PMA + Ionomycin), HPSE expression decreased, on the surface of primary human NK cells within the PBMCs cell suspension or in an enriched NK population setting. Moreover, indirect activation of primary NK cells promoted decay of HPSE expression over time. Caruana et al had already demonstrated that the stimulation of primary CD8 T cells with OKT3 and anti-CD28 antibodies leads to the loss of HPSE expression [65]. The decrease in HPSE expression is verified as early as 18h after stimulation and it is maintained in 15-day period that the cells are maintained in culture [65].

The expression of HPSE upon activation with PMA and Ionomycin was different between primary NK cells and NK-92$^{CD3/CD8}$ cells, with a decrease in expression only being verified in primary NK cells. This could be explained by the differences in NK populations their capacities to be activated and consequently, which could affect the HPSE expression upon chemical activation. While peripheral blood primary NK cells are mostly CD56^{dim} cells, associated with high cytotoxic capacity, NK-92$^{CD3/CD8}$ cells are CD56^{bright} cells, described as immunomodulatory and more prone for activation that induces cytokine secretion [84], like the one resulting from the incubation with PMA and Ionomycin. Interestingly, when NK-92$^{CD3/CD8}$ cells were co-cultured with target tumor cells, the HPSE surface expression decrease. This could also indicate that different stimuli lead to specific modulation of HPSE in NK-92$^{CD3/CD8}$ cells.

To study NK cell infiltration capacity, I isolated primary NK cells from HPSE-KO [67] and WT mice spleens and incubated these cells with TC-1 spheroids. NK cells lacking HPSE showed substantial reduction in the infiltration capability, which suggests that HPSE is required for mobility of NK through tumor structures. Similar results have been described for macrophages, while using the same HPSE-KO model [63]. The Vlodasvsky's group showed that macrophages populate the entire lung carcinoma tumor mass in wild-type mice xenografted with Lewis lung carcinoma cells [63]. In contrast, macrophages accumulate at the tumor periphery in HPSE-KO mice [63]. In CD8+ T cells, the loss of HPSE is accompanied by decreased capacity to migrate

through ECM *in vitro* [65]. The data supports that HPSE is required for the correct infiltration capacity of several immune populations.

Caruana et al. went further in the study of HPSE in T cells and showed that when the CD8+ T cells were genetically engineered to co-express a CAR and HPSE, they presented improved capacity to degrade ECM *in vitro* and show enhanced tumor infiltration in xenograft tumor models, associated with improved overall animal survival, when compared to the activity of T cells only engineered with the CAR [65]. However, it is important to consider that the strategy of using HPSE-overexpressing immune cells that are releasing HPSE to the TME could potentially have negative implications for tumor progression. This can happen due to cancer cells using the higher presence of HPSE in their favor and promote pro-tumor cell signaling, tumor cell mobility through the ECM and metastasis. Thus, taking in consideration the results obtained so far and the knowledge about HPSE, this thesis proposed to validate a strategy to promote NK cell infiltration by increasing HPSE expression on NK cell surface. This would be accomplished by transfecting NK cells with a membrane bound constitutively active HPSE.

5.2 Strategy to improve NK cell infiltration

The first step for an optimal treatment efficacy is that the adoptively transferred cells must access and abundantly infiltrate the tumor mass [85]. Thus, several research groups have been focusing on developing new strategies to improve NK and T cell infiltration into solid tumors.

In preclinical tumors models, several strategies that aimed improving NK cell recruitment to the TME, proved to be effective [85, 86]. These strategies focus mainly on overexpressing chemokine receptors associated with enhancing NK cell migratory capacity [85, 86]. For instance, overexpression of CXCR2 in primary human NK cells, by retroviral transduction, lead to enhanced migration capacity towards renal cell carcinoma supernatants [87]. Another study showed that by overexpressing both CXCR2 and IL-2 in NK-92 cells, these cells were present in higher numbers in the tumor sites, with inhibition of tumor growth *in vivo* [88]. Ng YY et al genetically engineered NK cells to co-express the CXCR1 and a CAR targeting tumor associated NKG2D ligands. These cells showed enhanced infiltration into ovarian peritoneal carcinoma xenograft [89]. In the cases mentioned above, results are dependent on the expression of chemokine ligands by tumor cells, which are in constant dynamic change according to the tumor context [90]. This can then impact the outcome of a clinically viable protocol.

Regarding T cells, strategies to overcome the lack of infiltration are focused on targeting the tumor vasculature and the ECM, among others [91]. CAR-T cells targeting antigens overexpressed in tumor vasculature, such as VEGFR1, PSMA and TEM8, have been developed to promote T cell extravasation and infiltration [92-94]. In these preclinical studies, authors observed ablation of tumors vessels and regression of tumor growth and tumor burden [92-94]. Several reports have also shown that targeting the tumor ECM can have successful results [95]. CAR-T cells engineered to target fibroblast activation protein, overexpressed by cancer-associated fibroblasts, inhibited tumor growth in mouse models and these animals presented significantly prolonged survival [96-98]. Moreover, CAR-T cells targeting a specific extra domain of fibronectin, an important ECM structural glycoprotein, inhibited the progression of tumors *in vivo* [99, 100].

In my thesis, the focus was on ECM rearrangement, through the degradation of HS side chains of HSPGs by HPSE. Combining the knowledge that HPSE is important for ECM remodeling and the results from my thesis which suggest that HPSE is important for NK cell infiltration, while also taking in consideration that tumor cells use the HPSE present in the TME for their advantage, a strategy to promote NK cell infiltration was developed.

As immune cell model, NK-92$^{CD3/CD8}$ cells [68] were chosen. These cells are a derivative of the NK-92 cell line [101], that express constitutively the human CD3 and CD8, thus also allowing the expression and further testing of TCRs and CARs [102]. The NK-92 cell line has been widely studied and developed for clinical use, with more than hundred cancer patients been treated so far with unmodified or genetically engineered NK-92 cells [101]. In the clinical studies conducted so far, the NK-92 cells and variants have been subjected to irradiation before infusion, since these cells derive from a leukemia [101].

Using NK-92$^{CD3/CD8}$ cells, the first approach to improve NK cell infiltration was to clone a fusion gene coding a protein composed of an N-terminal extracellular GS3, linked to a CD28 hinge and transmembrane domain and an intracellular monomeric green fluorescence protein (mWasabi, mWas).This first approach was not successful, since NK-92$^{CD3/CD8}$/GS3-mWas cells presented similar HPSE surface expression, surface distribution, enzymatic activity and NK cell infiltration capacity, comparing to the non-transfected NK-92$^{CD3/CD8}$ cells. A possible explanation for this situation is that the fusion protein is aggregating in the intracellular compartment, preventing the correct transport to the cell surface. However, this was not further investigated, and a new approach was taken. It is important to mention that the Hpa 733 polyclonal antibody used for the FC protocols detects both the pro-HPSE and the active form of HPSE [103]. Thus, since the only difference between these two cell lines is the transfection

with GS3-mWsabi fusion protein, the difference in HPSE expression should be translated into the expression of the GS3-mWsabi on the surface of the transfected cells. Nevertheless, a technique such as western blot could have been used to detect the expression of the GS3-mWsabi fusion protein.

In the second approach, the intracellular mWasabi protein was removed and a myc-tag was added to the N-terminus of the GS3, linked to a CD28 hinge and transmembrane domains (GS3^{TM}). This allowed to decrease the size of the fusion protein and avoid the possible aggregation that could be occurring with the first construct. NK-92$^{CD3/CD8}$/GS3^{TM} cells have higher HPSE expression, with the HPSE/GS3^{TM} protein being distributed throughout the cell surface. These cells also have higher HPSE activity compared to the non-transfected NK-92$^{CD3/CD8}$ cells.

The surface expression of the NKp44, NKp46 and NKG2D receptors was diminished in NK-92$^{CD3/CD8}$/GS3^{TM} cells, compared with that of the non-transfected NK-92$^{CD3/CD8}$ cell line. A possible explanation for the lower expression of NKp44, NKp46 and NKG2D is that the higher expression of active HPSE on NK-92$^{CD3/CD8}$/GS3^{TM} cell surface is promoting the shedding of membrane bound HSPGs and indirectly interfering with the expression of these receptors. HSPGs, such as syndecan-4, are expressed by NK cells and are reported to interact with NK receptors, serving as ligands/co-ligands, promoting their stabilization, modification, or shedding [104, 105]. Moreover, higher expression of HPSE in the microenvironment can promote HSPGs shedding of cell surface and consequently can alter receptor-HSPGs complexes and lead to reduce expression of these receptors [34, 106]. Both cell lines have high NKG2A expression and residual KIR2DL4 expression. These results are in accordance with what is described in literature, that the CD56^{bright} subset of NK cells expresses uniformly high CD94/NKG2A but lacks the expression of KIRs [22].

Despite having a decrease in NKp44, NKp46 and NKG2D expression, the activation capacities of NK-92$^{CD3/CD8}$/GS3^{TM} cells were preserved. NK and CD8+ T cells, the higher expression of degranulation proteins like CD107a, is associated with phenotype more prone for activation and cytotoxicity [107-109], which goes in accordance to the results presented in this thesis for NK-92$^{CD3/CD8}$/GS3^{TM} cells. Further studies could be performed to address this activation phenotype of NK-92$^{CD3/CD8}$/GS3^{TM} cells, such as the measurement of cytokine release (eg. IFNg) upon activation and co-culture with target cells. Interestingly, the co-culture of NK-92$^{CD3/CD8}$/GS3^{TM} cells with FaDu tumor cells lead to higher expression of CD107a than when these cells were co-cultured with UPCI-SCC-154 tumor cells. One explanation for this could be that FaDu cells express higher levels of NKG2D and NKp30 ligands than the UPCI-SCC-154,

leading to a higher activation of the NK cells. Different expression levels of NK cell ligand on cancer cell lines have been previously described and associated with NK cell activation and response [110, 111]. To further confirm this, the measurement of ligands expression to other important NK receptors could be assessed in tumor cells.

5.3 NK-92$^{CD3/CD8}$/GS3^{TM} cells have higher migration and infiltration capacity

Having a new cell line with increased active HPSE surface expression and enzymatic activity, I sought to know if this would be translated into an improved migration and infiltration capacity.

To assess NK cells migration, a transwell assay was used. A higher amount of NK-92$^{CD3/CD8}$/GS3^{TM} cells was able to degrade the matrix and migrate towards a chemoattractant, comparing to the non-transfected NK-92$^{CD3/CD8}$ cells. This result suggests that the GS3^{TM} fusion protein is giving an advantage to NK-92$^{CD3/CD8}$ cells, by increasing their migration capacity, through the cleavage of the HS side chains of HSPGs.

The most important evaluated feature to confirm the success of the GS3^{TM} fusion protein strategy was the NK cell infiltration capacity. To this end, co-cultures of NK-92$^{CD3/CD8}$/GS3^{TM} cells and NK-92$^{CD3/CD8}$ cells with HNSCC spheroids were conducted. NK-92$^{CD3/CD8}$/GS3^{TM} cells were found in higher number within the spheroids and promoted a decrease in spheroid size, which indicates that these cells have an enhanced infiltration capacity *in vitro*. By degrading the HS side chains of proteoglycans present in the surface of tumor cells, the GS3^{TM} fusion protein promoted changes in tumor cell-cell interactions and consequently cause tumor cells to desegregate, thus giving NK cells more access to tumors cells deeper into the 3D structure. Interestingly, the NK-92$^{CD3/CD8}$/GS3^{TM} cells infiltration and consequent decrease of spheroid size is seen at an earlier time point in the UPCI-SCC-154 experiments, compared to what was observed in FaDu co-culture experiments. One explanation for this is the increase in HPSE/GS3^{TM} substrate since UPCI-SCC-154 spheroids were generated with tumor cells and Geltrex^{TM}.

The experiments done *in vitro* in this thesis focused on the NK cells infiltration capacity. However, measurements of NK cells cytotoxicity upon co-cultures with target cells could have been performed to understand if by promoting more infiltration, the GS3^{TM} fusion protein is also inducing more cytotoxicity.

The next and final experiment was to determine if the NK-92$^{CD3/CD8}$/GS3^{TM} cells presented increased infiltration capacity *in vivo*. The injection of NK cells in tumor bearing mice is a suitable method to assess the real effects of NK cells at the tumor location [112]. Moreover, the repeated injection of these cells, like it was done in my thesis, promotes the enhancement and sustainment of therapeutic efficacy by maintaining cell functionality and persistence. This also better mimics the clinical scenario, where periodic NK cell infusions might be necessary for durable responses in patients [112]. The FaDu xenograft experiments in immunodeficient mice showed reduced tumor growth in mice treated with NK-92$^{CD3/CD8}$/GS3^{TM} cells, which were correlated with higher numbers of CD56 infiltrating cells into these tumors. The results from the *in vivo* xenograft experiment corroborate the higher infiltration capacity of NK-92$^{CD3/CD8}$/GS3^{TM} cells observed in the spheroid co-cultures. Even though, NK cells were injected in three different occasions the direct result of their infiltration capacity was only collected at the end point of the experience. To monitor the *in vivo* distribution of NK cells throughout the experiment, labelling of NK cells with contrast agents could be a solution. This technique was already applied in other studies to better understand NK cell behaviour [113, 114].

Taken together, the results from my thesis demonstrate that the GS3^{TM} fusion protein is giving an advantage to NK-92$^{CD3/CD8}$ cells, supporting the anti-tumor efficacy of these effector immune cells.

5.4 Concluding remarks and Future perspectives

The strategy to transfect NK-92$^{CD3/CD8}$ cells with a constitutively active membrane bound HPSE proved to be efficient in improving NK cell infiltration into tumor spheroids, as well as into xenograft tumors in immunodeficient mice. Moreover, my results suggest that HPSE is important for NK cell infiltration.

In this work, all experiments were conducted with non-irradiated NK-92$^{CD3/CD8}$ cells, which can proliferate indefinitely, since they derive from a leukemia. Thus, to allow the potential application of NK-92$^{CD3/CD8}$/GS3^{TM} cells in immunotherapy, similar experiments to the ones described in this work and suggested improvements should be performed with irradiated NK-92$^{CD3/CD8}$/GS3^{TM} cells. This is an important next step to understand if the higher HPSE expression, the higher enzymatic activity and the higher infiltration capacity are maintained after irradiation. Moreover, it would be of interest to test the GS3^{TM} fusion protein function in primary human NK cells.

Considering that enhancing tumor targeted cytotoxicity is always necessary, it would also be of interest to combine NK-92$^{CD3/CD8}$/GS3^{TM} cells with the expression of a TCR and/or a CAR. This way, NK cells would potentially have a higher capacity to access tumor cells, through the breakdown of ECM tumor barriers, while presenting increased targeted cytotoxicity.

6 Appendix

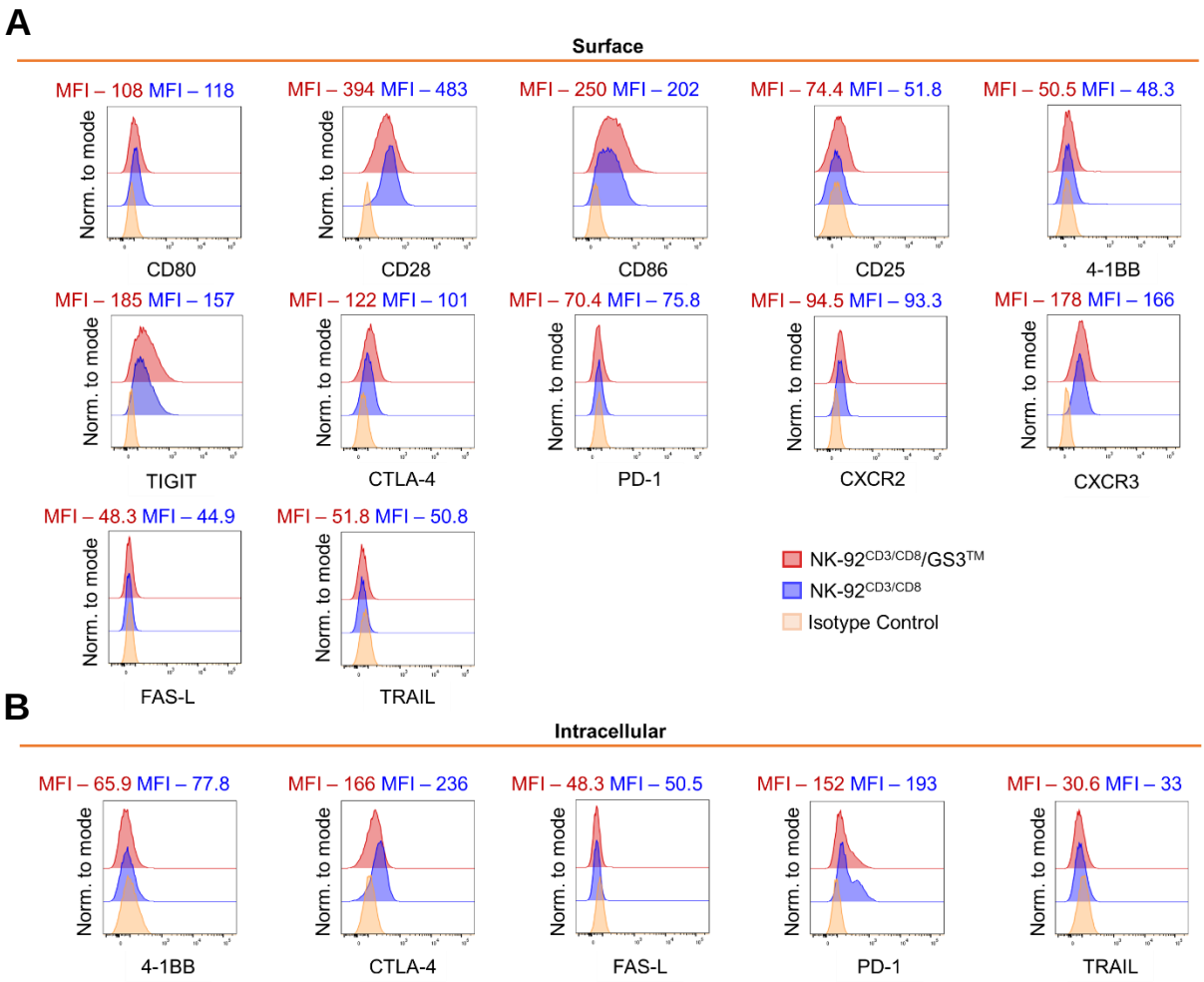

Supplementary Figure 1 - Comparative flow cytometric profile of NK-92$^{CD3/CD8}$ and NK-92$^{CD3/CD8}$/GS3^{TM}

(**A**) Surface receptors were stained on live cells with the indicated antibodies. (**B**) Intracellular proteins were stained on fixed cells with the indicated antibodies. Histograms are normalized to the mode. Representative results of three independent experiments are shown.

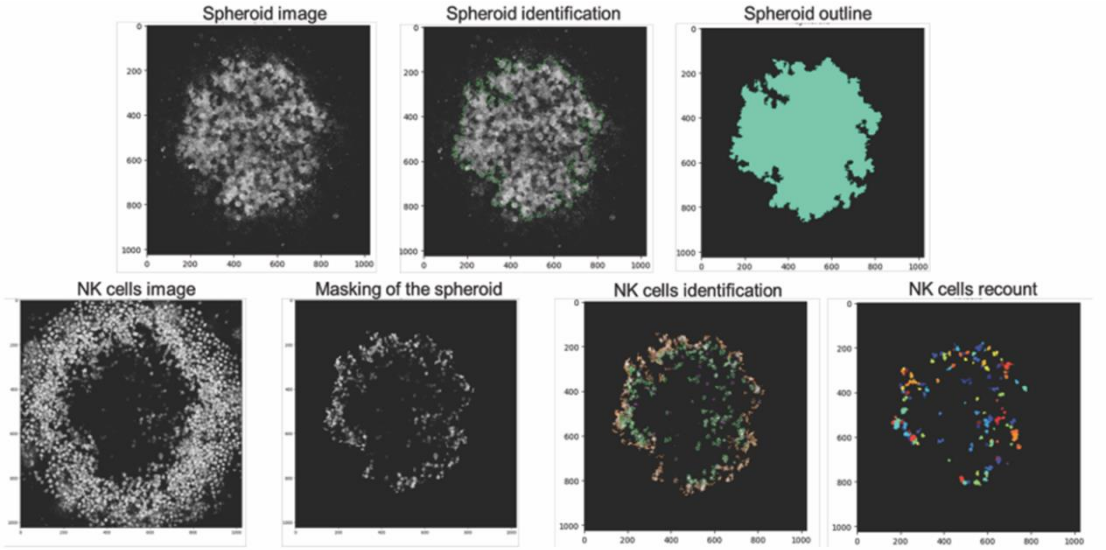

Supplementary Figure 2 - Automatic image analysis pipeline for NK cell quantification

Images were converted from green and blue channel images to grayscale, followed by the identification of the primary objects, spheroids, based on their intensity (green channel) and size. After, a mask was applied to the blue channel images to make sure that only NK cells present within the spheroid area would be identified. The final step was to identify and quantify the NK cells, based on the intensity, size and shape of the masked blue channel images

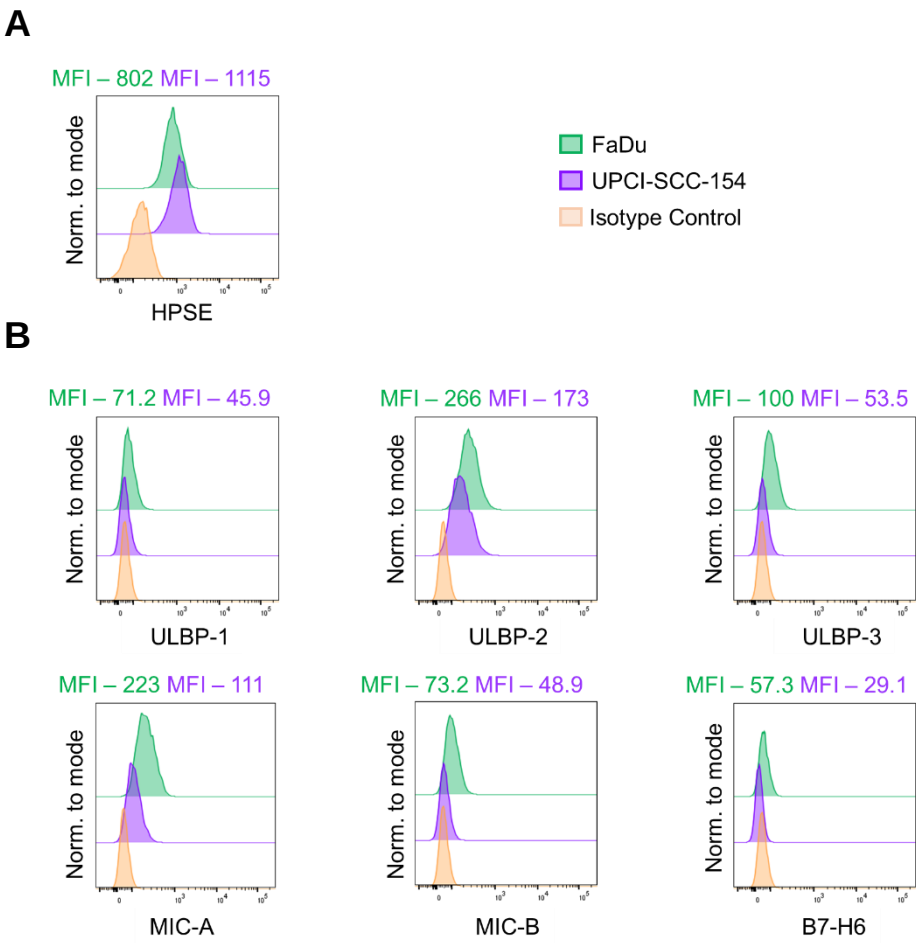

Supplementary Figure 3 - Expression of HPSE, NKG2D and NKp30 ligands in FaDu and UPCI-SCC-154 cells

(**A**) Surface expression of HPSE in FaDu (green) and UPCI-SCC-154 (purple) HNSCC cell lines detected with Hpa 733 polyclonal antibody and analyzed by FC. (**B**) Surface expression of the NKG2D ligands ULBP-1, ULBP-2, ULBP-3, MIC-A and MIC-B and the NKp30 ligand B7-H6 in UPCI-SCC-154 and FaDu cells. Cells were stained with the respective antibodies and analyzed by FC. Histograms are normalized to mode and represent MFI of each ligand. Data correspond to two independent experiments.

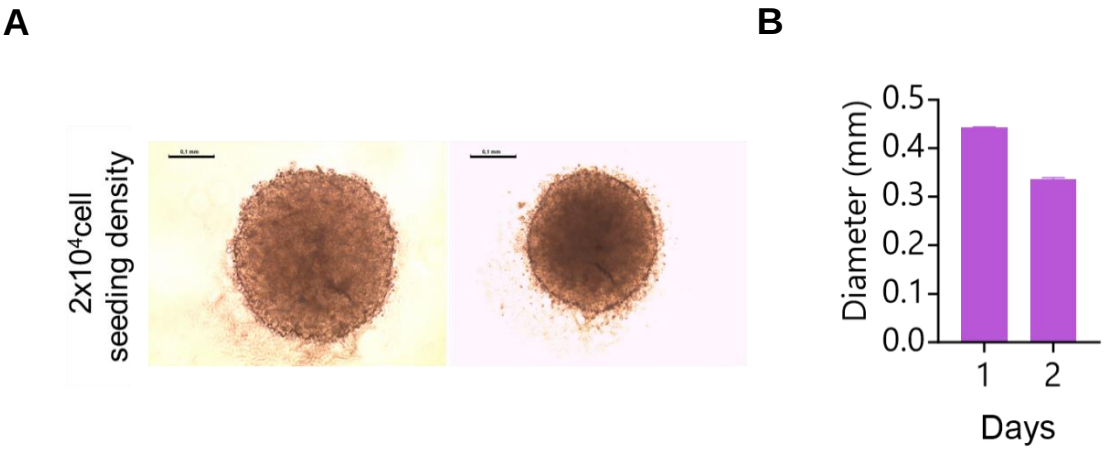

Supplementary Figure 4 - Spheroid culture optimization example

(**A**) Representative brightfield images of UPCI-SCC-154 spheroid at day 1 and day 2 after platting $2x10^4$ cells per well in ultra-low attachment plates. Spheroid culture was optimized by testing different cell densities, centrifugation and incubation conditions. Spheroid formation and size was monitored daily until they reached approximately 0.3 mm. (**B**) Measurements of spheroid diameters showed a significant compaction at day 2, which was chosen for NK infiltration tests. Brightfield images were taken daily and diameters were measured using ImageJ software (n=6).

7 References

1. de Visser, K.E. and J.A. Joyce, *The evolving tumor microenvironment: From cancer initiation to metastatic outgrowth.* Cancer Cell, 2023. **41**(3): p. 374-403.

2. Bejarano, L., M.J.C. Jordao, and J.A. Joyce, *Therapeutic Targeting of the Tumor Microenvironment.* Cancer Discov, 2021. **11**(4): p. 933-959.

3. Debela, D.T., et al., *New approaches and procedures for cancer treatment: Current perspectives.* SAGE Open Med, 2021. **9**: p. 20503121211034366.

4. Sanghera, C. and R. Sanghera, *Immunotherapy - Strategies for Expanding Its Role in the Treatment of All Major Tumor Sites.* Cureus, 2019. **11**(10): p. e5938.

5. Morotti, M., et al., *Promises and challenges of adoptive T-cell therapies for solid tumours.* Br J Cancer, 2021. **124**(11): p. 1759-1776.

6. Waldman, A.D., J.M. Fritz, and M.J. Lenardo, *A guide to cancer immunotherapy: from T cell basic science to clinical practice.* Nat Rev Immunol, 2020. **20**(11): p. 651-668.

7. Leko, V. and S.A. Rosenberg, *Identifying and Targeting Human Tumor Antigens for T Cell-Based Immunotherapy of Solid Tumors.* Cancer Cell, 2020. **38**(4): p. 454-472.

8. June, C.H. and M. Sadelain, *Chimeric Antigen Receptor Therapy.* N Engl J Med, 2018. **379**(1): p. 64-73.

9. Fowler, N.H., et al., *Tisagenlecleucel in adult relapsed or refractory follicular lymphoma: the phase 2 ELARA trial.* Nat Med, 2022. **28**(2): p. 325-332.

10. Locke, F.L., et al., *Long-term safety and activity of axicabtagene ciloleucel in refractory large B-cell lymphoma (ZUMA-1): a single-arm, multicentre, phase 1-2 trial.* Lancet Oncol, 2019. **20**(1): p. 31-42.

11. Munshi, N.C., et al., *Idecabtagene Vicleucel in Relapsed and Refractory Multiple Myeloma.* N Engl J Med, 2021. **384**(8): p. 705-716.

12. Berdeja, J.G., et al., *Ciltacabtagene autoleucel, a B-cell maturation antigen-directed chimeric antigen receptor T-cell therapy in patients with relapsed or refractory multiple myeloma (CARTITUDE-1): a phase 1b/2 open-label study.* Lancet, 2021. **398**(10297): p. 314-324.

13. Abramson, J.S., et al., *Lisocabtagene maraleucel for patients with relapsed or refractory large B-cell lymphomas (TRANSCEND NHL 001): a multicentre seamless design study.* Lancet, 2020. **396**(10254): p. 839-852.

14. Wang, M., et al., *KTE-X19 CAR T-Cell Therapy in Relapsed or Refractory Mantle-Cell Lymphoma.* N Engl J Med, 2020. **382**(14): p. 1331-1342.

15. Hong, D.S., et al., *Autologous T cell therapy for MAGE-A4(+) solid cancers in HLA-A*02(+) patients: a phase 1 trial.* Nat Med, 2023. **29**(1): p. 104-114.

16. Laskowski, T.J., A. Biederstadt, and K. Rezvani, *Natural killer cells in antitumour adoptive cell immunotherapy.* Nat Rev Cancer, 2022. **22**(10): p. 557-575.

17. Nersesian, S., et al., *NK cell infiltration is associated with improved overall survival in solid cancers: A systematic review and meta-analysis.* Transl Oncol, 2021. **14**(1): p. 100930.

18. Mitra, A., et al., *From bench to bedside: the history and progress of CAR T cell therapy.* Front Immunol, 2023. **14**: p. 1188049.

19. Jiao, Y., et al., *Type 1 Innate Lymphoid Cell Biology: Lessons Learnt from Natural Killer Cells.* Front Immunol, 2016. **7**: p. 426.

20. Mace, E.M., *Human natural killer cells: Form, function, and development.* J Allergy Clin Immunol, 2023. **151**(2): p. 371-385.

21. Chiossone, L., et al., *Maturation of mouse NK cells is a 4-stage developmental program.* Blood, 2009. **113**(22): p. 5488-96.

22. Cooper, M.A., T.A. Fehniger, and M.A. Caligiuri, *The biology of human natural killer-cell subsets.* Trends Immunol, 2001. **22**(11): p. 633-40.

23. Paul, S. and G. Lal, *The Molecular Mechanism of Natural Killer Cells Function and Its Importance in Cancer Immunotherapy.* Front Immunol, 2017. **8**: p. 1124.

24. Vivier, E., et al., *Targeting natural killer cells and natural killer T cells in cancer.* Nat Rev Immunol, 2012. **12**(4): p. 239-52.

25. Chan, C.J., M.J. Smyth, and L. Martinet, *Molecular mechanisms of natural killer cell activation in response to cellular stress.* Cell Death Differ, 2014. **21**(1): p. 5-14.

26. Barrow, A.D., C.J. Martin, and M. Colonna, *The Natural Cytotoxicity Receptors in Health and Disease.* Front Immunol, 2019. **10**: p. 909.

27. Siemaszko, J., A. Marzec-Przyszlak, and K. Bogunia-Kubik, *NKG2D Natural Killer Cell Receptor-A Short Description and Potential Clinical Applications.* Cells, 2021. **10**(6).

28. Pende, D., et al., *Killer Ig-Like Receptors (KIRs): Their Role in NK Cell Modulation and Developments Leading to Their Clinical Exploitation.* Front Immunol, 2019. **10**: p. 1179.

29. Perera Molligoda Arachchige, A.S., *Human NK cells: From development to effector functions.* Innate Immun, 2021. **27**(3): p. 212-229.

30. Wei, S., et al., *Control of lytic function by mitogen-activated protein kinase/extracellular regulatory kinase 2 (ERK2) in a human natural killer cell line: identification of perforin and granzyme B mobilization by functional ERK2.* J Exp Med, 1998. **187**(11): p. 1753-65.

31. Lo Nigro, C., et al., *NK-mediated antibody-dependent cell-mediated cytotoxicity in solid tumors: biological evidence and clinical perspectives.* Ann Transl Med, 2019. **7**(5): p. 105.

32. Prakash, J. and Y. Shaked, *The Interplay between Extracellular Matrix Remodeling and Cancer Therapeutics.* Cancer Discov, 2024. **14**(8): p. 1375-1388.

33. Huang, J., et al., *Extracellular matrix and its therapeutic potential for cancer treatment.* Signal Transduct Target Ther, 2021. **6**(1): p. 153.

34. Sarrazin, S., W.C. Lamanna, and J.D. Esko, *Heparan sulfate proteoglycans.* Cold Spring Harb Perspect Biol, 2011. **3**(7).

35. Vlodavsky, I., et al., *Biology of the Heparanase-Heparan Sulfate Axis and Its Role in Disease Pathogenesis.* Semin Thromb Hemost, 2021. **47**(3): p. 240-253.

36. Vlodavsky, I., et al., *Involvement of heparan sulfate and related molecules in sequestration and growth promoting activity of fibroblast growth factor.* Cancer Metastasis Rev, 1996. **15**(2): p. 177-86.

37. Nagarajan, A., P. Malvi, and N. Wajapeyee, *Heparan Sulfate and Heparan Sulfate Proteoglycans in Cancer Initiation and Progression.* Front Endocrinol (Lausanne), 2018. **9**: p. 483.

38. Hassan, N., et al., *Cell-surface heparan sulfate proteoglycans as multifunctional integrators of signaling in cancer.* Cell Signal, 2021. **77**: p. 109822.

39. Miao, H.Q., et al., *Cloning, expression, and purification of mouse heparanase.* Protein Expr Purif, 2002. **26**(3): p. 425-31.

40. Gaskin, S.M., T.P. Soares Da Costa, and M.D. Hulett, *Heparanase: Cloning, Function and Regulation.* Adv Exp Med Biol, 2020. **1221**: p. 189-229.

41. Rivara, S., F.M. Milazzo, and G. Giannini, *Heparanase: a rainbow pharmacological target associated to multiple pathologies including rare diseases.* Future Med Chem, 2016. **8**(6): p. 647-80.

42. Shteingauz, A., N. Ilan, and I. Vlodavsky, *Processing of heparanase is mediated by syndecan-1 cytoplasmic domain and involves syntenin and alpha-actinin.* Cell Mol Life Sci, 2014. **71**(22): p. 4457-70.

43. Abboud-Jarrous, G., et al., *Site-directed mutagenesis, proteolytic cleavage, and activation of human proheparanase.* J Biol Chem, 2005. **280**(14): p. 13568-75.

44. Levy-Adam, F., et al., *Heterodimer formation is essential for heparanase enzymatic activity.* Biochem Biophys Res Commun, 2003. **308**(4): p. 885-91.

45. Mayfosh, A.J., T.K. Nguyen, and M.D. Hulett, *The Heparanase Regulatory Network in Health and Disease.* Int J Mol Sci, 2021. **22**(20).

46. Baraz, L., et al., *Tumor suppressor p53 regulates heparanase gene expression.* Oncogene, 2006. **25**(28): p. 3939-47.

47. Li, R.W., et al., *Dramatic regulation of heparanase activity and angiogenesis gene expression in synovium from patients with rheumatoid arthritis.* Arthritis Rheum, 2008. **58**(6): p. 1590-600.

48. Vlodavsky, I., et al., *Involvement of heparanase in atherosclerosis and other vessel wall pathologies.* Matrix Biol, 2013. **32**(5): p. 241-51.

49. Rabelink, T.J., et al., *Heparanase: roles in cell survival, extracellular matrix remodelling and the development of kidney disease.* Nat Rev Nephrol, 2017. **13**(4): p. 201-212.

50. Waterman, M., et al., *Heparanase upregulation by colonic epithelium in inflammatory bowel disease.* Mod Pathol, 2007. **20**(1): p. 8-14.

51. Vlodavsky, I., et al., *Opposing Functions of Heparanase-1 and Heparanase-2 in Cancer Progression.* Trends Biochem Sci, 2018. **43**(1): p. 18-31.

52. Takaoka, M., et al., *Heparanase expression correlates with invasion and poor prognosis in gastric cancers.* Lab Invest, 2003. **83**(5): p. 613-22.

53. Rodrigues, A.A.N., et al., *Heparanase 1 Upregulation Promotes Tumor Progression and Is a Predictor of Low Survival for Oral Cancer.* Front Cell Dev Biol, 2022. **10**: p. 742213.

54. Arvatz, G., et al., *Heparanase and cancer progression: New directions, new promises.* Hum Vaccin Immunother, 2016. **12**(9): p. 2253-6.

55. Jayatilleke, K.M. and M.D. Hulett, *Heparanase and the hallmarks of cancer.* J Transl Med, 2020. **18**(1): p. 453.

56. Mohan, C.D., et al., *Targeting Heparanase in Cancer: Inhibition by Synthetic, Chemically Modified, and Natural Compounds.* iScience, 2019. **15**: p. 360-390.

57. Fux, L., et al., *Structure-function approach identifies a COOH-terminal domain that mediates heparanase signaling.* Cancer Res, 2009. **69**(5): p. 1758-67.

58. Yang, J., et al., *Targeting PI3K in cancer: mechanisms and advances in clinical trials.* Mol Cancer, 2019. **18**(1): p. 26.

59. Riaz, A., et al., *Characterization of heparanase-induced phosphatidylinositol 3-kinase-AKT activation and its integrin dependence.* J Biol Chem, 2013. **288**(17): p. 12366-75.

60. Amin, R., K. Tripathi, and R.D. Sanderson, *Nuclear Heparanase Regulates Chromatin Remodeling, Gene Expression and PTEN Tumor Suppressor Function.* Cells, 2020. **9**(9).

61. Mayfosh, A.J., N. Baschuk, and M.D. Hulett, *Leukocyte Heparanase: A Double-Edged Sword in Tumor Progression.* Front Oncol, 2019. **9**: p. 331.

62. Benhamron, S., et al., *Translocation of active heparanase to cell surface regulates degradation of extracellular matrix heparan sulfate upon transmigration of mature monocyte-derived dendritic cells.* J Immunol, 2006. **176**(11): p. 6417-24.

63. Gutter-Kapon, L., et al., *Heparanase is required for activation and function of macrophages.* Proc Natl Acad Sci U S A, 2016. **113**(48): p. E7808-E7817.

64. de Mestre, A.M., et al., *Regulation of inducible heparanase gene transcription in activated T cells by early growth response 1.* J Biol Chem, 2003. **278**(50): p. 50377-85.

65. Caruana, I., et al., *Heparanase promotes tumor infiltration and antitumor activity of CAR-redirected T lymphocytes.* Nat Med, 2015. **21**(5): p. 524-9.

66. Mayfosh, A.J., et al., *Heparanase is a regulator of natural killer cell activation and cytotoxicity.* J Leukoc Biol, 2022. **111**(6): p. 1211-1224.

67. Zcharia, E., et al., *Newly generated heparanase knock-out mice unravel co-regulation of heparanase and matrix metalloproteinases.* PLoS One, 2009. **4**(4): p. e5181.

68. Quiros-Fernandez, I., et al., *Dual T cell receptor/chimeric antigen receptor engineered NK-92 cells targeting the HPV16 E6 oncoprotein and the tumor-associated antigen L1CAM exhibit enhanced cytotoxicity and specificity against tumor cells.* J Med Virol, 2024. **96**(5): p. e29630.

69. Ai, H.W., et al., *Hue-shifted monomeric variants of Clavularia cyan fluorescent protein: identification of the molecular determinants of color and applications in fluorescence imaging.* BMC Biol, 2008. **6**: p. 13.

70. Kowarz, E., D. Loscher, and R. Marschalek, *Optimized Sleeping Beauty transposons rapidly generate stable transgenic cell lines.* Biotechnol J, 2015. **10**(4): p. 647-53.

71. Mates, L., et al., *Molecular evolution of a novel hyperactive Sleeping Beauty transposase enables robust stable gene transfer in vertebrates.* Nat Genet, 2009. **41**(6): p. 753-61.

72. Vlodavsky, I., et al., *Mammalian heparanase: gene cloning, expression and function in tumor progression and metastasis.* Nat Med, 1999. **5**(7): p. 793-802.

73. Zetser, A., et al., *Heparanase induces vascular endothelial growth factor expression: correlation with p38 phosphorylation levels and Src activation.* Cancer Res, 2006. **66**(3): p. 1455-63.

74. Nardella, C., et al., *Mechanism of activation of human heparanase investigated by protein engineering.* Biochemistry, 2004. **43**(7): p. 1862-73.

75. Murugin, V.V., et al., *Reduced degranulation of NK cells in patients with frequently recurring herpes.* Clin Vaccine Immunol, 2011. **18**(9): p. 1410-5.

76. Shinkai, Y., et al., *RAG-2-deficient mice lack mature lymphocytes owing to inability to initiate V(D)J rearrangement.* Cell, 1992. **68**(5): p. 855-67.

77. Greiner, D.L., R.A. Hesselton, and L.D. Shultz, *SCID mouse models of human stem cell engraftment.* Stem Cells, 1998. **16**(3): p. 166-77.

78. Shultz, L.D., et al., *Multiple defects in innate and adaptive immunologic function in NOD/LtSz-scid mice.* J Immunol, 1995. **154**(1): p. 180-91.

79. Liu, Y., *Survival correlation of immune response in human cancers.* Oncotarget, 2019. **10**(64): p. 6885-6897.

80. Kirtane, K., et al., *Adoptive cellular therapy in solid tumor malignancies: review of the literature and challenges ahead.* J Immunother Cancer, 2021. **9**(7).

81. Chen, N., et al., *Driving CARs on the uneven road of antigen heterogeneity in solid tumors.* Curr Opin Immunol, 2018. **51**: p. 103-110.

82. Yuan, Z., et al., *Extracellular matrix remodeling in tumor progression and immune escape: from mechanisms to treatments.* Mol Cancer, 2023. **22**(1): p. 48.

83. Liu, Z., et al., *Immunosuppression in tumor immune microenvironment and its optimization from CAR-T cell therapy.* Theranostics, 2022. **12**(14): p. 6273-6290.

84. Shin, E., et al., *Understanding NK cell biology for harnessing NK cell therapies: targeting cancer and beyond.* Front Immunol, 2023. **14**: p. 1192907.

85. Tong, L., et al., *NK cells and solid tumors: therapeutic potential and persisting obstacles.* Molecular Cancer, 2022. **21**(1).

86. Page, A., et al., *Development of NK cell-based cancer immunotherapies through receptor engineering.* Cell Mol Immunol, 2024. **21**(4): p. 315-331.

87. Kremer, V., et al., *Genetic engineering of human NK cells to express CXCR2 improves migration to renal cell carcinoma.* J Immunother Cancer, 2017. **5**(1): p. 73.

88. Gao, L., et al., *Engineering NK-92 Cell by Upregulating CXCR2 and IL-2 Via CRISPR-Cas9 Improves Its Antitumor Effects as Cellular Immunotherapy for Human Colon Cancer.* J Interferon Cytokine Res, 2021. **41**(12): p. 450-460.

89. Ng, Y.Y., J.C.K. Tay, and S. Wang, *CXCR1 Expression to Improve Anti-Cancer Efficacy of Intravenously Injected CAR-NK Cells in Mice with Peritoneal Xenografts.* Mol Ther Oncolytics, 2020. **16**: p. 75-85.

90. Wu, T., et al., *The Role of CXC Chemokines in Cancer Progression.* Cancers (Basel), 2022. **15**(1).

91. Rodriguez-Garcia, A., et al., *CAR-T Cells Hit the Tumor Microenvironment: Strategies to Overcome Tumor Escape.* Front Immunol, 2020. **11**: p. 1109.

92. Wang, W., et al., *Specificity redirection by CAR with human VEGFR-1 affinity endows T lymphocytes with tumor-killing ability and anti-angiogenic potency.* Gene Ther, 2013. **20**(10): p. 970-8.

93. Santoro, S.P., et al., *T cells bearing a chimeric antigen receptor against prostate-specific membrane antigen mediate vascular disruption and result in tumor regression.* Cancer Immunol Res, 2015. **3**(1): p. 68-84.

94. Byrd, T.T., et al., *TEM8/ANTXR1-Specific CAR T Cells as a Targeted Therapy for Triple-Negative Breast Cancer.* Cancer Res, 2018. **78**(2): p. 489-500.

95. Mai, Z., et al., *Modulating extracellular matrix stiffness: a strategic approach to boost cancer immunotherapy.* Cell Death Dis, 2024. **15**(5): p. 307.

96. Schuberth, P.C., et al., *Treatment of malignant pleural mesothelioma by fibroblast activation protein-specific re-directed T cells.* J Transl Med, 2013. **11**: p. 187.

97. Wang, L.C., et al., *Targeting fibroblast activation protein in tumor stroma with chimeric antigen receptor T cells can inhibit tumor growth and augment host immunity without severe toxicity.* Cancer Immunol Res, 2014. **2**(2): p. 154-66.

98. Kakarla, S., et al., *Antitumor effects of chimeric receptor engineered human T cells directed to tumor stroma.* Mol Ther, 2013. **21**(8): p. 1611-20.

99. Zhang, Z., et al., *CAR-T-Cell Therapy for Solid Tumors Positive for Fibronectin Extra Domain B.* Cells, 2022. **11**(18).

100. Martin-Otal, C., et al., *Targeting the extra domain A of fibronectin for cancer therapy with CAR-T cells.* J Immunother Cancer, 2022. **10**(8).

101. Klingemann, H., *The NK-92 cell line-30 years later: its impact on natural killer cell research and treatment of cancer.* Cytotherapy, 2023. **25**(5): p. 451-457.

102. Poorebrahim, M., et al., *A costimulatory chimeric antigen receptor targeting TROP2 enhances the cytotoxicity of NK cells expressing a T cell receptor reactive to human papillomavirus type 16 E7.* Cancer Lett, 2023. **566**: p. 216242.

103. Zetser, A., et al., *Processing and activation of latent heparanase occurs in lysosomes.* J Cell Sci, 2004. **117**(Pt 11): p. 2249-58.

104. Brusilovsky, M., et al., *Carbohydrate-mediated modulation of NK cell receptor function: structural and functional influences of heparan sulfate moieties expressed on NK cell surface.* Front Oncol, 2014. **4**: p. 185.

105. Brusilovsky, M., et al., *Regulation of natural cytotoxicity receptors by heparan sulfate proteoglycans in -cis: A lesson from NKp44.* Eur J Immunol, 2015. **45**(4): p. 1180-91.

106. Manon-Jensen, T., Y. Itoh, and J.R. Couchman, *Proteoglycans in health and disease: the multiple roles of syndecan shedding.* FEBS J, 2010. **277**(19): p. 3876-89.

107. Aktas, E., et al., *Relationship between CD107a expression and cytotoxic activity.* Cell Immunol, 2009. **254**(2): p. 149-54.

108. Alter, G., J.M. Malenfant, and M. Altfeld, *CD107a as a functional marker for the identification of natural killer cell activity.* J Immunol Methods, 2004. **294**(1-2): p. 15-22.

109. Betts, M.R., et al., *Sensitive and viable identification of antigen-specific CD8+ T cells by a flow cytometric assay for degranulation.* J Immunol Methods, 2003. **281**(1-2): p. 65-78.

110. Byrd, A., et al., *Expression analysis of the ligands for the Natural Killer cell receptors NKp30 and NKp44.* PLoS One, 2007. **2**(12): p. e1339.

111. Chitadze, G., et al., *Generation of soluble NKG2D ligands: proteolytic cleavage, exosome secretion and functional implications.* Scand J Immunol, 2013. **78**(2): p. 120-9.

112. Parodi, M., et al., *Murine models to study human NK cells in human solid tumors.* Front Immunol, 2023. **14**: p. 1209237.

113. Galli, F., et al., *Immune cell labelling and tracking: implications for adoptive cell transfer therapies.* EJNMMI Radiopharm Chem, 2021. **6**(1): p. 7.

114. Daldrup-Link, H.E., et al., *In vivo tracking of genetically engineered, anti-HER2/neu directed natural killer cells to HER2/neu positive mammary tumors with magnetic resonance imaging.* Eur Radiol, 2005. **15**(1): p. 4-13.